U. S. DEPARTMENT OF COMMERCE
Charles Sawyer, Secretary
NATIONAL BUREAU OF STANDARDS
E. U. Condon, Director

APRIL 1950
VOLUME • 44
NUMBER 4

JOURNAL OF RESEARCH

of the

NATIONAL BUREAU OF STANDARDS

Contents

RP		Page
2082	Factors affecting the water-vapor permeability of leather. Joseph R. Kanagy and Robert A. Vickers, III. (Price 10 cents)	347
2083	Reduction of halomethanes with lithium aluminum hydride. Vernon H. Dibeler. (Price 10 cents)	363
2084	Crystallization and second-order transitions in silicone rubbers. C. E. Weir, W. H. Leser, and L. A. Wood. (Price 10 cents)	367
2085	Refractive index as a function of wavelength for sixty API–NBS hydrocarbons. Alphonse F. Forziati. (Price 10 cents)	373
2086	Heats of combustion and formation of cellulose and nitrocellulose (cellulose nitrate). Ralph S. Jessup and Edward J. Prosen. (Price 10 cents)	387
2087	Thermal and moisture expansion studies of some domestic granites. Arthur Hockman and Daniel W. Kessler. (Price 10 cents)	395
2088	Separation of 2,3-dimethylpentane, 1, cis-3-dimethylcylcopentane, and 3-ethylpentane from petroleum. Augustus R. Glasgow, Jr., Charles B. Willingham, and Frederick D. Rossini. (Price 10 cents)	411
2089	Interference methods for producing and calibrating end standards. Chauncey G. Peters and Walter B. Emerson. (Price 15 cents)	419
2090	A note on the formation and structure of iron dendrites in a magnesium alloy. Harry C. Burnett, Jr., and Herbert C. Vacher. (Price 10 cents)	443

For sale by the Superintendent of Documents, U. S. Government Printing Office, Washington 25, D. C. • Price 75 cents
$4.50 per year on subscription

UNITED STATES GOVERNMENT PRINTING OFFICE, WASHINGTON : 1950

U. S. Department of Commerce
National Bureau of Standards

Research Paper RP2082
Volume 44, April 1950

Part of the Journal of Research of the National Bureau of Standards

Factors Affecting the Water-Vapor Permeability of Leather[1]

By Joseph R. Kanagy and Robert A. Vickers, III

This investigation was undertaken at the request of the Office of the Quartermaster General, which is endeavoring to obtain fundamental information on the transfer of water vapor through leather, which may be applied in the development of improved Army shoes. The method used for measuring the water vapor permeability is based on the present approved procedure of the American Leather Chemists' Association, but considerable improvement was made in the technique of assembling the permeability cell and in the procedure applied in making the determinations.

The water vapor permeability of leather depends upon a number of factors including thickness of sample, grease content, and the relative humidity and temperature of the atmosphere. It is greatly reduced by the presence of the natural glyceride greases. The grain layer of the leather appears to be the first stratum to become saturated with grease and consequently is a highly influential stratum with respect to water vapor permeability. The finish on the grain layer also has an influence on water vapor transmission. There is no dependent correlation between water vapor permeability and air permeability.

Studies on leathers impregnated with different types of materials, including rubber and acrylate resins, show that the water vapor permeability decreases in the following order: sulfonated oils, acrylate resins, rubber, and stuffing greases. The comparatively high water vapor permeability of the leathers treated with the sulfonated oils and acrylate resins is attributed to the influence of the polar groups in these impregnants.

Studies indicated that flexing of the specimen had no influence on the water vapor permeability of degreased leathers; however, for leathers that contained grease, there was an increase in water vapor permeability on flexing.

The results of the experiments indicate that, in addition to gaseous diffusion, water is transmitted through leather by conduction over the surface or by some form of activated diffusion. Evidence for the conduction mechanism is given by the behavior at low relative humidities, existence of an energy of activation, influence of temperature, comparison of air permeability and water vapor permeability, experiments with fabrics and glass disks, variations of diffusion constants, and the results of studies of the effect of gross air pressure with the dynamic equipment.

I. Introduction

The ability to transmit water vapor is one of the important properties of leather that makes it so desirable for use in the construction of shoes. A knowledge of the factors involved in this property is, therefore, important in the proper selection and manufacture of materials that will give improved service and yet maintain a sufficiently high level of water vapor permeability to assure comfort to the wearer.

The water vapor permeability of leather is inherently high. However, the use of fats and greases to improve water resistance of shoe leather may lower water vapor transmission to the point below the critical level, which has not been determined, at which the foot may be comfortable

[1] This report is made as a part of the Leather Research Program sponsored by the Research and Development Branch, Military Planning Division of the Office of the Quartermaster General, Department of the Army. This program is under the Advisory Direction of the National Research Council.

under a particular set of temperature and humidity conditions which the wearer of the shoes may encounter. It would be desirable to maintain water vapor transmission at a high level while simultaneously liquid water transmission is maintained at a low level.

The purpose of the present investigation was to study the mechanism of water vapor transmission and to attempt to develop and standardize a more suitable method for measuring it. In this connection the work of Bradley, McKay, and Worswick [1],[2] Edwards [2], Mitton [3], Hobbs [4], and Maeser [5] on leather has given considerable information which has been applied in this study. The work of the Institute of Paper Chemistry [6] and Carson and Worthington [7] on paper, a study of the permeability to moisture of synthetic resins for aircraft by Kline [8], the work of Doty, Aiken, and Mark [9, 10] on organic films, and the work by Harris and Fourt [11] on fabrics have been helpful in this investigation.

II. Test Method

The basic principle in all water vapor permeability tests developed for leather is the use of the specimen as a diaphragm with a region of high relative humidity on one side and one of low relative humidity on the other. The gain in weight per unit area on the low relative humidity side in unit time is expressed as the water vapor permeability. One of the earliest and simplest tests was developed by Wilson and Lines [13]. They put sulfuric acid in a bottle, over which a leather specimen was placed by fastening it in the cap, which was then screwed down on the top. The bottle and contents were weighed from time to time to determine the gain in weight.

Work by Mitton [3] and by the Institute of Paper Chemistry [6] has shown that a static air space between the specimen and the desiccant influences the result since the diffusion of water vapor is retarded by air. Thus, for highly permeable leathers the result may be the permeability of the underlying air space rather than that for the specimen. The atmospheres of high and low relative humidities should, therefore, make immediate contact with the opposite faces of the specimen.

This condition is readily achieved on the outer face by rapid ventilation. On the low relative humidity side, circulation involves complicated apparatus, but has been accomplished by the rapid passing of dry air. The necessary conditions can be more conveniently met in a cell (dish) by placing the desiccant in contact with the leather. The former has been used successfully by Edwards [27] and by Maeser [5], whereas the latter has been used successfully by Carson [7] and by the Institute of Paper Chemistry [6] and is applied in the present ALCA test [12].

1. Description of Method Used

The method used in this work is a modification of the ALCA test. This procedure was adopted because of its speed, convenience, ease of application, and ease of duplication of conditions.

The water vapor permeability cell devised is shown in figure 1, A. It consists of a circular aluminum cup with a flange. The total diameter

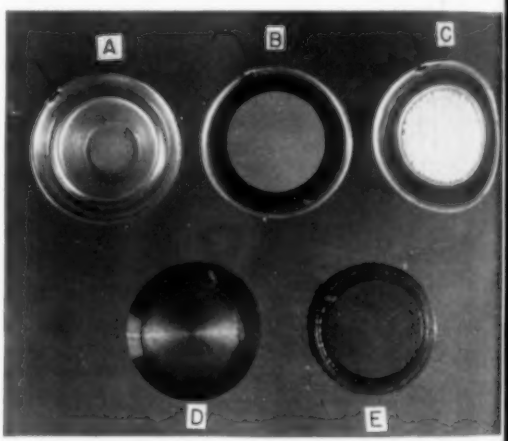

FIGURE 1. *A, Empty aluminum cell used in the water vapor permeability studies; B, assembled cell and leather specimen ready for measurements; C, assembled cell with transparent cellulose film showing desiccant; D, template used in assembling the cell; E, side of leather specimen next to desiccant after determination of water vapor permeability was made.*

is about 4 in. The flange is bent in such a way that a raised rim is formed at the edge of the cup upon which the leather fits tightly. In preparing the cells, the cup is filled with the desiccant, and the leather specimen having a larger diameter than the cup is placed over the rim. A circular copper template (fig. 1, D) having one surface

[2] Figures in brackets indicate the literature references at the end of this paper.

machined to have the same diameter as the cup is then fitted as nearly as possible directly over the cup. Molten microcrystalline wax is poured around the groove formed by the template and the flange. This seals the edge of the leather and fastens it to the cell. After the wax has hardened, the copper template is removed, leaving an area of 25 cm² of the leather exposed. Cooling the template in a refrigerator prior to use assists in preventing adhesion of the wax.

In figure 1, C the position of the desiccant with respect to the specimen is shown, and figure 1, E shows the side next to the desiccant of a leather specimen on which tests have been completed.

The completed cell is hung in a cabinet of the type described by Carson and Worthington [7] at the desired temperature and relative humidity. The cells are weighed at various intervals of time in place without removal from the cabinet to determine the rate at which the leather transmits moisture.

Unless otherwise stated, the temperature at which the measurements are made is 100° F. This temperature is used because it closely approximates body temperature. Less time is also required to reach a steady state at this temperature than at a lower temperature. Conditions of relative humidity in the range 40 to 65 percent were found satisfactory. The time required for a measurement by this method is 4 to 5 hrs compared to 4 or 5 days required in the present ALCA test. The cells may be prepared in about 5 percent of the time required by the ALCA test. The period over which the rate of gain of the cell was most nearly constant was taken as the value for the water vapor permeability. This was usually over the time interval of 2 to 4 hrs. The rates of gain during this period were averaged and expressed as gain per 100 min.

The success of the desiccant method depends upon the capacity for water vapor of the particular salt used. The salt used as the desiccant should maintain a high capacity for water over a great enough time period for completion of a test. This time period must permit the specimen to come to equilibrium and then continue the adsorption of water at a constant rate. The rate of adsorption per unit time may be taken at any point after a constant rate of gain has been reached. In figure 2 the behavior of anhydrous calcium chloride, anhydrous magnesium perchlorate, and

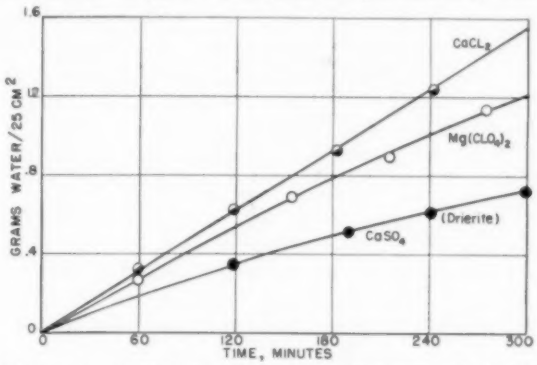

FIGURE 2. *Rate of moisture pickup by various desiccants used in the cells.*

Drierite (anhydrous calcium sulfate) when used in the cell is shown. The results were obtained with chrome-tanned calfskin at 44-percent relative humidity on the high vapor pressure side. They show that calcium chloride is highly superior to Drierite and better than magnesium perchlorate with respect to the maintenance of a high capacity for water vapor over an extended period of time. The curve for calcium chloride is a straight line, whereas the other two curves tend to level off.

All of the following determinations, unless otherwise stated, were made at 100° F with a relative humidity of 53 percent on the high-pressure side and calcium chloride in contact with the specimen on the low-pressure side.

2. Some Typical Results With the Method

In table 1 [3] are shown water vapor permeability

[3] In this study water vapor permeability is expressed in grams passing through 25 cm² of the specimen in 100 min. This unit was chosen for convenience in calculation. The total area exposed was 25 cm², and 100 is a convenient figure to handle arithmetically. The results were not expressed in the unit, grams/m²×24 hours, which is used by the ALCA, since they could not be directly compared because of the difference in conditions under which the tests were made. The ALCA test was designed to be run at 70° F and 65-percent relative humidity, whereas the test applied in this study was performed at 100° F and 53-percent relative humidity. From our present knowledge of water vapor permeability, the results have only relative significance, and comparisons can be made only under uniform sets of conditions. As a result of this work, the need for the clarification of definitions and a standard unit for the expression of water vapor permeability was emphasized with the result that a committee was appointed at this Bureau to consider these matters. Recently this committee has recommended that water vapor permeability be expressed in cgs units; namely, grams/cm²×sec. This recommendation will be offered for consideration by the Federal Specification Committee, the ASTM, and other scientific associations.

In order to show the relation between these units, the results in table 1 are expressed in three different ways: (1) By the unit used for all the data in this study, grams/25 cm²×100 min, (2) by the cgs unit which may be standard in the near future for all water vapor permeability measurements, grams/cm²×sec, and (3) by the unit used in the ALCA test, grams/m²×24 hr. The data expressed in grams/25 cm²×100 min may be converted to grams/cm²×sec by dividing by 15×10^6, and it may be converted to grams/m²24 hr by multiplying by 5760.

TABLE 1. *Water vapor permeabilities of various leathers at 100° F with 53-percent relative humidity on the high vapor pressure side and 0 relative humidity on the low vapor pressure side*

Type of leather	Thickness	Grease	Water vapor permeability		
	Mils	*Percent*	*g/cm²×sec*	*g/25 cm²×100 min*	*g/m²×24 hr*
Vegetable-tanned sealskin	107	1.0	3.00×10^{-4}	0.45	2592
Chrome-tanned calfskin	36	5.1	3.33	.50	2880
Vegetable-tanned calfskin	37	13.8	2.47	.37	2131
Vegetable-tanned sheepskin	43	6.7	5.07	.76	4378
Chrome-retanned upper	78	10.2	2.07	.31	1786
Do	81	10.2	1.73	.26	1498
Do	85	22.8	0.14	.02	115
Vegetable-tanned strap	105	4.7	2.13	.32	1152
Vegetable-tanned sole	200	5.9	1.93	.29	1670
Do	271	3.1	0.47	.07	403
Do	179	6.5	.08	.12	691
Chrome-retanned sole	215	1.2	1.93	.29	1670
Chrome hydraulic packing	165	7.1	1.07	.16	922
Alum-formaldehyde	42	6.9	3.80	.57	3283
Indian-tanned lace	129	25.4	0.07	.01	58
Rawhide lace	128	43.8	.02	.003	17

values obtained with the above-described method for a number of different types of leather. The thickness and grease contents of the leathers are also given. It may be observed that the water vapor transmission is dependent upon both grease content and thickness.

The correlation between the ALCA method [12] and the new method used in making the tests in this invesigation is shown in figure 3. In the ALCA method, a cell is prepared by cementing the leather specimen on the top of a tannin dish. This is a circular dish, about 3 in. in diameter and 1.5 in. deep. Drierite is placed in the dish prior to the sealing of the specimen. The prepared cell is placed on a rack in a room at a constant temperature and relative humidity. The cell is turned specimen side down, so that the desiccant is in contact with the specimen. Weighings are made from time to time to determine the rate at which water vapor passes through the leather. The results obtained with this method shown in figure 3 were obtained at 50-percent relative humidity and 73° F. The correlation is good except that it is curvilinear. The nature of the correlation is undoubtedly caused by the fact that Drierite is used in the ALCA test. Its capacity for holding water is low, and therefore the rate of pickup will decrease rapidly with time. There will then be a tendency for the curve showing increasing water vapor permeabilities to become asymptotic to some maximum value that would approach the saturation point of the Drierite used in the cup.

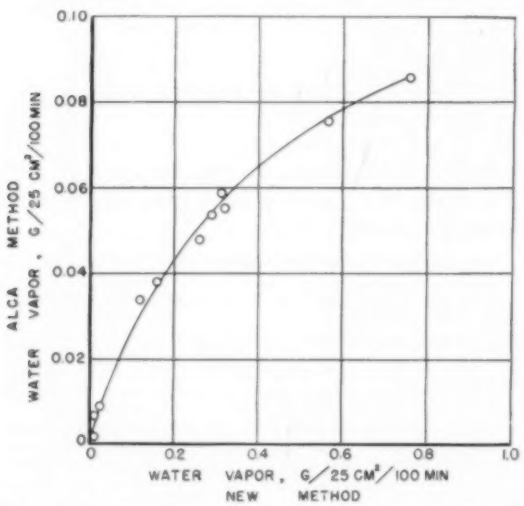

FIGURE 3. *Correlation of ALCA method with the new method for determining water vapor permeability.*

III. Mechanisms of Transmission of Water Vapor

The mechanism of water vapor transmission through a fibrous organic material or through an organic film has generally been accepted as consisting of gaseous diffusion through pores or by conduction. By conduction is meant migration by means of solution, activated diffusion, or capillary action from a region of high concentration to a region of low concentration over a water attracting surface. In transmission by capillary action

It is conceived that water condenses in small pores on the high relative humidity side and the migration proceeds automatically toward the region of low concentration on the low relative humidity side. Mitton [3] states that the diffusion of water vapor occurs mainly in the free spaces within the leather. On the other hand, Wilson [13] and Edwards [2] believed that the water vapor was transmitted by capillary action.

According to the most generally accepted concept of the fibrous structure of leather, long parallel chains of polypeptides form submicroscopic fibrils. These fibrils, in turn, form larger fibrils. The fibrils form fibers that are interwoven to give the physical structure that is visible on close examination of the hide or leather. Such a network produces a large number of pores or capillaries that vary in size. These might be divided into four categories according to Schulze (See Paine) [17]: (1) Macroscopic and microscopic cracks and spaces, (2) submicroscopic capillaries and canals, (3) intermolecular spaces, (4) intramolecular spaces. It would be expected that the macroscopic and microscopic spaces would be associated with gaseous diffusion. Submicroscopic capillaries would be involved in capillary flow and activated diffusion, categories (3) and (4) would be associated only with activated diffusion. According to Doty, Aiken, and Mark [9], two types of activated diffusion are involved in water vapor transmission—one in which the transmission takes place through preformed pores and one where the transmission takes place through the formation of temporary pockets caused by the kinetic action of the molecules. The former type of activated diffusion would occur through both macroscopic and microscopic pores, whereas the latter type would occur only through inter- and intramolecular spaces.

Results from X-ray studies [18] indicate that when water enters the region of the submicroscopic fibrils composed of polypeptide chains, swelling occurs and the distance between chains is increased. It appears, therefore, that a certain energy change must be involved when water becomes associated with these groups, and therefore transmission through this fine structure could occur only by an activated diffusion. The activated diffusion through the macroscopic and microscopic capillaries proceeds by the adsorption of the water molecules on the water attracting group on the surface. When the energy of adsorption has been dissipated, the water molecule will vibrate and acquire the kinetic energy for desorption. The molecule will then proceed further over the surface of the fiber to another active spot. This action will continue until the water molecule passes through the leather. The migration will proceed from the region of high concentration to that of a low concentration. The activated diffusion through intermolecular spaces will proceed by the same mechanism, except that the molecules will have to depend upon temporary openings consisting of pockets and crevices formed at random, and the rate of transmission will be much lower.

It is conceivable that capillary action occurs in the microscopic and submicroscopic pores by condensation on the high relative humidity side and then migration and evaporation on the low relative humidity side. Migration by solution is not considered to be important in leather. However, the behavior of the water in the region of the polypeptide groups might be interpreted as a solution process. The ways in which water vapor transmission depends upon important variables provide clues to mechanisms involved in the process. The succeeding sections of this paper give results of such studies.

IV. Effect of Important Variables on Water Vapor Permeability

1. Fundamental Equation for Diffusion

Many attempts have been made to represent water vapor transmission data by means of the linear diffusion equation, one form of which is given:

$$m = KA \frac{(C_2 - C_1)}{h} t,$$

where m = mass of water in grams passing in t seconds;
A = the area of the diaphragm in square centimeters;
$C_2 - C_1$ = difference in concentration at the two surfaces in grams per cubic centimeters;
h = thickness of the diaphragm in centimeters;
K = diffusion constant

This equation has the same form as the equation for the heat conductivity, where K depends upon the nature of the substance.

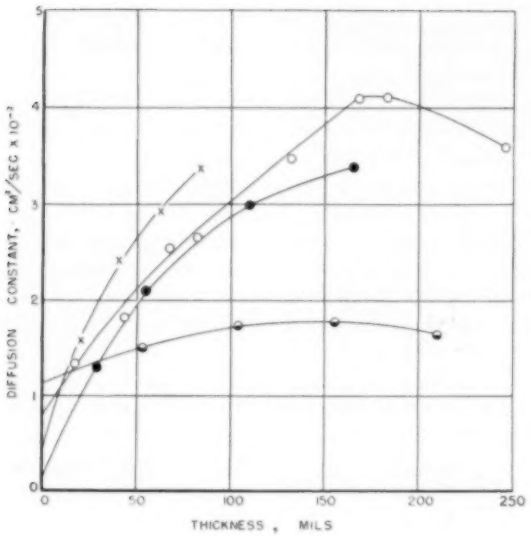

FIGURE 4. *Change of the diffusion constant of glass cloth, leather, cotton duck, and nylon with thickness.*
×, Glass cloth; ○, leather; ●, cotton duck; ◑, nylon.

In figure 4 the change in K with the thickness of the material is shown. The data show that K is not constant except possibly for nylon; therefore some mechanism other than or in addition to gaseous diffusion must be involved. With leather, cotton duck, and glass cloth, the values for K increase as the thickness increases, which indicates that the material has a specific influence on the diffusion. K values for nylon do not increase appreciably with thickness, which indicates that linear diffusion fairly well represents the behavior of this material and the material itself has little influence on the transmission of water vapor. The fact that the diffusion constant increases with increasing thicknesses for all except nylon indicates that there is an induction period involved in the process. This is probably in the initial contact of the water vapor with the material, some time apparently being required for the water molecules to attach themselves. After this has occurred, the diffusion proceeds more or less rapidly, depending on the type of material. The highly polar glass, cotton, and leather appear to be more influential on the conduction of the water vapor than the less polar nylon.

The variation of the diffusion constant with the relative humidity is shown in figure 5. The diffusion "constant" increases as the relative humidity increases and appears to decrease to [illegible] at a relative humidity of about 10. At low relative humidities the constant will necessarily be low, since the permeability is low for the reason given when figure 11 is discussed. However, at the higher relative humidities when the attracting groups in the protein become covered with water molecules, the conductivity of the material will be increased. It appears that water may be conducted most rapidly over other water molecules.

The results obtained for the diffusion coefficient of leather given in figure 4 are of the same order of magnitude as those obtained by Mitton [7]. Mitton's values for the diffusion coefficient also appear to be greater for the thicker samples of leather.

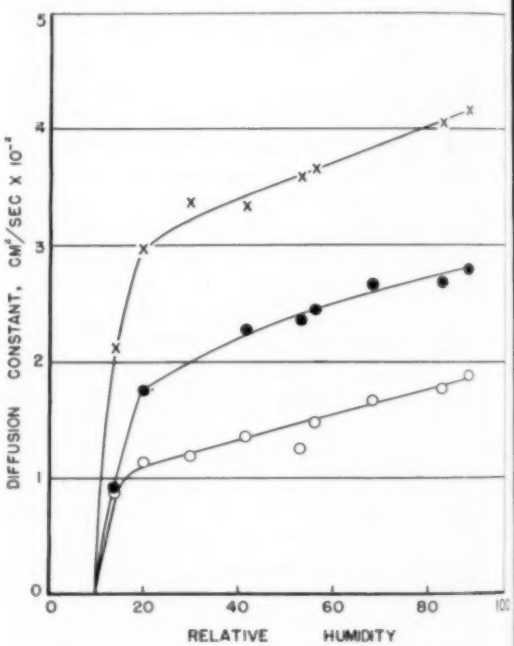

FIGURE 5. *Change in the diffusion constant of vegetable-tanned sealskin* ×, *vegetable-tanned sheepskin* ●, *and chrome-tanned calfskin* ○ *with relative humidity.*

2. Air Permeability Versus Water Vapor Permeability

The relation between air permeability and water vapor permeability for a number of leather splits is shown in table 2. The first four values given are for chrome-retanned sole leather. The others are for vegetable-tanned sole leather. Air permeability was determined by the method described

by Carson and Worthington [15]. The thickness and grease contents of the splits are given along with the air and water vapor permeabilities. It may be noted that as the air permeability decreases, the water vapor permeability also decreases; however, the range of the air permeability is about 200 to 1; whereas the range of the water vapor permeability is little more than 2 to 1. For the same types of leathers those having high water vapor permeability usually have high air permeability also; however, the relation between these two properties apparently involves other factors that are independent of each other.

TABLE 2. *Relation between air permeability and water vapor permeability of leather splits*

Thickness	Grease	Air permeability	Water vapor permeability at 53% relative humidity on wet side
Mils	*Percent*	*cm³/sec/cm²*	*g/25 cm²×100 min.*
24	1.43	9120	0.98
17	2.00	7540	1.13
33	0.74	6795	1.00
51	.54	5785	0.80
15	11.87	489	.81
25	11.25	285	.59
36	6.18	185	.66
35	5.71	162	.66
40	8.96	103	.54
33	8.24	93	.55
44	9.12	51	.48

Often new ideas and important information may be obtained by studying the properties of materials somewhat different in character from those with which the tests are directly concerned. For this reason some tests were made with various types of cloth fabrics and Pyrex-glass disks.

Figure 6 and table 3 compare the air permeability and water-vapor permeability of nylon and glass fabrics. Water-vapor permeability was determined on disks of the material about 2¾ in. in diameter by the same method as was used for the leather specimens. Air permeability was determined by the method described by Schiefer and Boyland [16]. Thickness of the fabrics was varied by increasing the number of plies. It may be observed that the ratio of the water-vapor permeability to air permeability for glass fabric is higher than that for nylon fabric.

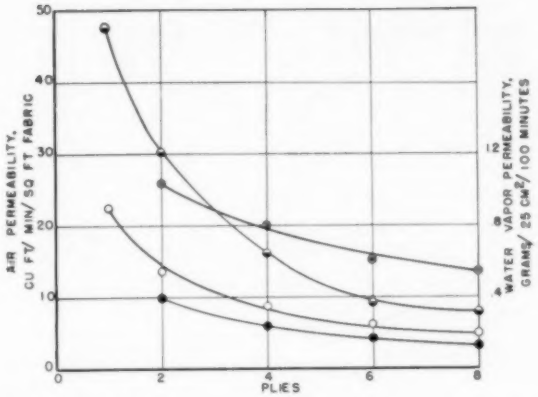

FIGURE 6. *Comparison of the air permeability and the water vapor permeability of glass and nylon fabrics, as a function of number of plies.*

Air permeability: ○, nylon; ◑, glass. Water vapor permeability: ●, nylon; ⊗, glass.

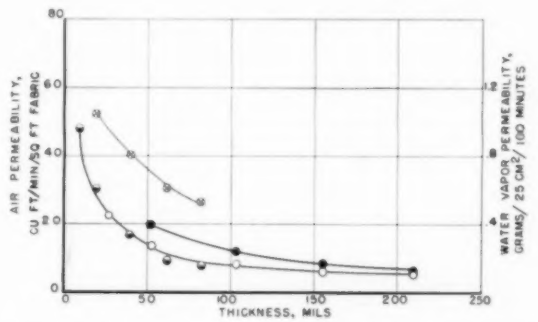

FIGURE 7. *Comparison of the air permeability and the water vapor permeability of glass and nylon fabrics as a function of thickness.*

Air permeability: ○, nylon; ◑, glass. Water vapor permeability: ●, nylon; ⊗, glass.

TABLE 3. *Comparison of air and water vapor permeabilities of glass and nylon fabrics*

(Air permeability determined at pressure of 0.5 in water)

	Plies	Thickness	Air permeability	Water-vapor permeability
		Mils	*ft³/min×ft² fabric*	*g/25 cm²×100 min*
Nylon	1	27	22.3	----
	2	53	13.4	0.41
	4	104	8.4	.35
	6	156	6.2	.18
	8	210	6.0	.13
Glass	1	10	48.2	----
	2	20	30.4	1.05
	4	40	16.8	.81
	6	62	9.4	.64
	8	83	8.0	.55

877106—50——2

In figure 7 the data obtained with the cloth fabrics are plotted against thickness. The air permeabilities of both types of cloth happen to be the same for given thickness, whereas the water-vapor permeabilities are different. This indicates that although the air permeabilities of the two types of cloth correlate with each other, the water-vapor permeabilities do not correlate and are obviously dependent upon the properties of the materials. The glass fabric shows much higher water-vapor permeability per unit thickness than the nylon.

Experiments were made with fritted Pyrex-glass disks about 2¾ in. in diameter and of the type used in filtering equipment. These disks were obtained from the Corning Glass Co. The approximate pore size for each disk and values for the air permeability and water penetration were furnished by the manufacturer. These values are given in table 4, along with the water-vapor permeabilities that were determined by the same method as was used for the leathers. It may be noted that both water penetration and air permeability increase rapidly with increase in pore size, whereas water-vapor permeability decreases for the two greatest pore sizes. Surface area would also decrease as the pore size increases, and it appears from these results that the water-vapor permeability is a function of the surface area.

TABLE 4. *Comparison of the water vapor permeability, liquid water permeability, and air permeability of Pyrex glass fritted disks*

Designated porosity	Average pore diameter	Liquid water penetration pressure difference 100 mm Hg	Air flow pressure difference 50 mm Hg	Water vapor permeability at 53% relative humidity on wet side	
				Trial No.	
				1	2
	Microns	*cm³/min*	*cm³/min*	*g/25 cm²×100 min*	*g/25 cm²×100 min*
Fine	5	9	190	0.251	0.249
Medium	14	70	1,200	.276	.283
Coarse	40	500	6,000	.261	.275
Extra coarse	160	3,500	20,000+	.172	.173

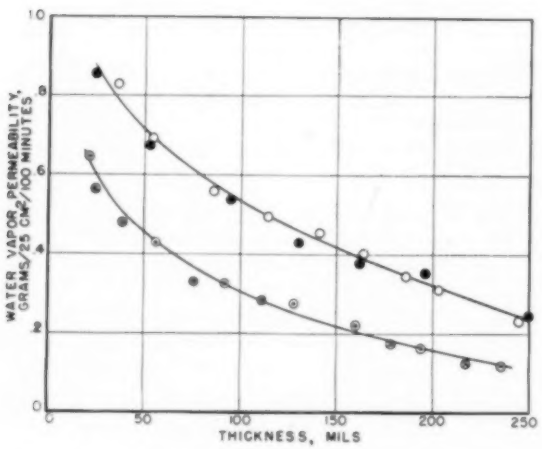

FIGURE 8. *Effect of thickness on the water vapor permeability of leather.*

Leather: ○, Vegetable tanned crust; ●, degreased crust; ⊗, vegetable tanned sole; ⊙, vegetable tanned sole degreased.

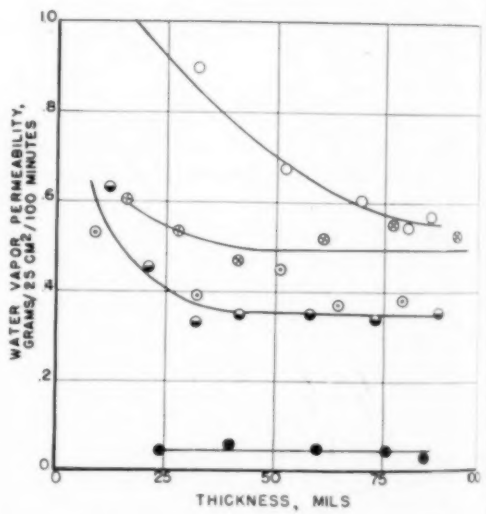

FIGURE 9. *Effect of grease content and thickness on the water vapor permeability of upper leather.*

Increments of flesh side split off. Upper leather, 22.8% grease: ◐, as received; ○, degreased. Upper leather 10.2% grease: ◑⊙, as received; ⊗, degreased.

Effect of Grease Content and Thickness on Water Vapor Permeability

The results of table 1 indicate that thickness and grease content influence water vapor permeability. A more detailed study of these factors was made. Figure 8 and table 5 show the effect of thickness on the water vapor permeability of vegetable-tanned crust and vegetable-tanned sole leathers. The curves for the two leathers are nearly parallel. Degreasing had little effect, since the grease content in these leathers was less than 5 percent. The water vapor permeability increases with decrease in thickness and is greater for crust leather than for sole leather. The differences in the water vapor permeabilities of these two types of leather can probably be explained by the differences in their densities.

In figure 9 and table 6 is shown the influence of grease and of thickness on the water vapor permeability of upper leather. The sample containing 22.8 percent of grease shows very low water vapor permeability, which does not increase with decrease in thickness. The thickness was varied by splitting successive layers off of the flesh side. Thus the results show definitely that the grain layer of this leather governs its transmission properties. After degreasing, this leather shows the same variation of water vapor permeability with thickness as was shown in figure 8. The leather containing 10.2 percent of grease was a fat-liquored type.[4] Degreasing had little effect on its permeability. The grain layer in this leather appears to influence the water vapor permeability

TABLE 5. *Effect of thickness on water vapor permeability*

(Thickness varied by removal of increments of flesh layer)

Chrome-retanned sole (as received)		Chrome-retanned sole (degreased)	
Thickness	Water vapor permeability	Thickness	Water vapor permeability
Mils	*g/25 cm² ×100 min*	*Mils*	*g/25 cm²×100 min.*
246	0.21	256	0.22
183	.32	203	.31
168	.35	161	.37
132	.38	95	.46
82	.46	77	.53
67	.55	34	.75
43	.61	23	.83
Vegetable-tanned sole (as received)		**Vegetable-tanned sole (degreased)**	
223	0.12	236	0.12
178	.18	194	.17
143	.22	160	.23
111	.29	128	.28
76	.33	92	.33
39	.48	56	.43
25	.57	22	.65
Vegetable-tanned crust (as received)		**Vegetable-tanned crust (degreased)**	
244	0.23	249	0.24
186	.34	196	.36
164	.40	162	.38
141	.46	139	.43
114	.50	95	.54
86	.56	53	.68
54	.70	24	.85
36	.83		

TABLE 6. *Effect of thickness and grease content on water vapor permeability of upper leather*

(Thickness varied by removal of increments of flesh layer)

Upper leather (1) (22.8% grease)		Upper leather (1) (degreased)	
Thickness	Water vapor permeability	Thickness	Water vapor permeability
Mils	*g/25 cm²×100 min*	*Mils*	*g/25 cm²×100 min*
85	0.03	86	0.57
76	.05	81	.55
60	.05	69	.61
40	.05	52	.68
24	.05	32	.90
		16	1.01

Upper leather (2) (10.2% grease)				Upper leather (2) (degreased)	
Sample No.		Sample No.			
1	2	1	2		
79	88	0.38	0.35	93	0.53
64	73	.38	.35	77	.55
51	58	.45	.35	61	.52
32	42	.39	.35	42	.47
9	33	.53	.35	28	.54
	21		.45	16	.61
	12		.64		

Increments of grain layer removed Upper leather (1) (22.8% grease)	
86	0.09
74	.34
64	.47
50	.54
32	.65
26	.72
*17	*.07

* Top grain layer.

[4] The addition of grease by tumbling the leather in an oil-in-water emulsion is known as fat-liquoring.

of both degreased and greased samples. This is apparently caused by the fact that the finish was sufficiently stable to resist the action of the chloroform, which was used in removing the grease. Mitton [3] and Wilson and Lines [13] have shown that the finish on the grain influences the water vapor permeability.

The variation of the water vapor permeability with thickness when increments of the grain side are removed is shown in figure 10 and table 6. The curve shows a very rapid increase in water vapor permeability with decrease in thickness. This is further proof that the grain layer of heavily greased upper leather exerts the predominating influence on the water vapor transmission.

4. Effect of Relative Humidity on Water Vapor Permeability

The dependence of water vapor permeability on relative humidity at constant temperature is shown in figure 11 and table 7. Approximately straight-line relationships are shown for each type

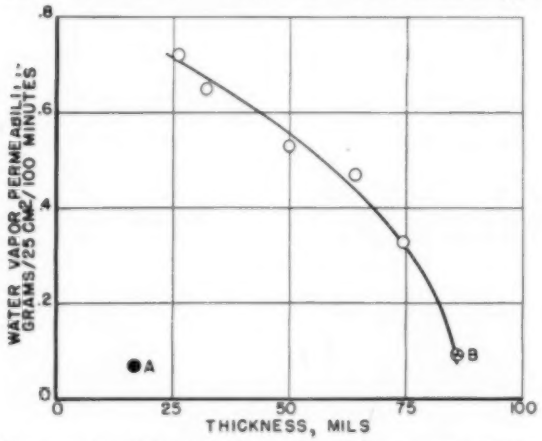

FIGURE 10. *Effect of thickness on water vapor permeability when increments of the grain side are split off.*

A, Grain split; B, full thickness; rest, flesh splits; ○, grain split off; ●, flesh split off; grain removed first.

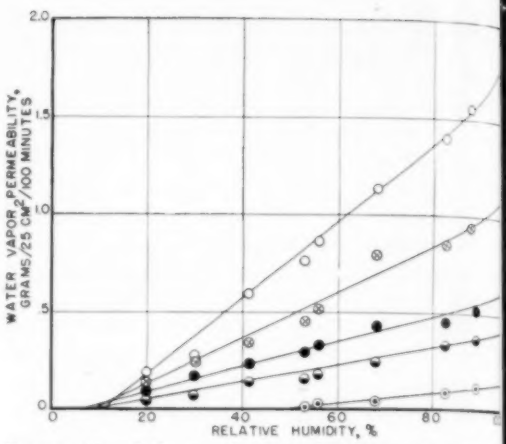

FIGURE 11. *Influence of relative humidity on water vapor permeability.*

Leather: ○, sheepskin; ⊗, sealskin; ●, sole; ◑, chrome; ⊙, Indian tanned lace.

of leather. These lines, with the exception of that for the heavily greased lace leathers, on extrapolation show zero transmission at about 10-percent relative humidity. This behavior is surprising and no definite explanation can be offered at this time. It has been shown that the heat of adsorption of water by leather is highest in atmospheres of less than 10-percent relative humidity, or when low concentrations of water are adsorbed. It is probable then that under these conditions the water is held within the leather so strongly that a steady state of transmission is not established under the conditions of the experiment. When the active sites within the leather are satisfied, which happens when higher concentrations of water are adsorbed, then the water vapor will be transmitted rapidly. These results again indicate that the leather surface has some influence on the water vapor that passes through, and therefore the mechanism must involve other factors than that of gaseous diffusion.

TABLE 7.—*Effect of relative humidity on water vapor permeability*

Water vapor permeability in g/25 cm²×100 min

Leather	Relative humidity (percent)							
	20	30	42	53	56	68	83	89
Vegetable-tanned sheepskin	0.19	0.31	0.60	0.79	0.87	1.14	1.40	1.56
Vegetable-tanned sealskin	.15	.26	.35	.45	.52	.80	.85	.94
Vegetable-tanned sole	.10	.18	.24	.29	.33	.44	.44	.51
Chrome	.05	.07	.14	.16	.19	.25	.34	.36
Indian-tanned lace	0	0	0	.01	.03	.04	.10	.11

Effect of Apparent Density on Water Vapor Permeability

Since the apparent density of leather varies inversely as the pore volume, it is expected that there might be a correlation between this factor and the water vapor permeability. In the study of the effect of apparent density, the same group of samples as shown in table 1 was used. All the leathers were degreased prior to the tests. However, they did not have uniform thicknesses, and the results are therefore modified somewhat by this factor, which was shown previously to be significant. In a study of the results, it was found that the best correlation was obtained if the water vapor permeability was plotted against the product of the thickness in centimeters and the apparent density. This is shown in figure 12, and the data are tabulated in table 8. These results suggest that the water vapor permeability is inversely proportional to the mass or density of fibers between the atmosphere of high and low relative humidity. However, a low apparent density not only is indicative of high pore volume, but also of high surface area. When the fibers are packed closely together, the leather loses not only pore volume but also surface area.

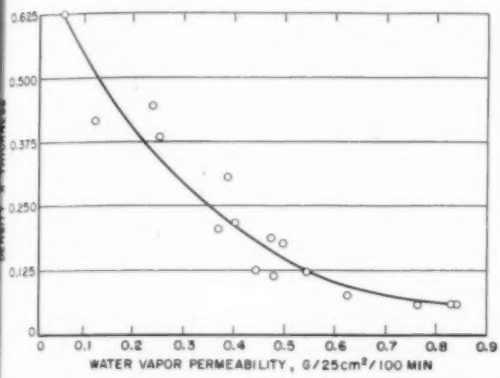

FIGURE 12. *Correlation of the water vapor permeability of leather with the product of the density and the thickness in centimeters.*

TABLE 8. *Effect of apparent density on the water vapor permeability*

Leather	Thickness	Apparent density	Density×thickness in cm	Water vapor permeability
	Mils			*g/25 cm²×100 min*
Vegetable-tanned sealskin	108	0.660	0.180	0.50
Chrome-tanned calfskin	42	.560	.061	.84
Chrome-retanned	80	.614	.124	.54
Chrome hydraulic packing	175	.704	.312	.39
Vegetable-tanned sole	199	.772	.391	.26
Indian-tanned lace	131	.666	.221	.40
Chrome-retanned	79	.639	.127	.45
Rawhide lace	122	.616	.191	.47
Vegetable-tanned strap	104	.789	.208	.37
Alum-formaldehyde	45	.696	.079	.63
Chrome-retanned	79	.574	.114	.48
Vegetable-tanned sole	184	.906	.424	.12
Vegetable-tanned calfskin	37	.649	.051	.83
Van Tassel chrome-retanned sole	242	.738	.452	.24
Vegetable-tanned sole	246	1.022	.638	.06
Vegetable-tanned sheepskin	47	.502	.061	.78

6. Effect of Temperature on Water-Vapor Permeability

Since the kinetic energy of the water molecules increases with increase in temperature, it might be expected that the water-vapor permeability should also increase. In these tests duplicate specimens of different types of leather were used as received. Tests were made at 30° and 45° C at three different relative humidities for each temperature. These results are given in table 9 and figure 13. In figure 13 the logarithm of the permeability is plotted against the logarithm of the vapor pressure. These parameters were chosen because their relation can be shown fairly well by a straight line. The numbers at the ends of the curves signify the leather specimens. The curves show the variation of the log of the permeability with the log of the vapor pressure for each temperature. The unfilled dots are for 30° C, whereas the filled dots are for 45° C. All points except that for one specimen at the lowest

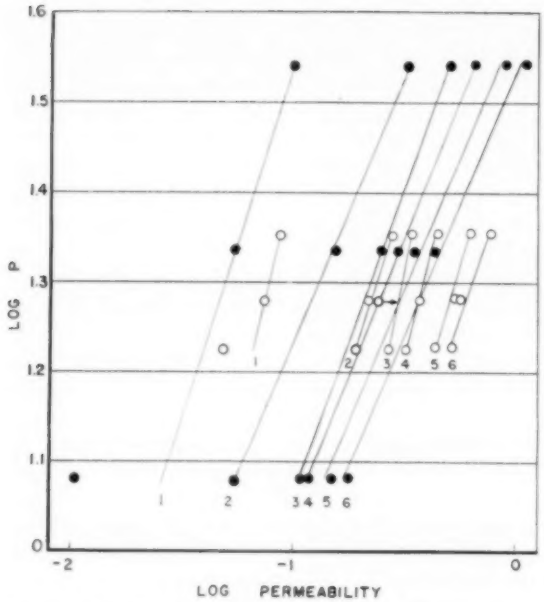

FIGURE 13. *Influence of temperature on water vapor permeability.*

Relation between the logarithm of the vapor pressure and the logarithm of the permeability. Determinations made at 30° C, ○; at 45° C, ● ⊙.

TABLE 9. *Effect of temperature on water-vapor permeability*

(Water-vapor permeability expressed in g/25 cm²×100 min)

Temperature	30° C			45° C		
Relative humidity, percent	54	61	72	17	31	49
Chrome-hydraulic packing	0.05	0.07	0.09	0.01	0.05	0.10
Chrome-retanned sole	.19	.22	.28	.05	.16	.32
Vegetable-tanned strap	.27	.24	.34	.11	.25	.50
Retanned upper (degreased)	.32	.37	.45	.12	.30	.64
Alum-formaldehyde	.44	.54	.62	.15	.34	.91
Vegetable-tanned sheepskin	.52	.55	.77	18	.43	1.11

relative humidity at both 30° and 45° C show fairly good straight-line relationships.

The results indicate that at the same vapor pressure the permeability is less at 45° than at 30° C. The relation of temperature and relative humidity to permeability is often confused. This is because for equal relative humidities the vapor pressure is much greater at the higher temperature, and the absolute humidity or total moisture content must be considered. Therefore the statement is often made that the permeability increases with temperature. Bradley, McKay, and Worswick [1] have stated that the water vapor permeability increases 6.5 percent for each degree rise in temperature. This occurs probably under conditions of constant relative humidity.

Work on the adsorption of water vapor by leather and collagen has shown that at the same vapor pressure the adsorption decreases with increase in temperature [14]. This indicates, therefore, that the permeability may be influenced by the amount adsorbed or by the ease with which the water makes contact with the leather surface. Work on plastic films [9, 10] has shown that permeability increases with temperature. This work was also done at constant relative humidity rather than constant vapor pressure. The plastic films, however, do not adsorb appreciable amounts of water, and it is probable that the mechanism of penetration of these two types of materials is different.

According to the activated diffusion mechanism postulated for water vapor transmission, a certain amount of energy is required to free adsorbed or bound water from an active site before it can go on to the next one. This energy is analogous to heat of vaporization and is often called "energy of activation for permeation." A value for this energy of activation for leather can be evaluated from the data in figure 13. For equal permeability values at the two temperatures, the logarithm of the vapor pressure difference is read off corresponding to each temperature, and the values substituted in the Clausius-Clapeyron equation

$$\Delta H = 2.303R \frac{\log P_2 - \log P_1}{\frac{1}{T_1} - \frac{1}{T_2}}.$$

Log P_1 was taken at 1.3 on each of the 30° C lines. The corresponding value of P_2 in each case was found by going vertically upward to the intersection with the 45° C line for the same sample of leather.

The average value obtained from the six curves in figure 11 was 3,575 calories/mole. That there is an energy of activation for permeation is further evidence that the water vapor permeability of leather is not solely gaseous diffusion, but involves also some form of "activated diffusion" or surface conduction.

7. Effect of Type of Impregnant on Water Vapor Permeability

In an application of the hypothesis that water is transmitted more rapidly over a polar than a nonpolar medium, experiments were made in

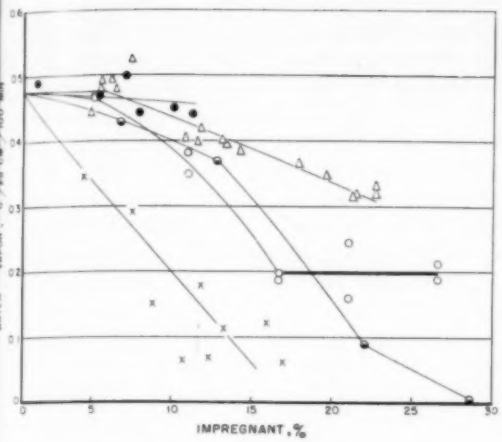

FIGURE 14. *Effect of various leather impregnants on the water vapor permeability.*

●, sulfonated oil; △, acrylate resins; ◑, solvent stuffing; ○, rubber; ×, wet stuffing.

which degreased chrome-retanned upper leather was treated with various types of impregnants. These impregnants included sulfonated oils, stuffing greases, rubber, and acrylate resins. The stuffing greases were added in two ways: (1) by the customary procedure, which is by wetting the leather and then applying the molten greases to the surface, and (2) by using a solvent. The solvent method was used principally so that a legitimate comparison could be made between the grease and the rubber and the resins, the last two of which were added in a solvent. The addition of a small amount of the stuffing grease by the usual procedure cannot be done uniformly, and considerable variation was obtained, as is indicated by the results that are given in table 10 and plotted in figure 14. The stuffing mixture used was obtained from a manufacturer of upper leather and consisted of petroleum wax, moellen, and fatty oils and greases.

TABLE 10. *Water vapor permeability of leathers treated with various types of impregnants*

(Water vapor permeability in g/25 cm²×100 min)

Stuffing grease				Sulfonated oil	
Customary procedure		Solvent method			
Grease in leather	Water vapor permeability	Grease in leather	Water vapor permeability	Grease in leather	Water vapor permeability
Percent	*g/25 cm²×100 min*	*Percent*	*g/25 cm²×100 min*	*Percent*	*g/25 cm²×100 min*
Blank	0.48	Blank	0.48	Blank	0.48
4.4	.35	6.8	.44	1.1	.49
7.5	.29	12.8	.37	5.3	.47
8.8	.15	22.0	.09	7.1	.50
10.7	.07	28.6	.01	7.9	.44
11.8	.18			10.1	.45
12.3	.07			11.3	.44
13.2	.11	Acrylate resins			
15.9	.12			Rubber	
16.9	.06	Blank	0.48		
		4.9	.44		
		5.5	.48	Blank	0.48
		5.6	.49	5.2	.46
		6.2	.49	5.2	.47
		6.5	.48	11.0	.38
		7.5	.53	11.0	.35
		10.8	.41	16.6	.19
		11.6	.40	16.6	.20
		11.8	.42	20.9	.24
		13.1	.40	20.9	.16
		13.4	.40	26.5	.22
		14.2	.38	26.5	.19
		17.9	.37		
		19.6	.35		
		21.3	.31		
		21.5	.32		
		22.7	.32		
		22.7	.33		

As shown in this figure, the stuffing procedure forms a film over the surface of the leather, and a nearly impermeable membrane is formed for low concentrations of grease. This is also shown in figure 9. The stuffing grease added by means of a solvent shows a less rapid decrease in water vapor permeability with increasing grease content, probably because a more uniform distribution of the grease is obtained. The leathers treated with rubber show less decrease in water vapor permeability than the stuffing greases. Sulfonated oil shows very little effect on the water vapor permeability, and the acrylate resins appear to maintain fairly high rates of transmission. These results are in agreement with the hypothesis that polar groups influence the water vapor permeability, since both sulfonated oils and the acrylates contain these types of groups. Rubber also maintains fairly high permeability in leather. This might be explained by assuming that it enters and fills only the larger pores, the smaller pores remaining intact for the transmission of water vapor. The latter hypothesis might be applied to all types of resinous materials. Thus it might be assumed that these particles can enter only those pores that are above a definite range in size. This hypothesis can be further studied by making experiments with polymers with varying molecular weight ranges.

8. Effect of Gross Air Pressure and Flexing on Water Vapor Permeability

In order to perform some tests that would approach more nearly the conditions to which shoes are subjected in actual service, a method of measuring the water vapor permeability of leather during flexing was developed. A sketch of the equipment is shown in figure 15. The principle of dynamic gas streams used by Edwards [2] and by Maeser [5] was applied. The apparatus consists of two chambers separated by a diaphragm of the leather under test. The conditions of relative humidity and pressure in each chamber may be varied as desired. The amount of moisture that penetrates the leather is determined by the pickup in the dry gas stream, the moisture being removed from this stream after it leaves the chamber by passing it through a tube containing a drying agent. The leather specimen may be flexed as a diaphragm, to simulate the flexing of a shoe vamp in walking. The flexing is done by a rod fastened to the center of the specimen and connected by an adjustable cam to a variable speed transmission. Any speed up to 220 rpm with any stroke up to 1.5 in. may be attained. Tests may also be made with the leather diaphragm under static conditions (no flexing).

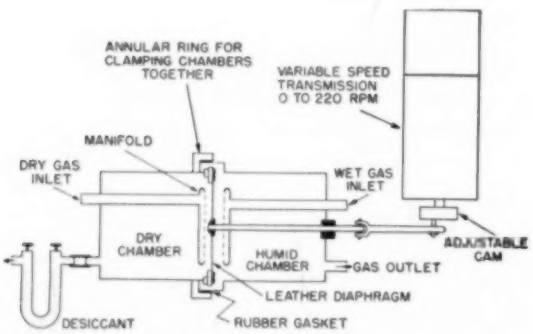

FIGURE 15. *Sketch of the equipment used to determine water vapor permeability under dynamic conditions.*

The results obtained with the dynamic equipment on degreased upper leather are shown in figure 16, where the water vapor permeability is plotted against the difference in pressure of air between the two chambers in centimeters of diamyl phthalate (approximately g/cm.^{2}). The dry air was passed through one chamber at the rate of 2.0 ft^3/hr, whereas air saturated with water vapor at 73° F was passed through the other chamber at different rates to give the differences in pressures of air shown in the figure. Since it was difficult to obtain exactly equal pressures on both sides to give a zero difference, tests were made varying the pressure from a high on one side to a high on the other. The point where the curve crosses the zero pressure line is equivalent to the water vapor permeability at zero air

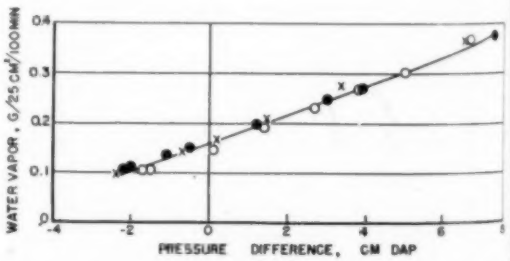

FIGURE 16. *Influence of flexing on the water vapor permeability of degreased upper leather.*

●, Static, before flex; ○, static, after flex; ×, flexing.

pressure difference. The negative pressure given on the graph is indicative of highest pressure on the side through which dry air was passed. The flexing in these experiments was done at a rate of 60/min, and the stroke was $\frac{3}{8}$ in.

According to the graph, the water vapor permeability of the degreased leather is the same whether or not the specimen is flexed. The slope of the curve indicating the rate of water vapor transmission with difference in air pressure is the same whether the pressure is high on the dry or moist chambers. This appears to indicate that some of the moisture passes through independently of the air stream and even counter to it. If the moisture moved entirely within the air stream, zero water vapor permeability would be expected at zero pressure. It might be expected that the value for the water vapor permeability at the point where the curve crosses zero pressure is that normally obtained by the difference in concentration of water vapor. The slope of the curve would then be caused by the moisture that passes through the pores of the leather in the air stream. However, the slope of the curve above zero pressure is slightly greater than that which can be accounted for by the moisture content of the air. It is therefore probable that the moisture is adsorbed by the leather and is conducted over its surface more rapidly than if it were carried along with the air stream. The increase in transmission with increase in pressure must be partially caused by increased adsorption of moisture by the leather.

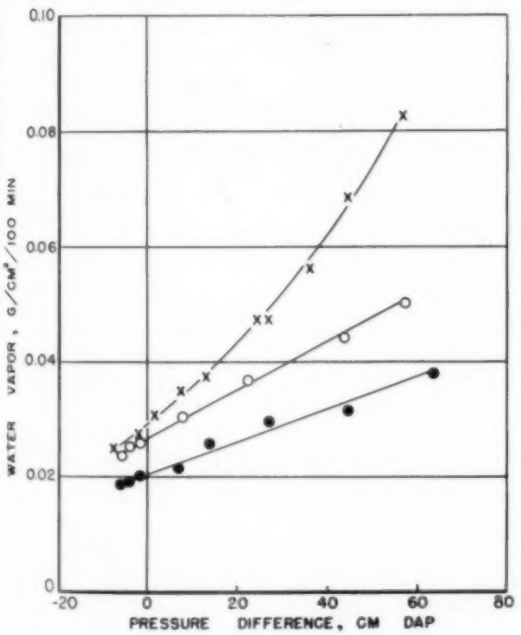

FIGURE 17. *Influence of flexing on the water vapor permeability of upper leather containing a high percentage of grease.*

●, Static, before flex; ○, static, after flex; ×, flexing.

The influence of flexing on the water vapor permeability of upper leather containing grease is shown in figure 17. These experiments were performed by the same procedure as that for the degreased leather. The results show that the water vapor permeability under static conditions after flexing is increased, and the permeability during flexing is substantially increased. In the discussion of figure 5, it was shown that the barrier offering the main resistance to the passing of water vapor for the highly greased upper leather was the thin top grain split. Flexing would undoubtedly break this impermeable film, and after flexing, its permeability to water vapor should be increased as is shown. The further increase in water vapor permeability shown during flexing is probably caused by a wider opening of this film, allowing the moisture to pass on through in the air stream. The difference between the rate of the water vapor permeability at zero air pressure for the flexed leather and that obtained on increasing the air pressure is equal to the amount present in the air stream that passes through the leather. The explanation for the difference in behavior in this respect between the degreased and the greased leather is the lower adsorbing power of the latter.

The fact that the water vapor permeability of heavily greased leather increases on flexing has an important practical significance. The percentage of the total area of the upper of a shoe that is flexed to any extent is probably about 50 percent, so that the increase in total water vapor permeability might be significant. The water vapor permeability increases further on flexing with increase in pressure. There is undoubtedly some increase in pressure in a shoe on walking; however, the amount is not known.

V. Conclusion

The results of the experiments indicate that in addition to gaseous diffusion, water is transmitted

through leather by conduction over the surface or by some form of activiated diffusion. The evidence for the conduction mechanism has been pointed out briefly within the paper. This evidence consists of the behavior at low relative humidities, existence of energy of activation, influence of temperature, comparison of air permeability and water vapor permeability, experiments with fabrics and glass disks, variations of diffusion constants, and studies of the effect of gaseous air pressure with the dynamic equipment.

The behavior at low relative humidity shows the influence of strong adsorption forces that appear to hold the water within the leather so that a definite pressure head seems to be required to force it through. The effect of temperature on water vapor permeability also shows the influence of the surface. At a higher temperature the water molecules have a greater kinetic energy so that the diffusion forces are greater; however, for the same vapor pressure, the permeability is actually lower, which is in line with the fact that the adsorption of moisture is decreased as the temperature is increased. Here again is shown the influence of the surface properties.

The fact that water vapor passes through glass disks having small pores at a greater rate than through those having larger pores can be explained only by the fact that the smaller pores are associated with greater surface areas. Likewise the variation of the diffusion constants with the thickness of the materials and with relative humidity gradient shows the influence of the material itself on the permeability. These results indicate the greater activity of the highly polar glass, leather, and cotton surfaces as compared to the less polar nylon surface. The influence of polarity is also shown in the studies of the effects of different impregnants.

Studies of the effect of gross air pressure in the dynamic equipment indicate that the water vapor permeability is not dependent on the air permeability and may proceed counter to it. The variation of water vapor permeability with apparent density is believed to magnify the importance of diffusion; since the surface area will also increase with decrease in apparent density, and this may be the reason for the increased permeability under these conditions. As a result of these studies, it appears that activated diffusion is an important mechanism in the transference of water vapor through leather.

As stated in the introduction, the purpose of this work was to study the mechanism of water vapor permeability and to develop a test method. It would be well to follow this with a study of the comfort and health of the foot as influenced by water vapor permeability. A study of this property as influenced by special treatments and by the use of a variety of materials might lead to the development of a more comfortable and more serviceable shoe and would be extremely valuable to the Armed Services.

VI. References

[1] H. Bradley, A. T. McKay, and B. Worswick, J. Int. Soc. Leather Trades Chem. **13,** 87 (1929).

[2] R. S. Edwards, J. Int. Soc. Leather Trades Chem. **16,** 439 (1932).

[3] R. G. Mitton, J. Int. Soc. Leather Trades Chem. **31,** 44 (1947).

[4] R. B. Hobbs, J. Am. Leather Chem. Assoc. **36,** 346 (1941).

[5] M. Maeser. Report submitted to OQMG.

[6] The Institute of Paper Chemistry. Instrumentation Studies **44, 49, 50, 51, 52, 53,** and **54.**

[7] Frederick T. Carson and Vernon Worthington, NBS Circular C453 (1946).

[8] G. M. Kline, J. Research NBS **18,** 235 (1937) RP974.

[9] Paul M. Doty, Captain Wm. H. Aiken, and Hermann Mark, Ind. and Eng. Chem. Anal. Ed. **16,** 686 (1944).

[10] Paul M. Doty, W. H. Aiken, and H. Mark, Ind. and Eng. Chem. **38,** 788 (1946).

[11] Lyman Fourt and Milton Harris, Textile Research J. **17,** 256 (1947).

[12] The American Leather Chemists Assoc. Methods of sampling and analysis, Section E, physical testing of leather.

[13] J. A. Wilson and G. O. Lines, Ind. Eng. Chem. **17,** 570 (1925).

[14] J. R. Kanagy, J. Research NBS **44,** 31 (1950) RP2056; J. Am. Leather Chem. Assoc. **45,** 12 (1950).

[15] F. T. Carson and Vernon Worthington, J. Research NBS **26,** 467 (1941) RP1390.

[16] Herbert F. Schiefer and Paul M. Boyland, J. Research NBS **28,** 637 (1942) RP1471.

[17] F. A. Paine, The permeability of organic membranes to gases and vapours (The Printing and Allied Trades Research Association, Charterhouse Chambers, Charterhouse Square, London, E. C. 1, April 1949).

[18] R. S. Bear, J. Am. Chem. Soc. **64,** 727 (1942); **66,** 1297 (1944).

WASHINGTON, November 3, 1949.

U. S. Department of Commerce
National Bureau of Standards

Research Paper RP2083
Volume 44, April 1950

Part of the Journal of Research of the National Bureau of Standards

Reduction of Halomethanes with Lithium Aluminum Hydride

By Vernon H. Dibeler

A study has been made of the reactions of lithium aluminum hydride with methyl bromide, methylene chloride, methylene bromide, methylene iodide, chloroform, bromoform, and carbon tetrachloride. Except for hydrogen and unreacted halide, essentially pure methane was formed in each case. The amount of hydrogen evolved increased with the number of halogen atoms in the molecule, reaching a maximum in the reduction of carbon tetrachloride. This fact, together with the absence of hydrocarbons heavier than methane, indicates that the reaction proceeds by a step-wise process rather than a simultaneous stripping of several halogen atoms from the molecule.

I. Introduction

The discovery of lithium aluminum hydride and its effectiveness as a reducing agent [1] [1] has been followed by its application to the reduction of a wide variety of organic compounds including alkyl and allyl halides, nitriles, aromatic nitro compounds, azoxy compounds, aldimines, epoxides amides, carboxylic acids, aldehydes, ketones, esters, acid chlorides and anhydrides [2, 3, 4]. The reagent has also been used to determine active hydrogen [5]. It does not attack olefinic double bonds; and consequently, has been used to demonstrate the structures of the stereoisomers of 1,3-dichloropropene [6]. It is also reported to reduce anthracene and phenanthrene [7].

In general, reactions that proceed smoothly with lithium aluminum hydride are also those that can be carried out readily with Grignard reagents. An example is the reduction of alkyl halides recently studied by Johnson, Blizzard, and Carhart [3]. These experiments were limited to monohalides with the exception of 1,2-dibromooctane, which in addition to *n*-octane, gave 14-percent unidentified olefin calculated as octene.

Apparent exceptions to the analogy of lithium aluminum hydride and the Grignard reagent have previously been ascribed to differences in the degree of reactivity rather than mode of reaction. This paper reports the reduction of a number of halomethanes containing one to four halogen atoms; i. e., methyl bromide, methylene chloride, methylene bromide, methylene iodide, chloroform, bromoform, and carbon tetrachloride. The results show that lithium aluminum hydride is able to react with compounds known to be inert toward the Grignard reagent; viz, the more highly halogenated methanes. Since the experiments were in the nature of a survey, no attempt was made to obtain maximum yields of any of the products.

II. Experimental Method

A diagram of the apparatus used in the preparations is given in figure 1. A 250-ml distilling flask (*D*) was connected to a condenser (*E*) by a standard tapered joint. The condenser was provided with connections to a vacuum system, an open-end manometer (*F*), a trap (*G*), and a Toepler pump (*H*). The latter was used to pump reaction products into sample bulbs attached to the standard tapered joint (*I*). The halides were introduced into the reaction flask at *C* either by distillation from a break-seal tube (*A*) or drop-wise from a dropping funnel (*B*). Standard precautionary techniques used in Grignard reactions were applied throughout. The following description of the reduction of methylene bromide serves to illustrate the method. Approximately 0.5 g (13 millimoles)

[1] Figures in brackets indicate the literature references at the end of this paper.

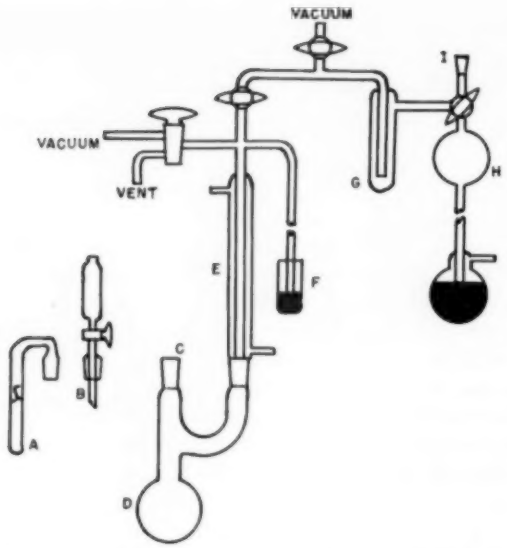

FIGURE 1. *Apparatus for the reduction of halomethanes.*

of powdered (under dry nitrogen) lithium aluminum hydride and 50 ml of anhydrous dibutyl ether were introduced into the reaction flask. A break-seal tube containing 1.7 g (10 millimoles) of methylene bromide in vacuum was attached to the flask. The flask was cooled to 0° C and cautiously evacuated to degas the mixture. The flask, condenser, and manometer were isolated from the rest of the system and the flask slowly warmed to 60° C and held at that temperature for about 3 hrs. Under these conditions gentle refluxing occurred sufficient to stir the mixture. The solution plus some insoluble material was cooled with liquid nitrogen, the flask was thoroughly evacuated and isolated from the pumps. The break-seal tube was opened and the halide condensed onto the frozen ether solution. The flask was allowed to warm slowly until a moderate reaction occurred at about the melting point of the halide. The flask was intermittently cooled to maintain moderate reaction if necessary. When no further rise in pressure was indicated on the manometer, the flask was surrounded with an ice bath at 0° C. After thermal equilibrium was attained, the pressure of the evolved gases was measured as the difference between the initial and final readings of the manometer. A sample of the product for mass spectrometric analysis was withdrawn by the Toepler pump through the cold trap at 0° C.

The haloforms and carbon tetrachloride were reduced in a similar manner, except that portions of these compounds were mixed with ether and added drop-wise to the gently refluxing hydride solution at 60° C.

Dibutyl ether and the halides were laboratory-grade chemicals and were used without purification except for drying. The ether was refluxed for several hours over molten sodium and distilled off. The liquid halides stood for several days over calcium sulfate with occasional shaking. Required samples were removed by pipet through a porous plug. The methyl bromide was not dried.

Mass spectrometric analyses were made with a Consolidated model 21–102 mass spectrometer using conventional procedures [8].

III. Results

The experimental results are summarized in table 1. The halomethanes are listed in the first column. Column two gives the nominal temperature at which reduction occurred. Column three gives the ratio of the number of moles of hydride to the number of moles of halide used in the reaction. Column four gives the ratio of the mole percentage of methane to the mole percentage of hydrogen in the evolved gases. Column five gives the percentage yield of methane computed from the halide.

TABLE 1. *Summary of experimental results for the reduction of several halomethanes by lithium aluminum hydride*

Halide	Nominal temperature of reduction	$LiAlH_4$/halide (molar ratio)	CH_4/H_2 (Ratio of mole %)	Yield
	°C			%
CH_3Br	Below −80	1.0	99	98
CH_2Cl_2	−80	1.1	19	81
CH_2Br_2	−50	1.3	13	93
CH_2I_2	10	1.0	7.3	85
$CHCl_3$	60	1.6	1.2	52
$CHBr_3$	60	1.5	1.1	60
CCl_4	60	2.0	0.87	36

Except for hydrogen and unreacted halide, mass spectrometric analysis showed that essentially methane was obtained from each halide. The amount of hydrogen produced during the reduction of methyl bromide was less than 1 per-

cent of the total gas evolved. As shown in table 1, however, a striking increase in the amount of evolved hydrogen was observed in the reduction of the heavier halides. Some hydrogen was due to water remaining after the halides were dried with calcium sulfate; however, this must be small. It also appears that the over-all yields of methane decrease as the amount of hydrogen increases. The mode of formation of the hydrogen will be considered further in connection with a study with lithium aluminum deuteride.

No hydrocarbons other than methane with appreciable vapor pressures at 0° C were observed in any of the products. A small amount of nitrogen retained in the reaction mixture was sometimes evolved with the methane. Since, in the mass spectrum, the most sensitive peak ($m/e=28$) of both ethylene and ethane coincides with the molecule ion of nitrogen, the low limit of detection of these hydrocarbons was somewhat higher than under ideal conditions. It is estimated, however, that less than 0.1 percent of either compound was formed in any case. Other hydrocarbons were estimated as less than 0.03 percent.

V. Discussion

The prior observations that lithium aluminum hydride can be used to replace the halide of monoalkyl halides with hydrogen has been extended in this paper to show that treatment of halomethanes containing two to four halogen atoms likewise gives methane but in smaller yields. Better yields were obtained with di- and tribromomethane and diiodomethane than with the corresponding chloromethanes. With the mono- and dihalogenated methanes, reactions proceeded smoothly at about the melting point of the halide. At room temperature the reaction with the haloforms was slow, and in the case of carbon tetrachloride, little methane was obtained. Accordingly, these reactions were accomplished at higher temperatures.

It is of considerable interest that no hydrocarbons other than methane were detected in any of the reactions. This would indicate that the reduction is a step-wise process, since the simultaneous stripping off of several halogen atoms would greatly increase the probability of coupling to form unsaturated and saturated molecules. It seems equally certain that the reaction does not proceed by a free radical mechanism.

The ability of lithium aluminum hydride to reduce polyhalogenated hydrocarbons as demonstrated above, together with its previously reported effectiveness in reducing monoalkyl halides without attacking olefinic double bonds, indicate that the hydride offers an attractive method for the preparation of a wide variety of deuterium-substituted compounds, both saturated and unsaturated. Some preliminary work in this laboratory using lithium aluminum deuteride shows that the halomethanes are similarly reduced to give the expected deuterated molecules. However, reactions are somewhat slower and require the utmost in care for high isotopic purity. Further work is in progress and will be described in a later report.

V. References

[1] A. E. Finholt, A. C. Bond, Jr., and H. I. Schlesinger, J. Am. Chem. Soc. **69,** 1199 (1947).

[2] R. F. Nystrom and W. G. Brown, J. Am. Chem. Soc. **69,** 1197, 2548 (1947).

[3] J. E. Johnson, R. H. Blizzard, and H. W. Carhart, J. Am. Chem. Soc. **70,** 3664 (1948).

[4] R. F. Nystrom and W. G. Brown, J. Am. Chem. Soc. **70,** 3738 (1948).

[5] J. A. Krynitsky, J. E. Johnson, and H. W. Carhart, J. Am. Chem. Soc. **70,** 486 (1948).

[6] L. F. Hatch and R. H. Perry, Jr., J. Am. Chem. Soc **71,** 3262 (1949).

[7] J. R. Sampey and J. M. Cox, J. Am. Chem. Soc. **71,** 1507 (1949).

[8] For a review of recent publications on mass spectrometric techniques, see: J. A. Hipple and M. Shepherd, Anal. Chem. **21,** 32 (1949).

Washington, January 9, 1950.

U. S. Department of Commerce
National Bureau of Standards

Research Paper RP2084
Volume 44, April 1950

Part of the Journal of Research of the National Bureau of Standards

Crystallization and Second-Order Transitions in Silicone Rubbers[1]

By C. E. Weir, W. H. Leser, and L. A. Wood

In the course of an investigation to determine which rubbers might be suitable for use at low temperatures, interferometric measurements of the length-temperature relationships of silicone rubbers have been made. Crystallization was found between −60° and −67° C in Dow-Corning Silastic X–6160 and in General Electric 9979G silicone rubber, the latter of which contains no filler. Crystallization between −75° and −85° C was found in Silastic 250. Melting occurred over a range of temperature above the temperature of crystallization. The volume change on crystallization varied from 2.0 to 7.8 percent. No crystallization or melting phenomena were observed in Silastic X–6073 between −180° and +100° C. All types of silicone rubber exhibited a second-order transition at about −123° C, the lowest temperature at which such a transition has been observed in a polymer. The coefficient of linear thermal expansion of silicone rubbers containing no filler was found to be about 40×10^{-5}/deg C between −35° and 0° C.

I. Introduction

Most of the properties of the silicone rubbers (polysiloxanes), developed especially for use at high temperatures, have been found to show less change with temperature than those of other polymers [1, 6].[2] Recently there has been particular interest in the properties of all types of rubbers at low temperatures. Consequently the behavior of the silicone rubbers at low temperatures has taken on additional importance.

The fundamental phenomena related to the stiffening of rubbers at low temperatures are the second-order transition [4] and crystallization [8]. Both of these phenomena influence the relationship between the dimensions of a specimen and the temperature. In the present investigation the change of length at different temperatures was measured with an interferometer.

II. Materials Investigated

The samples of silicone rubber were of commercial origin. Two of them contained no fillers or vulcanizing agents and were highly elastic brown solids of low strength. They transmitted light relatively well and had refractive indices of 1.4028 and 1.4040, respectively. The densities measured by the method of hydrostatic weighing were found to be 0.973 and 0.974 g/cm^3 at 25° C, respectively. These densities appear to be slightly higher than densities of liquid silicones previously reported [2,5]. These samples were produced by the General Electric Co. and were supplied through the kind cooperation of the Connecticut Hard Rubber Co. They are designated General Electric 9979G silicone rubber and in this paper are referred to as gum silicones for convenience.

The other samples of silicone rubber contained filler and were vulcanized. These were obtained through the cooperation of the Dow-Corning Co. and were designated Silastic X–6073 and Silastic X–6160. These types were especially designed for use at low temperatures. Silastic X–6160 is described as differing only slightly from Silastic 160, which has been reported [6] to contain 60 percent of filler consisting of equal weights of zinc oxide and titanium dioxide. No data are available on the other varieties of Silastic.

A vulcanizate of Silastic 250, a new variety of silicone rubber, was also furnished by the Dow-Corning Co.

[1] The work reported here was supported by the Office of Naval Research and the Office of The Quartermaster General as part of Project ONR (QMC) NR-053-314.

[2] Figures in brackets indicate the literature references at the end of this paper.

III. Experimental Method

The interferometer arrangement described by Wood, Bekkedahl, and Peters [10] was used, with minor modifications, to determine the thickness of rubber specimens as a function of temperature. The apparatus was modified by surrounding the lower removable portion of the interferometer container with close-wound, close-fitting helix of ⅛-in. copper tubing. The lower end of the helix was terminated in a wye, one leg of which was terminated in a fine orifice. The other leg of the wye passed through the wall of the container and was terminated in a somewhat larger orifice. Dry carbon-dioxide-free air was used to eliminate clogging of lines by freezing of vapors. This air flowed into the upper end of the helix at a pressure of 1 cm of mercury, circulated through the coil, and was discharged into both the surrounding Dewar and the interferometer chamber. Internal and external stirring and a markedly lower temperature gradient resulted from the use of this air stream. After the air had passed through the interferometer chamber it was discharged across the top glass plate of the container, thereby effectively eliminating condensation of moisture on this plate. Liquid nitrogen, used as a coolant, produced temperatures as low as −196° C. The cooling was effected in a manner similar to that described previously [10].

The light source consisted of a helium discharge tube. Essentially monochromatic light of wavelength 5,876 A was obtained by use of appropriate filters.

The top interferometer plate, a semicircular disk of fused quartz 2 cm in diameter and 2 mm thick, which was supported by the test specimens, weighed 0.82 g.

No correction for change in refractive index of air with temperature was applied to the data obtained.

Slabs of silicone rubber were accurately cut with parallel faces by means of a sharp blade and a small miter box. One to three specimens, generally 4-mm cubes, cut from a slab were placed between the two interferometer plates with the parallel faces of the specimens in contact with the plates. After removing the eyepiece of the telescope, the elastic specimens were moved about between the interferometer plates until the images of the slit reflected from the upper and lower plates appeared to coincide. Fringes of the desired width were clearly visible when the eyepiece of the telescope was replaced.

Measurements below temperatures at which rubbers crystallized presented two main difficulties: maintaining visible fringes during the dimensional changes occurring on freezing; and maintaining a uniform rate of cooling at low temperatures.

Attempts were made to obtain fringes with crystalline material by cooling the specimens by immersion in liquid nitrogen and then manipulating the frozen specimens with suitable prods so as to produce fringes. These attempts were unsuccessful principally because of frosting of all exposed surfaces, and therefore measurements were made below −100° C only in a few fortuitous experiments in which fringes were maintained during crystallization.

Measurements of expansion were found to be difficult to obtain on cooling at very low temperatures, since the height of the liquid nitrogen in the surrounding Dewar was necessarily such that intermittent contact occurred between the coolant and the exterior of the interferometer container. Such contact produced rapid and nonuniform cooling. A rate of cooling or heating of about 1 deg C per minute was considered desirable in these experiments [10]. Most measurements at low temperatures were made on heating and were carried out by cooling the interferometer to −196° C, insulating the system, and permitting it to warm by absorption of heat from the surroundings.

IV. Results and Discussion

Graphical results shown in the succeeding figures are typical but do not include measurements on all specimens of silicone rubber investigated. In most instances only those portions of the curves are shown that are considered pertinent to the discussion.

Crystallization on cooling to low temperatures, manifested as a radical decrease in specimen length on cooling over a narrow temperature interval, was observed in all samples except Silastic X–6073. Melting, observed as the reverse process on heating, was found above the crystallization temperature in all samples except X–6073.

Expansion curves on cooling and heating a gum silicone are shown in figure 1. Crystallization is believed to occur between −60° and −67° C.

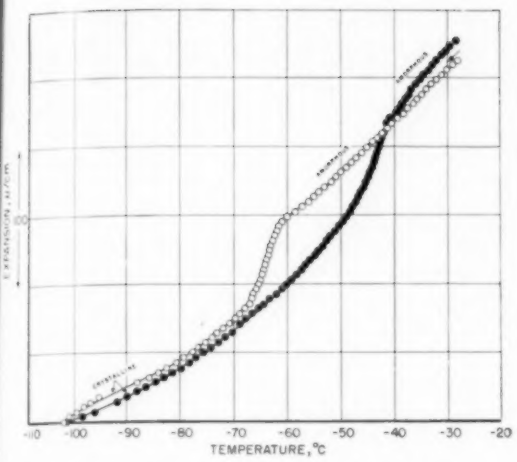

FIGURE 1. *Crystallization and melting of gum silicone.*

Average thickness at 20° C, 0.414 cm. Values for expansion are calculated in terms of the thickness at 20° C. ○, Observations on cooling; ●, observations on heating.

This temperature range of crystallization was found in the gum silicones and Silastic X–6160 (fig. 5). Results obtained with Silastics X–6073 and 250 are somewhat different and will be described in detail later. The crystallization depicted by figure 1 appears to be a rapid process in contrast to the crystallization of natural rubber studied by Bekkedahl and Wood [3, 9]. Attempts to vary the temperature at which crystallization occurred or to produce supercooled material by rapidly chilling the interferometer in a liquid nitrogen bath were not successful, as specimens invariably crystallized near −60° C. The values for hardness of several varieties of Silastic at temperatures as low as −62° C are reported by Konkle, Selfridge, and Servais [6]. All of the values show a rapid rise at the lowest temperature measured. They found that the equilibrium hardness values at temperatures below −55° C were not attained until after 3½ hrs. Both of these observations are indicative of the crystallization reported in the present paper.

The onset of melting with increasing temperature is not sharp. It is believed that melting begins a few degrees above the crystallization temperature and is complete at about −39° C.

The magnitude of the volume change associated with crystallization of gum silicones appears to be variable and as calculated from linear changes ranges from 2.0 to 7.8 percent. The maximum volume change on crystallization of natural rubber has been found to be slightly over 3 percent [8].

If specimens of gum silicone are alternately cooled and heated cyclically at temperatures somewhat above −60° C, no evidence of crystallization or melting is observed. Experiments of this nature, carried out between −30° and −50° C gave the results shown in figure 2. If crystallization occurred at a measurable rate in this temperature interval, the length of the specimen would gradually decrease as a function of time. Consequently, the expansion curves on successive heating or cooling would be displaced in the direction corresponding to a smaller length of specimen. The behavior of the gum silicones is in contrast to that of natural rubber, which undergoes slow crystallization at temperatures higher than the optimum crystallization temperature [8, 9].

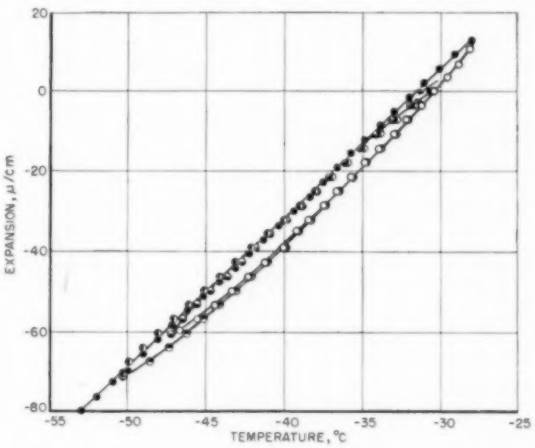

FIGURE 2. *Behavior of gum silicone above the crystallization temperature.*

Average thickness of 20° C, 0.414 cm. Values for expansion are calculated in terms of the thickness at 20° C. ◐, Observations on first cooling; ◓, observations on first heating; ◒, observations on second cooling; ○, observations on second heating; ●, observations on third cooling.

The results of expansion measurements of the gum silicones at temperatures far below the crystallization temperature are shown in figure 3. The second-order transition temperature is located as the point of change of slope and is fairly well defined in all curves. The temperatures of the transitions, defined as the intersections of the extrapolated linear segments, are in good agreement on repeated runs. Curvature near the transition temperature produces obvious difficulties in draw-

ing the linear segments. Differences as large as 5° C in transition temperatures as indicated by intersections of projected linear segments have been observed between the curves obtained by heating and cooling at the rate of 1° C per minute. From consideration of these factors it appears that the second-order transition of silicone rubbers may be set at −123° C with a maximum estimated uncertainty of ±5° C. As far as can be ascertained, this represents the lowest second-order transition temperature yet reported for any polymer.

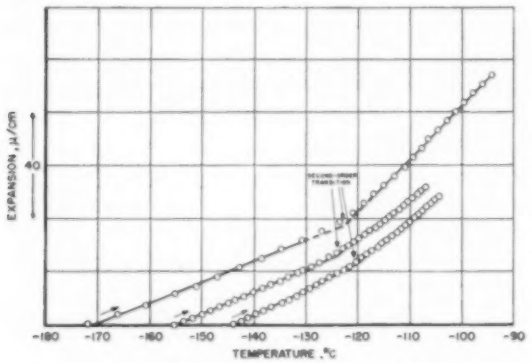

FIGURE 3. *Second-order transitions of GE 9979G gum silicone.*

Average thickness at 20° C, 0.424 cm. Curves plotted from different origins. Values for expansion are calculated in terms of the thickness at 20° C.

The transition temperature of −123° C appears to be unaffected by the addition of filler or by vulcanization. This behavior differs from that of natural rubber [4] in which filler and vulcanization change the transition temperature.

Silastic 250 differed from the other silicones in its temperature of crystallization, which was appreciably lower, and in the fact that it could be supercooled, with only partial crystallization. The results of expansion measurements obtained on this variety of silicone rubber are shown in figure 4.

Observations on heating and cooling shown in figure 4 were obtained separately. It is noted that while a normal second-order transition temperature of −121° C is obtained, crystallization on cooling and completion of melting on heating occur at lower temperatures than previously described. Crystallization on cooling occurs at approximately −75° C and completion of melting on heating at approximately −45° C.

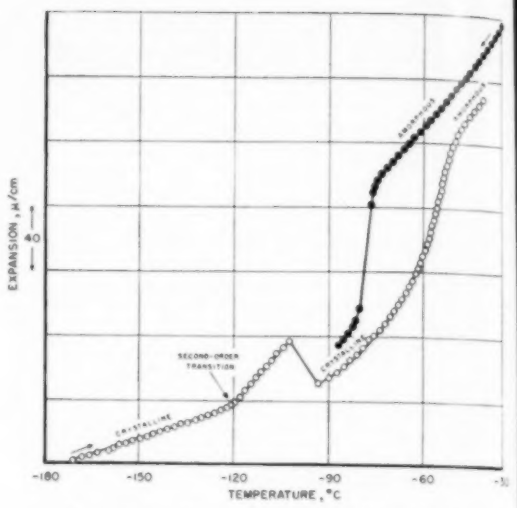

FIGURE 4. *Expansion curves of Silastic 250.*

Average thickness of specimens at 20° C, 0.386 cm. Curves plotted from different origins. Values for expansion are calculated in terms of the thickness at 20° C. ○, Observations on heating; ●, observations on cooling.

There is evidently a range of temperature favorable for crystallization extending from −75° to about −100° C, since crystallization of supercooled material was observed at the latter temperature on *increasing* temperature. This behavior is very similar to that of natural rubber [8, 9], which can be crystallized over a range of temperatures and which can be supercooled.

Silastic X–6073 differed from the other silicone rubbers in that it showed no evidence whatever of crystallization or melting between −180° and 0° C. A portion of the results of expansion measurements obtained with this variety together with those for Silastic X–6160, which are included for comparison are given in figure 5.

X–6073 shows no evidence of crystallization or melting at any temperature shown. Additional observations on heating this specimen were extended to +100° C (not shown in fig. 5) with no evidence of crystallization or melting or other transition evidenced by change of slope. The marked linearity shown when crystallization is absent is contrasted with the curvature existing in measurements of expansion on X–6160 below the crystallization range. This result may indicate that the amount of crystalline material is varying with consequent curvature of the graphs, over a considerable range of temperature.

The change in rate of expansion at the second-

order transition is greater for X–6073 than for X–6160, and the transition occurs at a slightly higher temperature.

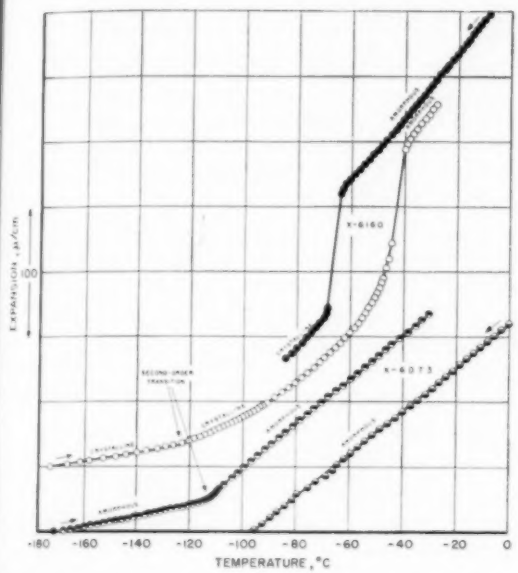

FIGURE 5. *Expansion curves of Silastics X–6073 and X–6160.*

Curves plotted from different origins. Values for expansion are calculated in terms of the thickness at 20° C. Silastic X-6073: average thickness at 20° C, 0.326 cm; ◓, observations on heating; ◒, observations on cooling. Silastic X-6160: average thickness at 20° C, 0.385 cm; ○, observations on heating; ●, observations on cooling.

The data obtained have been used to calculate coefficients of linear expansion of silicone rubbers. It is to be emphasized that there is some doubt concerning the reliability of the results, since no special precautions were taken to avoid possible tilting of the specimens as discussed by Saunders [7], and because the slopes of expansion curves were obtained graphically from single runs in most instances. The coefficients of expansion are given in table 1.

It will be noted that the gum silicones have very high coefficients of expansion. The coefficient of cubical expansion of such isotropic material would be about 120×10^{-5} per deg C between −35° and 0° C, which is as large as that of many organic liquids.

The coefficients of expansion of the other silicone rubbers are lower, as expected from the fact that they all contain fillers that reduce the coefficients. The coefficients of these rubbers observed below the second-order transition temperature are approximately 15 to 35 percent of the corresponding values above the transition.

V. Summary

This investigation has revealed a second-order transition in all silicone rubbers examined at a temperature of approximately −123° C. As far as can be ascertained this is the lowest temperature at which a second-order transition has been observed in a polymer. In one variety of silicone rubber (X–6073) no crystallization or melting was observed between −180° and +100° C; in the other varieties, crystallization and melting phenomena were observed at low temperatures.

TABLE 1. *Coefficients of linear thermal expansion of silicone rubbers*

Silicone rubber	Temperature range	Heating or cooling	Coefficients of expansion per degree C		
			Below second-order transition	Immediately above second-order transition	Above crystallization or melting range
	°C				
G. E. 9979G gum silicone $n=1.4040$	−35 to 0	Heating			39×10^{-4}
G. E. 9979G gum silicone $n=1.4028$	−35 to 0	do			40
	−120 to −100	do		18×10^{-4}	
	−180 to −125	do	9×10^{-4}		
Silastic 250	0 to −75	Cooling			22
	−120 to −102	Heating		25	
	−180 to −120	do	7		
Silastic X–6073	0 to −95	Cooling		16	
	−116 to +100	Heating		17	
	−180 to −116	do	3		
Silastic X–6160	0 to −65	Cooling			24
	−35 to 0	Heating			25
	−120 to −90	do		11	
	−180 to −120	do	4		

VI. References

[1] S. L. Bass, Silicone rubber—A new synthetic elastomer, Proceedings of Second Rubber Technology Conference, London, Paper No. 22, p. 17 (1948).

[2] O. K. Bates, Thermal conductivity of liquid silicones, Ind. Eng. Chem. **41,** 1966 (1949).

[3] N. Bekkedahl, Forms of rubber as indicated by the temperature-volume relationship, J. Research NBS **13,** 411 (1934) RP717.

[4] R. F. Boyer and R. S. Spencer, Second-order transition effects in rubber and other high polymers, Advances in Colloid Sci. **II,** chapter I, H. Mark and G. S. Whitby (Interscience Publishers Inc., New York, N. Y., 1946).

[5] M. J. Hunter, E. L. Warrick, J. F. Hyde, and C. C. Curie, Organosilicon polymers II—the open chain dimethylsiloxanes with trimethylsiloxy end groups, J. Am. Chem. Soc. **68,** 2284 (1946).

[6] G. M. Konkle, R. R. Selfridge, and P. C. Servais, Behavior of silastic on aging, Ind. Eng. Chem. **39,** 1410 (1947).

[7] J. B. Saunders, Improved interferometric procedure with application to expansion measurements, J. Research NBS **23,** 179 (1939) RP1227.

[8] L. A. Wood, Crystallization phenomena in natural and synthetic rubbers, Advances in Colloid Sci. **II,** chapter II, H. Mark and G. S. Whitby (Interscience Publishers Inc., New York, N. Y., 1946.

[9] L. A. Wood and N. Bekkedahl, Crystallization of unvulcanized rubber at different temperatures, J. Research NBS **36,** 489 (1946). RP1718. J. Applied Physics **17,** 362 (1946).

[10] L. A. Wood, N. Bekkedahl, and C. G. Peters, Application of the interferometer to the measurement of dimensional changes in rubber, J. Research NBS **23,** 571 (1939) RP1253.

WASHINGTON, September 13, 1949.

U. S. Department of Commerce
National Bureau of Standards

Research Paper RP2085
Volume 44, April 1950

Part of the Journal of Research of the National Bureau of Standards

Refractive Index as a Function of Wavelength for Sixty API–NBS Hydrocarbons[1]

By Alphonse F. Forziati [2]

Measurements of the refractive index at 20°, 25°, and 30° C and at seven wavelengths, from 6678.1 to 4358.3 Angstrom units, were made on 60 purified hydrocarbons of the API–NBS series. The apparatus consisted of a precision Abbe-type refractometer, calibrated by means of NBS Standard Samples of hydrocarbons certified with respect to refractive index at the three temperatures and seven wavelengths used. The light sources used were a mercury arc, a sodium vapor lamp, and hydrogen and helium discharge tubes, with suitable filters. A constant temperature bath maintained the temperature of the refractometer prisms constant within ±0.02° C.

The experimental data on the hydrocarbons were adjusted by means of a four constant Hartmann equation, $n_\lambda = n_\infty + C/(\lambda - \lambda^*)^{1.6}$, and a two constant modified Cauchy equation, $\Delta n_\lambda = a + b/\lambda^2$. ($\Delta n_\lambda$, the change in the refractive index at the wavelength, λ, when the temperature is changed from 20° to 25° C or 25° to 30° C, is used instead of n_λ of the Cauchy equation).

The computed refractive index at 20°, 25°, and 30° C, together with the values of the specific dispersions, and the constants of the Hartmann and modified Cauchy equations, applicable over the range of measurement, are reported for 60 API–NBS hydrocarbons, comprising 17 paraffins, 14 alkylcyclopentanes, 8 alkylcyclohexanes, and 21 alkylbenzenes.

I. Introduction

This investigation is part of the systematic program on the physical properties of highly purified hydrocarbons being prepared in the cooperative program of the American Petroleum Institute and the National Bureau of Standards.

Precision measurements of the refractive index were made on 60 hydrocarbons of the API-NBS series at 20°, 25°, and 30° C and at the seven wavelengths, helium 6678.1 and 5015.7 A, hydrogen 6562.8 and 4861.3 A, sodium (intensity-weighted mean) 5892.6 A, and mercury 5460.7 and 4358.3 A.

This paper gives the results of the adjustment of the data by means of the Hartmann and the modified Cauchy equations, together with the calculated specific dispersions, for 17 paraffin, 14 alkylcyclopentane, 8 alkylcyclohexane, and 21 alkylbenzene hydrocarbons.

II. Apparatus and Procedure

A precision Abbe-type Bausch and Lomb refractometer was used to measure the refractive index. In order to maintain the temperature of the refracting prism constant within the required limit of ±0.02° C, it was found necessary to remove the thermometer furnished with the instrument and to adapt a small cylinder to the water exit-tube. The top of this cylinder was threaded to accommodate a short platinum resistance thermometer (25 ohms) made specially for this purpose.[3] This cylinder permitted the water at constant temperature to flow freely through the exit-tube and provided for complete immersion of the thermometer in the water.[4]

A constant-temperature bath was assembled and connected to the refractometer, as shown in figure 1. The temperature of the water as it left the prism cell was measured by means of the

[1] This investigation was performed at the National Bureau of Standards as part of the work of the American Petroleum Institute Research Project 6 on the "Analysis, Purification, and Properties of Hydrocarbons".

[2] Research Associate on the American Petroleum Institute Research Project 6 at the National Bureau of Standards.

[3] Manufactured by Cyril H. Meyers, Arlington, Va.

[4] The bulb of the mercury-in-glass thermometer originally in the water exit-tube of the instrument throttled the flow of water to such an extent that it was impossible to attain adequate temperature control.

platinum resistance thermometer and a Mueller-type resistance bridge. The maximum drift observed over a period of 6 hr was ±0.02 deg C, whereas the temperature of the water in the bath itself varied only ±0.005 deg C. To obtain satisfactory control of temperature, it is very important that the connections from the constant-temperature bath to the refractometer be well insulated and as short as possible. Furthermore, the temperature of the water leaving the prism assembly should be measured before and after each group of measurements on each hydrocarbon and a suitable correction applied if necessary.

A diagram of the controls for the constant-temperature bath is shown in figure 2, with details given in the legend.

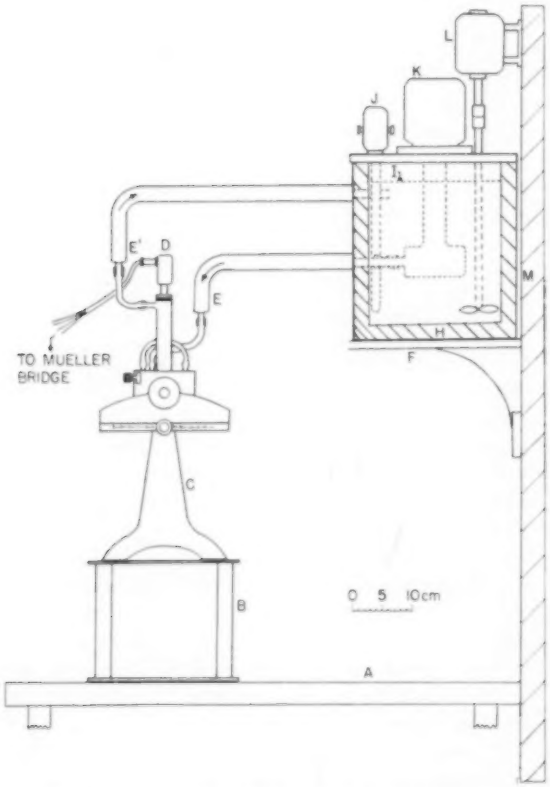

FIGURE 1. *Assembly of precision refractometer*

The letters have the following significance: A, table; B, metal supporting-stand for refractometer; C, refractometer (Bausch and Lomb Precision); *D*, platinum resistance thermometer; E, water inlet to prism assembly; E', water outlet from prism assembly; F, support for constant-temperature water bath; H, thermal insulation on water-bath; I, water level; J, mercury-type thermoregulator; K, water pump; L, motor with stirrer; M, wall of room.

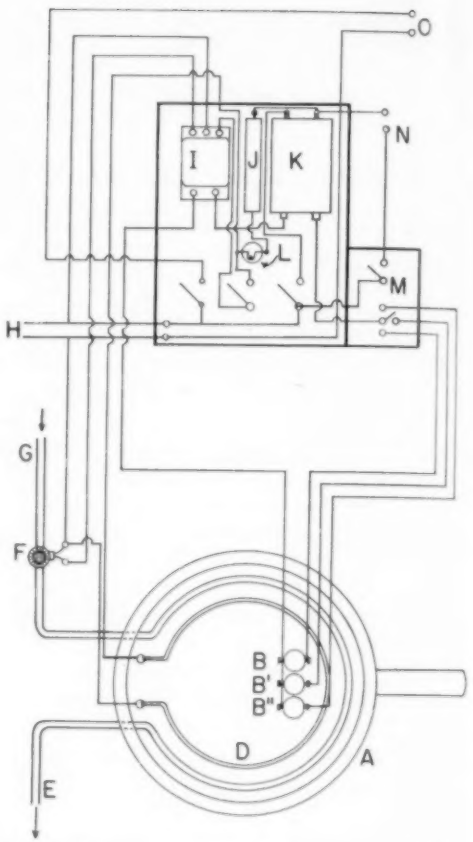

FIGURE 2. *Diagram of controls for precision refractometer*

The letters have the following significance: A, water bath; B, B', and B" mercury-type thermoregulators set at 20° C (±0.01° C), 25° C (±0.01° C), and 30° C (±0.01° C), respectively; D, heater; E, water discharge; F, solenoid valve; G, inlet for cooling water; H, power line, 110 volts, alternating current; I, relay; J, resistance, 1,000 ohms; K, rectifier and transformer; L, miniature lamp, 14 volts; M, switch assembly; N, to stirrer motor; O, to pump motor.

The sources of light used were as follows:

For the mercury lines, a mercury arc (General Electric type H4) was used. For isolating the line at 4358.3 A, a combination of Corning filter No. 5850 (melt 647, thickness of 3.98 mm) and Corning filter No. 3389 (melt 622, thickness of 3.05 mm) was used. For the line at 5460.7 A, a Wratten filter No. 62 was used.

For the hydrogen lines, a low-pressure discharge tube of the Texas Co. design [1] [5] filled with hydrogen was used. A Wratten filter No. 45 was used for the line at 4861.3 A. A Corning filter No.

[5] Figures in brackets indicate the literature references at the end of this paper.

2404 (thickness of 3.35 mm) was used for the line at 6562.8 A in order to improve the contrast of the light and dark portions of the field.

For the helium lines, a low-pressure discharge tube of the same type as for hydrogen, but filled with helium, was used. A Wratten filter No. 45 was used for the line at 5015.7 A. For the line at 6678.1 A, the same filter was used as for the hydrogen line at 6562.8 A.

For the sodium line, intensity-weighted mean at 5892.6 A, the standard sodium vapor lamp supplied with the refractometer was used.

The mercury arc and sodium vapor lamp were equipped with shields bearing a vertical slit, 1x25 mm in size.

At the beginning of each series of measurements, the refractometer was calibrated by means of the NBS Standard Samples of 2,2,4-trimethylpentane, methylcyclohexane, and toluene, each of which is certified with respect to refractive index at 20°, 25°, and 30° C, at each of the seven wavelengths given above. During the series of measurements, the refractometer was periodically checked with the standard used on that day. The complete calibration was repeated after a prolonged series and the change, if any, was prorated over the time interval. A table of corrections for each wavelength at 20°, 25°, and 30° C was prepared for each one of the three standards. These corrections were then applied to the observations in accordance with the standard liquid used. The calibrating values of the three standards used, as obtained by the NBS Optical Instruments Section, are given in table 1.

TABLE 1. *Certified values of refractive index for three NBS Standard Samples of Hydrocarbons*

Wavelength in Angstrom units	Designation of line	Index of refraction [a]								
		2,2,4-Trimethylpentane No. 217			Methylcyclohexane No. 218			Toluene No. 211a		
		20° C	25° C	30° C	20° C	25° C	30 C	20° C	25° C	30° C
6678.1	Helium	1.38916	1.38670	1.38424	1.42064	1.41812	1.41560	1.49180	1.48903	1.48619
6562.8	Hydrogen, C	1.38945	1.38698	1.38452	1.42094	1.41842	1.41591	1.49243	1.48966	1.48682
5892.6 [b]	Sodium, D_1, D_2	1.39145	1.38898	1.38650	1.42312	1.42058	1.41806	1.49693	1.49413	1.49126
5460.7	Mercury, e	1.39316	1.39068	1.38820	1.42497	1.42243	1.41989	1.50086	1.49803	1.49514
5015.7	Helium	1.39544	1.39294	1.39044	1.42744	1.42488	1.42233	1.50620	1.50334	1.50041
4861.3	Hydrogen, F	1.39639	1.39389	1.39138	1.42847	1.42590	1.42334	1.50847	1.50559	1.50265
4358.3	Mercury, g	1.40029	1.39776	1.39523	1.43269	1.43010	1.42752	1.51800	1.51506	1.51206

[a] These measurements were made by the NBS Section on Optical Instruments.
[b] Intensity-weighted mean of doublet, D_1, D_2.

III. Source and Purity of Compounds

The compounds whose refractive indices were measured in the present investigation were samples from the API-NBS series of highly purified hydrocarbons, which are being prepared through a cooperative undertaking of the American Petroleum Institute and the National Bureau of Standards. The description of the compounds is given in a preceding report [2]. The purification and determination of purity and freezing points of these compounds are described in references [3, 4, 5, 6, 7]. It is believed that in each case the impurity was of such nature and present in such small amount that the properties measured were not affected beyond the indicated limits of uncertainty.

IV. Adjustment of the Data

1. Method of Adjustment

The Hartmann dispersion formula, in its simple form,

$$n_\lambda = n_\infty + C/(\lambda - \lambda^*), \qquad (1)$$

where n_λ is the refractive index of the substance for light of wavelength λ, and n_∞, C, and λ^* are constants, is not sufficiently accurate for the representation of refractive indices to five decimal places. It is well known that some exponent other than unity is desirable for $(\lambda - \lambda^*)$ in accurate work over an extended range in wavelengths. Tilton and Gurewitz [8] found that the refractive indices of three standard hydrocarbons

could be accurately represented to within a few units of the sixth decimal when 1.6 was used as the exponent.

The data obtained in the present investigation have been adjusted by means of the Hartmann equation as used by Tilton and Gurewitz:

$$n_\lambda = n_\infty + C/(\lambda - \lambda^*)^{1.6}. \quad (2)$$

The results show that the equation is entirely adequate to represent the refractive indices of a wide variety of liquid hydrocarbons over the range of wavelength from 0.66781 to 0.43583 μ (or 6678 to 4358 A).

The constants in eq 2 were adjusted by means of a modification [6] of an interpolation precedure recommended by Tilton and Gurewitz [8]. The following abbreviations are used:

$$\beta = 1/(\lambda - \lambda^*)^{1.6}, \quad (3)$$

$$\gamma = (\beta_{0.44583} - \beta_{0.65628})/(\beta_{0.43583} - \beta_{0.54607}). \quad (4)\ [7]$$

To facilitate the calculations, values of β and γ were calculated over certain ranges. Table 2 gives the values of β for each of the seven wavelengths, for values of λ^* from 0.0700 to 0.1500 μ. Table 3 gives values of γ for values of λ^* from 0.07 to 0.15.

TABLE 2. *Values of $\beta = 1/(\lambda - \lambda^*)^{1.6}$, for each of seven wavelengths, λ, for the range $\lambda^* = 0.0700$ to 0.1500*

λ^*	Wavelength, λ in microns						
	0.6678149	0.6562793	0.5892620	0.5460740	0.5015675	0.4861327	0.4358142
	$\beta = 1/(\lambda - \lambda^*)^{1.6}$						
	β_{He-red}	β_C	$\beta_{D_1 \cdot D_2}$	β_e	$\beta_{He-blue}$	β_F	β_g
0.070	2.277683	2.349809	2.85352	3.278846	3.836384	4.066578	4.997411
	6109	6427	881	11050	14266	15684	21934
.071	2.283792	2.356236	2.86233	3.289896	3.850650	4.082262	5.019345
	6136	6456	886	11110	14353	15782	22092
.072	2.289928	2.362692	2.87119	3.301006	3.865003	4.098044	5.041437
	6163	6485	891	11171	14439	15882	22249
.073	2.296091	2.369177	2.88010	3.312177	3.879442	4.113926	5.063986
	6190	6513	895	11233	14528	15982	22410
.074	2.302281	2.375690	2.88905	3.323410	3.893970	4.129908	5.086996
	6217	6543	899	11295	14616	16083	22572
.075	2.308498	2.382233	2.89804	3.334705	3.908586	4.145991	5.108968
	6244	6572	904	11358	14705	16187	22734
.076	2.314742	2.388805	2.90708	3.346063	3.923291	4.162178	5.131402
	6272	6601	909	11420	14795	16290	22900
.077	2.321014	2.395406	2.91617	3.357483	3.938086	4.178468	5.154302
	6299	6631	913	11484	14887	16393	23066

[6] Harold Hurwitz, Scientific Aid on the API Research Project 6 at this Bureau, developed this modification and computed tables 2 and 3.

[7] Any three wavelengths may be used to define γ. Table 3 must then be recomputed for the selected wavelengths.

TABLE 2. *Values of $\beta = 1/(\lambda - \lambda^*)^{1.6}$, for each of seven wavelengths, λ, for the range $\lambda^* = 0.700$ to 0.1500*—CONT.

λ^*	Wavelength, λ in microns						
	0.6678149	0.6562793	0.5892620	0.5460740	0.5015675	0.4861327	0.4358142
	$\beta = 1/(\lambda - \lambda^*)^{1.6}$						
	β_{He-red}	β_C	$\beta_{D_1 \cdot D_2}$	β_e	$\beta_{He-blue}$	β_F	β_g
0.078	2.327313	2.402037	2.92530	3.368967	3.952973	4.194861	5.17758
	6327	6661	917	11548	14978	16409	2324
.079	2.333640	2.408698	2.93447	3.380515	3.967951	4.211360	5.20092
	6355	6691	923	11613	15070	16603	2341
.080	2.339995	2.415389	2.94370	3.392128	3.983021	4.227963	5.22466
	6383	6721	927	11677	15164	16707	2357
.081	2.346378	2.422110	2.95297	3.403805	3.998185	4.244670	5.24870
	6412	6752	932	11743	15258	16814	2374
.082	2.352790	2.428862	2.96229	3.415548	4.013443	4.261484	5.27310
	6441	6782	937	11809	15353	16923	2391
.083	2.359231	2.435644	2.97166	3.427357	4.028796	4.278407	5.29787
	6469	6814	942	11876	15448	17033	2407
.084	2.365700	2.442458	2.98108	3.439233	4.044244	4.295440	5.32302
	6498	6844	946	11942	15545	17144	2424
.085	2.372198	2.449302	2.99054	3.451175	4.059789	4.312584	5.34857
	6527	6876	951	12010	15642	17260	2441
.086	2.378725	2.456178	3.00005	3.463185	4.075431	4.329844	5.37452
	6556	6907	957	12078	15740	17372	2458
.087	2.385281	2.463085	3.00962	3.475263	4.091171	4.347216	5.40088
	6586	6938	961	12147	15839	17487	2475
.088	2.391867	2.470023	3.01923	3.487410	4.107010	4.364703	5.42767
	6615	6971	967	12216	15939	17602	2493
.089	2.398482	2.476994	3.02890	3.499626	4.122949	4.382305	5.45488
	6645	7002	971	12285	16040	17717	2510
.090	2.405127	2.483996	3.03861	3.511911	4.138989	4.400022	5.48252
	6675	7034	976	12355	16142	17831	2528
.091	2.411802	2.491030	3.04837	3.524266	4.155131	4.417853	5.51059
	6705	7067	982	12427	16244	17948	2546
.092	2.418507	2.498097	3.05819	3.536693	4.171375	4.435801	5.53910
	6735	7099	986	12497	16347	18067	2563
.093	2.425242	2.505196	3.06805	3.549190	4.187722	4.453868	5.56807
	6766	7133	992	12570	16453	18187	2582
.094	2.432008	2.512329	3.07797	3.561760	4.204175	4.472055	5.59749
	6797	7165	997	12642	16557	18307	2601
.095	2.438805	2.519494	3.08794	3.574402	4.220732	4.490362	5.59689
	6828	7199	1002	12716	16663	18430	2617
.096	2.445633	2.526693	3.09796	3.587118	4.237395	4.508792	5.62739
	6858	7232	1008	12789	16771	18553	2635
.097	2.452491	2.533925	3.10804	3.599907	4.254166	4.527345	5.64835
	6890	7267	1013	12864	16878	18677	2654
.098	2.459381	2.541192	3.11817	3.612771	4.271044	4.546022	5.67980
	6922	7300	1018	12938	16988	18803	2673
.099	2.466303	2.548492	3.12835	3.625709	4.288032	4.564825	5.70174
	6953	7334	1023	13014	17098	18930	2691
.100	2.473256	2.555826	3.13858	3.638723	4.305130	4.583755	5.73419
	6985	7369	1028	13090	17209	19058	2710
.101	2.480241	2.563195	3.14886	3.651813	4.322339	4.602813	5.75719
	7017	7403	1034	13166	17320	19186	2728
.102	2.487258	2.570598	3.15920	3.664979	4.339659	4.621999	5.78069
	7050	7438	1039	13243	17434	19318	2750
.103	2.494308	2.578036	3.16959	3.678222	4.357093	4.641317	5.81469
	7082	7473	1045	13322	17549	19448	2769
.104	2.501390	2.585509	3.18004	3.691544	4.374642	4.660765	5.84924
	7115	7508	1051	13400	17663	19582	2787
.105	2.508505	2.593017	3.19055	3.704944	4.392305	4.680347	5.88434
	7058	7544	1058	13479	17780	19715	2810
.106	2.515653	2.600561	3.20113	3.718423	4.410085	4.700062	5.89001
	7271	7579	1063	13560	17897	19851	2827

TABLE 2. *Values of $\beta=1/(\lambda-\lambda^*)^{1.6}$, for each of seven wavelengths, λ, for the range $\lambda^*=0.700$ to 0.1500*—Con.

λ^*	Wavelength, λ in microns						
	0.6678149	0.6562793	0.5892620	0.5460740	0.5015675	0.4861327	0.4358342
	$\beta=1/(\lambda-\lambda^*)^{1.6}$						
	$\beta_{\text{Ne-red}}$	β_C	β_{D_1,D_2}	β_e	$\beta_{\text{Ne-blue}}$	β_F	β_g
0.107	2.522834	2.608140	3.21176	3.731983	4.427982	4.719913	5.927026
	7214	7615	1070	13640	18016	19987	28953
.108	2.530048	2.615755	3.22246	3.745623	4.445998	4.739900	5.955979
	7248	7652	1075	13721	18135	20125	29185
.109	2.537296	2.623407	3.23321	3.759344	4.464133	4.760025	5.985164
	7282	7688	1081	13803	18255	20264	29417
.110	2.544578	2.631095	3.24402	3.773147	4.482388	4.780289	6.014581
	7316	7725	1086	13885	18376	20405	29652
.111	2.551894	2.638820	3.25488	3.787032	4.500764	4.800694	6.044233
	7350	7761	1092	13969	18499	20546	29891
.112	2.559244	2.646581	3.26580	3.801001	4.519263	4.821240	6.074124
	7385	7799	1098	14052	18624	20690	30131
.113	2.566629	2.654380	3.27678	3.815053	4.537887	4.841930	6.104255
	7419	7836	1103	14137	18748	20835	30376
.114	2.574048	2.662216	3.28781	3.829190	4.556635	4.862765	6.134631
	7454	7874	1110	14223	18874	20981	30622
.115	2.581502	2.670090	3.29891	3.843413	4.575509	4.883746	6.165253
	7489	7912	1116	14309	19002	21129	30871
.116	2.588991	2.678002	3.31007	3.857722	4.594511	4.904875	6.196124
	7525	7949	1122	14395	19130	21277	31122
.117	2.596516	2.685951	3.32129	3.872117	4.613641	4.926152	6.227246
	7560	7988	1129	14483	19261	21428	31378
.118	2.604076	2.693939	3.33258	3.886600	4.632902	4.947580	6.258624
	7596	8027	1134	14572	19391	21580	31636
.119	2.611672	2.701966	3.34392	3.901172	4.652293	4.969160	6.290260
	7632	8066	1141	14660	19524	21734	31897
.120	2.619304	2.710032	3.35533	3.915832	4.671817	4.990894	6.322157
	7668	8105	1147	14750	19657	21888	32160
.121	2.626972	2.718137	3.36680	3.930582	4.691474	5.012782	6.354317
	7705	8144	1154	14840	19792	22044	32426
.122	2.634677	2.726281	3.37834	3.945422	4.711266	5.034826	6.386743
	7742	8184	1160	14932	19928	22203	32697
.123	2.642419	2.734465	3.38994	3.960354	4.731194	5.057029	6.419440
	7779	8225	1166	15024	20065	22362	32969
.124	2.650198	2.742690	3.40160	3.975378	4.751259	5.079391	6.452409
	7816	8264	1173	15116	20204	22523	33246
.125	2.658014	2.750954	3.41333	3.990494	4.771463	5.101914	6.485655
	7853	8305	1180	15209	20344	22685	33524
.126	2.665867	2.759259	3.42513	4.005703	4.791807	5.124599	6.519179
	7891	8346	1186	15304	20484	22850	33807
.127	2.673758	2.767605	3.43699	4.021007	4.812291	5.147449	6.552986
	7930	8387	1193	15399	20628	23016	34093
.128	2.681688	2.775992	3.44892	4.036406	4.832919	5.170465	6.587079
	7967	8428	1200	15496	20772	23184	34382
.129	2.689655	2.784420	3.46092	4.051902	4.853691	5.193649	6.621461
	8006	8470	1207	15592	20917	23353	34675
.130	2.697661	2.792890	3.47299	4.067494	4.874608	5.217002	6.656136
	8045	8512	1213	15690	21064	23524	34971
.131	2.705706	2.801402	3.48512	4.083184	4.895672	5.240526	6.691107
	8084	8554	1220	15790	21212	23698	35270
.132	2.713790	2.809956	3.49732	4.098974	4.916884	5.264224	6.726377
	8124	8597	1228	15888	21362	23872	35574
.133	2.721914	2.818553	3.50960	4.114862	4.938246	5.288096	6.761951
	8163	8640	1234	15990	21513	24049	35881
.134	2.730077	2.827193	3.52194	4.130852	4.959759	5.312145	6.797832
	8203	8683	1241	16090	21666	24227	36192
.135	2.738280	2.835876	3.53435	4.146942	4.981425	5.336372	6.834024
	8243	8726	1248	16192	21820	24406	36504

TABLE 2. *Values of $\beta=1/(\lambda-\lambda^*)^{1.6}$, for each of seven wavelengths, λ, for the range $\lambda^*=0.700$ to 0.1500*—Con.

λ^*	Wavelength, λ in microns						
	0.6678149	0.6562793	0.5892620	0.5460740	0.5015675	0.4861327	0.4358342
	$\beta=1/(\lambda-\lambda^*)^{1.6}$						
	$\beta_{\text{Ne-red}}$	β_C	β_{D_1,D_2}	β_e	$\beta_{\text{Ne-blue}}$	β_F	β_g
0.136	2.746523	2.844602	3.54683	4.163134	5.003245	5.360778	6.870528
	8283	8770	1256	16296	21977	24588	36823
.137	2.754806	2.853372	3.55939	4.179430	5.025222	5.385366	6.907351
	8324	8814	1263	16399	22133	24772	37144
.138	2.763130	2.862186	3.57202	4.195829	5.047355	5.410138	6.944495
	8365	8858	1270	16504	22293	24958	37471
.139	2.771495	2.871044	3.58472	4.212333	5.069648	5.435096	6.981966
	8406	8903	1278	16609	22453	25145	37800
.140	2.779901	2.879947	3.59750	4.228942	5.092101	5.460241	7.019766
	8448	8948	1285	16714	22614	25335	38133
.141	2.788349	2.888895	3.61035	4.245656	5.114715	5.485576	7.057899
	8489	8993	1292	16822	22779	25527	38470
.142	2.796838	2.897888	3.62327	4.262478	5.137494	5.511103	7.096369
	8531	9039	1300	16931	22943	25720	38813
.143	2.805369	2.906927	3.63627	4.279409	5.160437	5.536823	7.135182
	8574	9084	1308	17040	23111	25916	39160
.144	2.813943	2.916011	3.64935	4.296449	5.183548	5.562739	7.174342
	8617	9131	1315	17152	23279	26114	39510
.145	2.822560	2.925142	3.66250	4.313601	5.206827	5.588853	7.213852
	8660	9177	1323	17265	23450	26313	39864
.146	2.831220	2.934319	3.67573	4.330866	5.230277	5.615166	7.253716
	8703	9224	1331	17378	23621	26514	40223
.147	2.839923	2.943543	3.68904	4.348244	5.253898	5.641680	7.293939
	8747	9271	1338	17493	23796	26719	40588
.148	2.848670	2.952814	3.70242	4.365737	5.277694	5.668399	7.334527
	8790	9319	1347	17606	23972	26926	40956
.149	2.857460	2.962133	3.71589	4.383343	5.301666	5.695325	7.375483
	8835	9367	1354	17723	24149	27134	41329
.150	2.866295	2.971500	3.72943	4.401066	5.325815	5.722459	7.416812

The value of γ was determined from the relation

$$\gamma=(n_{0.43583}-n_{0.65628})/(n_{0.43583}-n_{0.54607}). \quad (5)$$

Using table 3, the corresponding value of λ^* was interpolated. Further interpolation in table 2 yielded values for β for each of the seven wavelengths used. The constant C was then readily computed from the equation

$$C=(n_{0.43583}-n_{0.65628})/(\beta_{0.43583}-\beta_{0.65628}). \quad (6)$$

The Hartmann equation was written as

$$n_\lambda=n_\infty+C\beta_\lambda. \quad (7)$$

The remaining unknown constant, n_∞, was easily computed by inserting the observed values of the refractive index at $\lambda=0.65628$, 0.54607, and 0.43583μ, the numerical value of C, and appropriate values of β_λ, successively into the above

877106—50——3

equation and solving three times for n_∞. If no errors were made, the three computed values of n_∞ agreed within ± 0.00001. The same equation was used to compute the refractive index at $\lambda = 0.66781$, 0.58926, 0.50157, and 0.48613μ, by inserting the average value of n_∞, and the values of C and β_λ. Since it was found that this procedure reproduces good data to about ± 0.00001 units in the refractive index, it is obvious that attempts to better these constants of the Hartmann equation by least squares or any other method of adjustment would be of no practical value in this work where only fifth decimal data is to be considered.

TABLE 3. *Values of* $\gamma = (\beta_{0.48613} - \beta_{0.58926})/(\beta_{0.48613} - \beta_{0.54607})$, *for values of* λ^* *from 0.07 to 0.15*

Intervals of λ^*	λ^*							
	0.07000	0.08000	0.09000	0.10000	0.11000	0.12000	0.13000	0.14000
	$\gamma = (\beta_{0.48613} - \beta_{0.58926})/(\beta_{0.48613} - \beta_{0.54607})$							
0.000	1.540589	1.533190	1.525554	1.517667	1.509518	1.501096	1.492383	1.483368
	729	753	778	802	830	858	888	920
.001	1.539860	1.532437	1.524776	1.516865	1.508688	1.500238	1.491495	1.482448
	733	755	779	806	832	860	890	923
.002	1.539127	1.531682	1.523997	1.516059	1.507856	1.499378	1.490605	1.481525
	734	757	783	809	835	864	894	926
.003	1.538393	1.530925	1.523214	1.515250	1.507021	1.498514	1.489711	1.480599
	736	761	785	810	838	867	896	929
.004	1.537657	1.530164	1.522429	1.514440	1.506183	1.497647	1.488815	1.479670
	739	762	787	814	841	869	901	932
.005	1.536918	1.529402	1.521642	1.513626	1.505342	1.496778	1.487914	1.478738
	741	765	789	817	844	874	903	935
.006	1.536177	1.528637	1.520853	1.512809	1.504498	1.495904	1.487011	1.477803
	744	767	793	818	846	875	905	937
.007	1.535433	1.527870	1.520060	1.511991	1.503652	1.495029	1.486106	1.476866
	745	769	795	821	849	879	910	940
.008	1.534688	1.527101	1.519265	1.511170	1.502803	1.494150	1.485196	1.475926
	748	773	798	825	852	882	912	945
.009	1.533940	1.526328	1.518467	1.510345	1.501951	1.493268	1.484284	1.474981
	750	774	800	827	855	885	916	947

Instead of applying the above procedure separately to the data obtained at 20°, 25°, and 30° C, it was decided that the 21 measurements on each hydrocarbon would be better correlated if the change in refractive index in going from 20° to 25° C and from 25° to 30° C were first adjusted by means of the method of least squares and the Cauchy formula

$$\Delta n_\lambda = a + b/\lambda^2, \tag{8}$$

using Δn_λ instead of n_λ.

The computed values of Δn, for each wavelength, were then added to the 30° C refractive indices and subtracted from the 20° C indices to give two values at 25° C. These were averaged with the experimentally determined indices of refraction at 25° C, and the average fitted to the Hartmann equation by the interpolation method described above. By adding and subtracting the computed values of Δn from the refractive indices calculated by means of the constants of the Hartmann equation, the values of refractive index for 20° and 30° C were obtained. This procedure automatically "smoothed" the values for 20° and 30° C. In the case of the paraffins and cycloparaffins, the values of Δn for the range 20° to 25° C were so nearly equal to those for the range 25° to 30° C that average values of Δn were used.

2. Results of the Adjustment

Table 4 gives the values of the constants of the modified Cauchy equation for each of the 60 compounds. The last column of the table gives the root-mean-square value, $\rho \times 10^5$, of the deviations of the observed from the calculated refractive indices.

Table 5 gives the values of the constants of the Hartmann equation for each of the 60 compounds. As before, the last column of the table gives the root-mean-square value, $\rho \times 10^5$, of the deviations

of the observed from the calculated refractive indices.

Table 6 gives the calculated values of refractive index at 20°, 25°, and 30° C, at each of seven wavelengths, for each of the 60 compounds.

Table 7 gives values of the specific dispersion, $10^4(n_F - n_C)/d$ and $10^4(n_g - n_D)/d$, for each of the 60 compounds, from the values of refractive index given in this report and the values of density given in an earlier report [2].

TABLE 4. *Values of the constants of the modified Cauchy equation for 60 API–NBS hydrocarbons*

Compound	Formula	Constants in the equation $\Delta n = a \times b/\lambda^2$					
		$a \times 10^3$		$b \times 10^3$		$\rho \times 10^3$	
		20° to 25°C	25° to 30°C	20° to 25°C	25° to 30°C	20° to 25°C	25° to 30°C
PARAFFINS							
n-Heptane	C_7H_{16}	2.455	2.455	0.0273	0.0273	4.79	3.71
2-Methylhexane	C_7H_{16}	2.532	2.532	.0179	.0179	6.69	6.15
3-Methylhexane	C_7H_{16}	2.466	2.466	.0296	.0296	6.68	6.73
3-Ethylpentane	C_7H_{16}	2.491	2.491	.0215	.0215	3.28	3.39
2,2-Dimethylpentane	C_7H_{16}	2.528	2.528	.0253	.0253	5.29	3.92
2,3-Dimethylpentane	C_7H_{16}	2.430	2.430	.0283	.0283	3.52	4.92
2,4-Dimethylpentane	C_7H_{16}	2.554	2.554	.0268	.0268	3.93	4.68
3,3-Dimethylpentane	C_7H_{16}	2.407	2.407	.0313	.0313	4.38	4.70
2,2,3-Trimethylbutane	C_7H_{16}	2.422	2.422	.0351	.0351	4.98	1.95
n-Nonane	C_9H_{20}	2.230	2.230	.0293	.0293	4.69	3.82
2,2,5-Trimethylhexane	C_9H_{20}	2.392	2.392	.0157	.0157	4.83	2.65
2,4,4-Trimethylhexane	C_9H_{20}	2.234	2.234	.0227	.0227	3.06	2.11
3,3-Diethylpentane	C_9H_{20}	2.060	2.060	.0276	.0276	4.80	4.01
2,2,3,3-Tetramethylpentane	C_9H_{20}	2.132	2.132	.0250	.0250	2.18	1.52
2,2,3,4-Tetramethylpentane	C_9H_{20}	2.200	2.200	.0196	.0196	5.97	4.65
2,2,4,4-Tetramethylpentane	C_9H_{20}	2.322	2.322	.0106	.0106	4.68	4.10
2,3,3,4-Tetramethylpentane	C_9H_{20}	2.128	2.128	.0211	.0211	3.37	2.45
ALKYLCYCLOPENTANES							
Ethylcyclopentane	C_7H_{14}	2.438	2.438	0.0243	0.0243	3.45	3.47
1,1-Dimethylcyclopentane	C_7H_{14}	2.570	2.570	.0284	.0284	4.64	2.03
1,*cis*-2-Dimethylcyclopentane	C_7H_{14}	2.408	2.408	.0470	.0470	5.31	5.33
1,*trans*-2-Dimethylcyclopentane	C_7H_{14}	2.514	2.514	.0252	.0252	3.34	2.54
1,*cis*-3-Dimethylcyclopentane	C_7H_{14}	2.518	2.518	.0313	.0313	2.61	2.18
1,*trans*-3-Dimethylcyclopentane	C_7H_{14}	2.535	2.535	.0250	.0250	4.09	3.80
n-Propylcyclopentane	C_8H_{16}	2.272	2.272	.0337	.0337	3.58	3.20
Isopropylcyclopentane	C_8H_{16}	2.247	2.247	.0265	.0265	2.57	1.68
1-Methyl-1-ethylcyclopentane	C_8H_{16}	2.319	2.319	.0342	.0342	2.81	2.19
1-Methyl-*cis*-2-ethylcyclopentane	C_8H_{16}	2.360	2.360	.0071	.0071	3.90	2.41
1,1,2-Trimethylcyclopentane	C_8H_{16}	2.391	2.391	.0263	.0263	4.80	4.86
1,1,3-Trimethylcyclopentane	C_8H_{16}	2.371	2.371	.0412	.0412	6.41	4.91
1,*cis*-2,*trans*-4-Trimethylcyclopentane	C_8H_{16}	2.343	2.343	.0304	.0304	4.10	3.12
1,*trans*-2,*cis*-4-Trimethylcyclopentane	C_8H_{16}	2.413	2.413	.0216	.0216	4.87	4.00
ALKYLCYCLOHEXANES							
1,1-Dimethylcyclohexane	C_8H_{16}	2.296	2.296	0.0294	0.0294	5.23	4.99
n-Propylcyclohexane	C_9H_{18}	2.211	2.211	.0215	.0215	4.03	3.81
Isopropylcyclohexane	C_9H_{18}	2.192	2.192	.0226	.0226	4.50	3.10
1,1,3-Trimethylcyclohexane	C_9H_{18}	2.248	2.248	.0172	.0172	2.58	2.46
n-Butylcyclohexane	$C_{10}H_{20}$	2.156	2.156	.0170	.0170	3.06	1.32
Isobutylcyclohexane	$C_{10}H_{20}$	2.202	2.202	.0165	.0165	3.12	1.64
sec-Butylcyclohexane	$C_{10}H_{20}$	2.142	2.142	.0169	.0169	2.74	2.28
tert-Butylcyclohexane	$H_{16}C_{20}$	2.174	2.174	.0110	.0110	3.30	3.12

TABLE 4. *Values of the constants of the modified Cauchy equation for 60 API–NBS hydrocarbons*—Continued

Compound	Formula	Constants in the equation $\Delta n = a + b/\lambda^2$					
		$a \times 10^3$		$b \times 10^3$		$\rho \times 10^4$	
		20° to 25°C	25° to 30°C	20° to 25°C	25° to 30°C	20° to 25°C	25° to 30°C
ALKYLBENZENES							
Benzene	C_6H_6	2.988	3.020	0.0753	0.0424	0.94	1.97
Methylbenzene	C_7H_8	2.658	2.704	.0459	.0620	2.89	1.28
Ethylbenzene	C_8H_{10}	2.541	2.617	.0501	.0290	7.70	0.80
1,2-Dimethylbenzene	C_8H_{10}	2.331	2.503	.0590	.0432	1.55	1.49
1,3-Dimethylbenzene	C_8H_{10}	2.383	2.585	.0669	.0255	1.90	1.57
1,4-Dimethylbenzene	C_8H_{10}	2.394	2.616	.0595	.0325	2.62	1.02
n-Propylbenzene	C_9H_{12}	2.372	2.382	.0494	.0368	1.39	1.54
Isopropylbenzene	C_9H_{12}	2.428	2.328	.0419	.0398	3.21	1.34
1-Methyl-2-ethylbenzene	C_9H_{12}	2.340	2.396	.0478	.0193	3.86	2.12
1-Methyl-3-ethylbenzene	C_9H_{12}	2.390	2.439	.0535	.0271	1.54	3.22
1-Methyl-4-ethylbenzene	C_9H_{12}	2.428	2.348	.0443	.0356	1.20	1.94
1,2,3-Trimethylbenzene	C_9H_{12}	2.320	2.341	.0467	.0184	1.91	1.75
1,2,4-Trimethylbenzene	C_9H_{12}	2.337	2.337	.0457	.0457	2.81	1.93
1,3,5-Trimethylbenzene	C_9H_{12}	2.445	2.341	.0303	.0431	1.52	1.95
n-Butylbenzene	$C_{10}H_{14}$	2.246	2.376	.0421	.0075	2.78	2.61
Isobutylbenzene	$C_{10}H_{14}$	2.347	2.348	.0407	.0294	2.41	1.80
sec-Butylbenzene	$C_{10}H_{14}$	2.280	2.354	.0443	.0230	1.84	1.59
tert-Butylbenzene	$C_{10}H_{14}$	2.306	2.348	.0395	.0443	3.24	3.06
1,2-Diethylbenzene	$C_{10}H_{14}$	2.249	2.370	.0527	.0147	1.98	1.91
1,3-Diethylbenzene	$C_{10}H_{14}$	2.282	2.334	.0469	.0348	0.91	2.03
1,4-Diethylbenzene	$C_{10}H_{14}$	2.223	2.353	.0537	.0234	1.30	1.05

TABLE 5. *Values of the constants of the Hartmann equation for the 60 API–NBS hydrocarbons*

Compound	Formula	Constants in the equation $n_\lambda = n_\infty + C/(\lambda - \lambda^*)^{1.5}$ at 25°C			
		n_∞	C	λ^*	ρ
PARAFFINS					
n-Heptane	C_7H_{16}	1.37475	0.003341	0.09641	1.49
2-Methylhexane	C_7H_{16}	1.37195	.003307	.09832	1.34
3-Methylhexane	C_7H_{16}	1.37570	.003348	.09649	1.02
3-Ethylpentane	C_7H_{16}	1.38046	.003357	.09544	1.15
2,2-Dimethylpentane	C_7H_{16}	1.36927	.003274	.10022	0.87
2,3-Dimethylpentane	C_7H_{16}	1.37920	.003254	.10122	1.46
2,4-Dimethylpentane	C_7H_{16}	1.36860	.003296	.09907	1.12
3,3-Dimethylpentane	C_7H_{16}	1.37781	.003494	.08991	1.30
2,2,3-Trimethylbutane	C_7H_{16}	1.37620	.003536	.08921	1.22
n-Nonane	C_9H_{20}	1.39243	.003381	.10202	1.68
2,2,5-Trimethylhexane	C_9H_{20}	1.38657	.003389	.10208	0.93
2,4,4-Trimethylhexane	C_9H_{20}	1.39411	.003560	.09624	.37
3,3-Diethylpentane	C_9H_{20}	1.40733	.003566	.09624	1.07
2,2,3,3-Tetramethylpentane	C_9H_{20}	1.41030	.003503	.10282	0.93
2,2,3,4-Tetramethylpentane	C_9H_{20}	1.40146	.003494	.10082	.84
2,2,4,4-Tetramethylpentane	C_9H_{20}	1.39343	.003543	.10116	2.32
2,3,3,4-Tetramethylpentane	C_9H_{20}	1.40880	.003617	.09667	1.28

TABLE 5. *Values of the constants of the Hartmann equation for the 60 API–NBS hydrocarbons*—Continued

Compound	Formula	Constants in the equation $n\lambda = n_\infty + C/(\lambda - \lambda^*)^{1.6}$ at 25°C			
		n_∞	C	λ^*	ρ
ALKYLCYCLOPENTANES					
Ethylcyclopentane	C_7H_{14}	1.40579	0.003778	0.09084	0.62
1,1-Dimethylcyclopentane	C_7H_{14}	1.39941	.003750	.09273	1.15
1,*cis*-2-Dimethylcyclopentane	C_7H_{14}	1.40729	.004306	.07150	3.31
1,*trans*-2-Dimethylcyclopentane	C_7H_{14}	1.39830	.003559	.09830	1.78
1,*cis*-3-Dimethylcyclopentane	C_7H_{14}	1.39687	.003669	.09299	1.10
1, *trans*-3-Dimethylcyclopentane	C_7H_{14}	1.39522	.003559	.09830	2.42
n-Propylcyclopentane	C_8H_{16}	1.41247	.003640	.09991	1.03
Isopropylcyclopentane	C_8H_{16}	1.41210	.003624	.10076	1.22
1-Methyl-1-ethylcyclopentane	C_8H_{16}	1.41300	.003850	.09160	0.80
Ethylcyclopentane	C_8H_{16}	1.41529	.003799	.09320	.84
1,1,2-Trimethylcyclopentane	C_8H_{16}	1.40888	.003755	.09589	.54
1,1,3-Trimethylcyclopentane	C_8H_{16}	1.39691	.003956	.08384	1.45
1, *cis*-2, *trans*-4-Trimethylcyclopentane	C_8H_{16}	1.40481	.003641	.09694	0.68
1, *trans*-2, *cis*-4-Trimethylcyclopentane	C_8H_{16}	1.39683	.003668	.09405	1.17
ALKYLCYCLOHEXANES					
1,1-Dimethylcyclohexane	C_8H_{16}	1.41434	0.004109	0.08469	0.87
n-Propylcyclohexane	C_9H_{18}	1.42266	.003954	.09262	1.92
Isopropylcyclohexane	C_9H_{18}	1.42653	.003919	.09432	0.78
1,1,3-Trimethylcyclohexane	C_9H_{18}	1.41535	.003803	.09917	.84
n-Butylcyclohexane	$C_{10}H_{20}$	1.42646	.003911	.09522	.69
Isobutylcyclohexane	$C_{10}H_{20}$	1.42431	.003877	.09689	1.31
sec-Butylcyclohexane	$C_{10}H_{20}$	1.43238	.003942	.09460	1.54
tert-Butylcyclohexane	$C_{10}H_{20}$	1.43248	.003959	.09563	0.89
ALKYLBENZENES					
Benzene	C_6H_6	1.47421	0.006825	0.13003	0.60
Methylbenzene	C_7H_8	1.47132	.006556	.13046	.20
Ethylbenzene	C_8H_{10}	1.47152	.006276	.12843	3.08
1,2-Dimethylbenzene	C_8H_{10}	1.48037	.006500	.13012	1.48
1,3-Dimethylbenzene	C_8H_{10}	1.47249	.006349	.13126	0.87
1,4-Dimethylbenzene	C_8H_{10}	1.47098	.006393	.13089	1.79
n-Propylbenzene	C_9H_{12}	1.46895	.005968	.12771	1.98
Isopropylbenzene	C_9H_{12}	1.46850	.005898	.12886	2.51
1-Methyl-2-ethylbenzene	C_9H_{12}	1.48026	.006355	.12666	1.73
1-Methyl-3-ethylbenzene	C_9H_{12}	1.47258	.006239	.12745	1.97
1-Methyl-4-ethylbenzene	C_9H_{12}	1.47114	.006126	.13028	1.09
1,2,3-Trimethylbenzene	C_9H_{12}	1.48915	.006406	.13118	1.07
1,2,4-Trimethylbenzene	C_9H_{12}	1.48024	.006337	.13160	1.10
1,3,5-Trimethylbenzene	C_9H_{12}	1.47501	.006249	.13173	0.78
n-Butylbenzene	$C_{10}H_{14}$	1.46761	.005805	.12487	2.92
Isobutylbenzene	$C_{10}H_{14}$	1.46418	.005817	.12448	1.37
sec-Butylbenzene	$C_{10}H_{14}$	1.46803	.005784	.12527	0.84
tert-Butylbenzene	$C_{10}H_{14}$	1.47032	.005838	.12485	2.66
1,2-Diethylbenzene	$C_{10}H_{14}$	1.48014	.006059	.12832	1.18
1,3-Diethylbenzene	$C_{10}H_{14}$	1.47241	.006013	.12731	2.55
1,4-Diethylbenzene	$C_{10}H_{14}$	1.47172	.006001	.12838	1.71

TABLE 6. *Refractive indices at seven wavelengths and three temperatures for 60 API–NBS hydrocarbons*

Wavelength in Angstrom units	Spectral line	Index of refraction														
		20° C	25° C	30° C	20° C	25° C	30° C	20° C	25° C	30° C	20° C	25° C	30° C	20° C	25° C	30° C
		n-Heptane C_7H_{16}			2-Methylhexane C_7H_{16}			3-Methylhexane C_7H_{16}			3-Ethylpentane C_7H_{16}			2,2-Dimethylpentane C_7H_{16}		
6678.1	He_{red}	1.38545	1.38293	1.38041	1.38266	1.38009	1.37752	1.38643	1.38390	1.38137	1.39120	1.38866	1.38612	1.37995	1.37737	1.37[illegible]
6562.8	H_c	1.38572	1.38320	1.38068	1.38293	1.38036	1.37779	1.38671	1.38417	1.38163	1.39147	1.38893	1.38639	1.38023	1.37764	1.37[illegible]
5892.6	Na_D	1.38764	1.38511	1.38258	1.38485	1.38227	1.37969	1.38864	1.38609	1.38354	1.39339	1.39084	1.38829	1.38215	1.37955	1.37[illegible]
5460.7	Hg_e	1.38930	1.38675	1.38420	1.38650	1.38391	1.38132	1.39029	1.38773	1.38517	1.39504	1.39248	1.38992	1.38380	1.38119	1.37[illegible]
5015.7	He_{blue}	1.39149	1.38893	1.38637	1.38869	1.38609	1.38349	1.39249	1.38991	1.38733	1.39723	1.39465	1.39207	1.38601	1.38338	1.38[illegible]
4861.3	H_F	1.39241	1.38984	1.38727	1.38961	1.38700	1.38439	1.39342	1.39083	1.38824	1.39814	1.39556	1.39298	1.38699	1.38435	1.38[illegible]
4358.3	Hg_g	1.39617	1.39357	1.39097	1.39338	1.39075	1.38812	1.39719	1.39457	1.39195	1.40189	1.39929	1.39669	1.39071	1.38805	1.38[illegible]
		2,3-Dimethylpentane C_7H_{16}			2,4-Dimethylpentane C_7H_{16}			3,3-Dimethylpentane C_7H_{16}			2,2,3-Trimethylbutane C_7H_{16}			*n*-Nonane C_9H_{20}		
6678.1	He_{red}	1.38977	1.38728	1.38479	1.37927	1.37666	1.37405	1.38869	1.38621	1.38373	1.38719	1.38469	1.38219	1.40314	1.40084	1.39[illegible]
6562.8	H_c	1.39005	1.38755	1.38505	1.37954	1.37692	1.37430	1.38897	1.38649	1.38401	1.38746	1.38496	1.38246	1.40342	1.40112	1.39[illegible]
5892.6	Na_D	1.39196	1.38945	1.38694	1.38145	1.37882	1.37619	1.39092	1.38842	1.38592	1.38944	1.38692	1.38440	1.40542	1.40311	1.40[illegible]
5460.7	Hg_e	1.39362	1.39110	1.38858	1.38308	1.38044	1.37780	1.39259	1.39008	1.38757	1.39112	1.38858	1.38604	1.40715	1.40482	1.40[illegible]
5015.7	He_{blue}	1.39582	1.39328	1.39074	1.38527	1.38261	1.37995	1.39480	1.39227	1.38974	1.39335	1.39079	1.38823	1.40954	1.40710	1.40[illegible]
4861.3	H_F	1.39674	1.39419	1.39164	1.38618	1.38351	1.38084	1.39572	1.39318	1.39064	1.39428	1.39171	1.38914	1.41041	1.40806	1.40[illegible]
4358.3	Hg_g	1.40054	1.39796	1.39538	1.38993	1.38723	1.38453	1.39948	1.39691	1.39434	1.39807	1.39546	1.39285	1.41437	1.41199	1.40[illegible]
		2,2,5-Trimethylhexane C_9H_{20}			2,4,4-Trimethylhexane C_9H_{20}			3,3-Diethylpentane C_9H_{20}			2,2,3,3-Tetramethylpentane C_9H_{20}			2,2,3,4-Tetramethylpentane C_9H_{20}		
6678.1	He_{red}	1.39743	1.39500	1.39257	1.40510	1.40282	1.40054	1.41816	1.41604	1.41392	1.42122	1.41903	1.41684	1.41236	1.41012	1.40[illegible]
6562.8	H_c	1.39771	1.39528	1.39285	1.40540	1.40311	1.40082	1.41845	1.41633	1.41421	1.42152	1.41933	1.41714	1.41266	1.41041	1.40[illegible]
5892.6	Na_D	1.39972	1.39728	1.39484	1.40745	1.40515	1.40285	1.42051	1.41837	1.41623	1.42360	1.42140	1.41920	1.41472	1.41246	1.41[illegible]
5460.7	Hg_e	1.40143	1.39899	1.39655	1.40920	1.40689	1.40458	1.42226	1.42011	1.41796	1.42540	1.42318	1.42096	1.41648	1.41421	1.41[illegible]
5015.7	He_{blue}	1.40373	1.40128	1.39883	1.41153	1.40921	1.40689	1.42460	1.42243	1.42026	1.42778	1.42555	1.42332	1.41883	1.41655	1.41[illegible]
4861.3	H_F	1.40470	1.40224	1.39978	1.41251	1.41018	1.40785	1.42558	1.42340	1.42122	1.42879	1.42655	1.42431	1.41981	1.41753	1.41[illegible]
4358.3	Hg_g	1.40866	1.40618	1.40370	1.41650	1.41415	1.41180	1.42957	1.42737	1.42517	1.43291	1.43065	1.42839	1.42386	1.42150	1.41[illegible]
		2,2,4,4-Tetramethylpentane C_9H_{20}			2,3,3,4-Tetramethylpentane C_9H_{20}			Ethylcyclopentane C_7H_{14}			1,1-Dimethylcyclopentane C_7H_{14}			1,*cis*-2-Dimethylcyclopentane C_7H_{14}		
6678.1	He_{red}	1.40457	1.40222	1.39987	1.41984	1.41766	1.41548	1.41739	1.41490	1.41241	1.41113	1.40850	1.40587	1.41965	1.41714	1.41[illegible]
6562.8	H_c	1.40487	1.40252	1.40017	1.42016	1.41798	1.41580	1.41769	1.41520	1.41271	1.41144	1.40880	1.40616	1.41997	1.41745	1.41[illegible]
5892.6	Na_D	1.40694	1.40459	1.40224	1.42222	1.42003	1.41784	1.41981	1.41730	1.41479	1.41356	1.41091	1.40826	1.42217	1.41963	1.41[illegible]
5460.7	Hg_e	1.40874	1.40638	1.40402	1.42402	1.42182	1.41962	1.42162	1.41910	1.41658	1.41538	1.41271	1.41004	1.42405	1.42148	1.41[illegible]
5015.7	He_{blue}	1.41111	1.40875	1.40639	1.42638	1.42417	1.42196	1.42401	1.42148	1.41895	1.41778	1.41510	1.41242	1.42649	1.42380	1.42[illegible]
4861.3	H_F	1.41212	1.40975	1.40738	1.42737	1.42515	1.42293	1.42501	1.42247	1.41993	1.41878	1.41609	1.41340	1.42751	1.42490	1.42[illegible]
4358.3	Hg_g	1.41623	1.41385	1.41147	1.43144	1.42920	1.42696	1.42910	1.42653	1.42396	1.42290	1.42018	1.41746	1.43161	1.42895	1.42[illegible]
		1,*trans*-2-Dimethylcyclopentane C_7H_{14}			1,*cis*-3-Dimethylcyclopentane C_7H_{14}			1,*trans*-3-Dimethylcyclopentane C_7H_{14}			*n*-Propylcyclopentane C_8H_{16}			Isopropylcyclopentane C_8H_{16}		
6678.1	He_{red}	1.40963	1.40706	1.40449	1.40836	1.40577	1.40318	1.40657	1.40398	1.40139	1.42382	1.42147	1.41912	1.42339	1.42108	1.41[illegible]
6562.8	H_c	1.40992	1.40735	1.40478	1.40865	1.40606	1.40347	1.40686	1.40427	1.40168	1.42412	1.42177	1.41942	1.42369	1.42138	1.41[illegible]
5892.6	Na_D	1.41200	1.40941	1.40682	1.41074	1.40813	1.40552	1.40894	1.40633	1.40372	1.42626	1.42389	1.42152	1.42582	1.42350	1.42[illegible]
5460.7	Hg_e	1.41377	1.41117	1.40857	1.41250	1.40988	1.40726	1.41071	1.40809	1.40547	1.42809	1.42571	1.42333	1.42716	1.42502	1.42[illegible]
5015.7	He_{blue}	1.41612	1.41351	1.41090	1.41487	1.41223	1.40959	1.41307	1.41044	1.40781	1.43055	1.42814	1.42573	1.43010	1.42775	1.42[illegible]
4861.3	H_F	1.41717	1.41455	1.41193	1.41586	1.41321	1.41056	1.41411	1.41147	1.40883	1.43156	1.42915	1.42674	1.43112	1.42876	1.42[illegible]
4358.3	Hg_g	1.42118	1.41853	1.41588	1.41989	1.41721	1.41453	1.41812	1.41545	1.41278	1.43577	1.43332	1.43087	1.43533	1.43290	1.43[illegible]
		1-Methyl-1-ethylcyclopentane C_8H_{16}			1-Methyl-*cis*-2-ethylcyclopentane C_8H_{16}			1,1,2-Trimethylcyclopentane C_8H_{16}			1,1,3-Trimethylcyclopentane C_8H_{16}			1,*cis*-2,*trans*-4-Trimethylcyclopentane C_8H_{16}		
6678.1	He_{red}	1.42473	1.42233	1.41993	1.42689	1.42451	1.42213	1.42051	1.41806	1.41561	1.40872	1.40626	1.40380	1.41615	1.41374	1.41[illegible]
6562.8	H_c	1.42501	1.42261	1.42021	1.42719	1.42481	1.42243	1.42081	1.41836	1.41591	1.40904	1.40657	1.40410	1.41644	1.41403	1.41[illegible]
5892.6	Na_D	1.42718	1.42476	1.42234	1.42933	1.42695	1.42457	1.42298	1.42051	1.41804	1.41119	1.40870	1.40321	1.41855	1.41612	1.41[illegible]
5460.7	Hg_e	1.42903	1.42660	1.42417	1.43116	1.42878	1.42640	1.42482	1.42234	1.41986	1.41302	1.41051	1.40799	1.42035	1.41791	1.41[illegible]
5015.7	He_{blue}	1.43148	1.42903	1.42657	1.43360	1.43121	1.42882	1.42728	1.42478	1.42228	1.41543	1.41250	1.41037	1.42276	1.42030	1.41[illegible]
4861.3	H_F	1.43251	1.43005	1.42759	1.43461	1.43222	1.42983	1.42830	1.42580	1.42330	1.41644	1.41389	1.41134	1.42376	1.42129	1.41[illegible]
4358.3	Hg_g	1.43671	1.43421	1.43171	1.43877	1.43637	1.43397	1.43251	1.42998	1.42745	1.42053	1.41794	1.41535	1.42787	1.42537	1.42[illegible]

TABLE 6.—*Refractive indices at seven wavelengths and three temperatures for 60 API–NBS hydrocarbons*—Continued

Wavelength in Angstrom units	Spectral line	Index of refraction														
		20° C	25° C	30° C	20° C	25° C	30° C	20° C	25° C	30° C	20° C	25° C	30° C	20° C	25° C	30° C
		1, *trans*-2, *cis*-4-Trimethylcyclopentane C_8H_{16}			1,1-Dimethylcyclohexane C_8H_{16}			*n*-Propylcyclohexane C_9H_{18}			Isopropylcyclohexane C_9H_{18}			1,1,3-Trimethylcyclohexane C_9H_{18}		
6678.1	He_{red}	1.40821	1.40575	1.40329	1.42644	1.42408	1.42172	1.43450	1.43224	1.42998	1.43831	1.43607	1.43383	1.42702	1.42473	1.42244
6562.8	H_α	1.40851	1.40605	1.40359	1.42676	1.42440	1.42204	1.43481	1.43255	1.43029	1.43862	1.43638	1.43414	1.42734	1.42505	1.42276
5892.6	Na_D	1.41060	1.40812	1.40564	1.42900	1.42662	1.42424	1.43705	1.43478	1.43251	1.44087	1.43861	1.43635	1.42955	1.42725	1.42495
5460.7	Hg_e	1.41239	1.40990	1.40741	1.43090	1.42851	1.42612	1.43895	1.43667	1.43439	1.44277	1.44050	1.43823	1.43146	1.42915	1.42684
5015.7	He_{blue}	1.41475	1.41225	1.40975	1.43341	1.43100	1.42859	1.44149	1.43919	1.43689	1.44524	1.44296	1.44068	1.43399	1.43167	1.42935
4861.3	H_F	1.41574	1.41324	1.41074	1.43446	1.43204	1.42962	1.44254	1.44024	1.43794	1.44637	1.44408	1.44179	1.43504	1.43272	1.43040
4358.3	Hg_g	1.41980	1.41727	1.41474	1.43872	1.43627	1.43382	1.44686	1.44454	1.44222	1.45070	1.44839	1.44608	1.43940	1.43706	1.43472
		n-Butylcyclohexane $C_{10}H_{20}$			Isobutylcyclohexane $C_{10}H_{20}$			*sec*-Butylcyclohexane $C_{10}H_{20}$			*tert*-Butylcyclohexane $C_{10}H_{20}$			Benzene C_6H_6		
6678.1	He_{red}	1.43819	1.43600	1.43381	1.43606	1.43382	1.43158	1.44416	1.44198	1.43980	1.44435	1.44215	1.43995	1.49578	1.49262	1.48950
6562.8	H_α	1.43852	1.43632	1.43412	1.43637	1.43413	1.43189	1.44446	1.44228	1.44010	1.44467	1.44247	1.44027	1.49643	1.49327	1.49015
5892.6	Na_D	1.44075	1.43855	1.43635	1.43861	1.43636	1.43411	1.44673	1.44454	1.44235	1.44694	1.44473	1.44252	1.50112	1.49792	1.49478
5460.7	Hg_e	1.44266	1.44045	1.43824	1.44052	1.43826	1.43600	1.44864	1.44644	1.44424	1.44887	1.44666	1.44445	1.50521	1.50197	1.49881
5015.7	He_{blue}	1.44520	1.44298	1.44076	1.44307	1.44080	1.43853	1.45120	1.44899	1.44678	1.45145	1.44923	1.44701	1.51077	1.50748	1.50429
4861.3	H_F	1.44627	1.44404	1.44181	1.44412	1.44185	1.43958	1.45219	1.44998	1.44777	1.45252	1.45030	1.44808	1.51313	1.50982	1.50662
4358.3	Hg_g	1.45061	1.44837	1.44613	1.44849	1.44620	1.44391	1.45664	1.45441	1.45218	1.45693	1.45470	1.45247	1.52302	1.51964	1.51640
		Methylbenzene C_7H_8			Ethylbenzene C_8H_{10}			1,2-Dimethylbenzene C_8H_{10}			1,3-Dimethylbenzene C_8H_{10}			1,4-Dimethylbenzene C_8H_{10}		
6678.1	He_{red}	1.49180	1.48903	1.48619	1.49102	1.44837	1.48569	1.50037	1.49791	1.49531	1.49221	1.48968	1.48704	1.49079	1.48827	1.48558
6562.8	H_α	1.49243	1.48966	1.48682	1.49162	1.48896	1.48628	1.50100	1.49853	1.49593	1.49283	1.49029	1.48765	1.49141	1.48888	1.48619
5892.6	Na_D	1.49693	1.49413	1.49126	1.49588	1.49320	1.49050	1.50545	1.50295	1.50032	1.49722	1.49464	1.49198	1.49582	1.49325	1.49054
5460.7	Hg_e	1.50086	1.49803	1.49514	1.49960	1.49689	1.49418	1.50935	1.50682	1.50417	1.50105	1.49844	1.49577	1.49966	1.49707	1.49434
5015.7	He_{blue}	1.50620	1.50334	1.50041	1.50465	1.50191	1.49918	1.51463	1.51207	1.50940	1.50626	1.50361	1.50092	1.50489	1.50226	1.49951
4861.3	H_F	1.50847	1.50559	1.50265	1.50678	1.50403	1.50129	1.51688	1.51430	1.51161	1.50847	1.50580	1.50311	1.50712	1.50447	1.50172
4358.3	Hg_g	1.51800	1.51506	1.51206	1.51575	1.51295	1.51018	1.52630	1.52366	1.52093	1.51777	1.51503	1.51231	1.51644	1.51373	1.51094
		n-Propylbenzene C_9H_{12}			Isopropylbenzene C_9H_{12}			1-Methyl-2-ethylbenzene C_9H_{12}			1-Methyl-3-ethylbenzene C_9H_{12}			1-Methyl-4-ethylbenzene C_9H_{12}		
6678.1	He_{red}	1.48742	1.48494	1.48248	1.48688	1.48436	1.48194	1.49968	1.49723	1.49479	1.49179	1.48928	1.48678	1.49021	1.48768	1.48525
6562.8	H_α	1.48799	1.48550	1.48303	1.48744	1.48492	1.48250	1.50028	1.49783	1.49539	1.49238	1.48987	1.48737	1.49079	1.48826	1.48583
5892.6	Na_D	1.49202	1.48951	1.48702	1.49145	1.48890	1.48646	1.50456	1.50208	1.49963	1.49660	1.49406	1.49154	1.49500	1.49244	1.48999
5460.7	Hg_e	1.49555	1.49301	1.49051	1.49498	1.49239	1.48993	1.50828	1.50578	1.50332	1.50028	1.49771	1.49518	1.49866	1.49608	1.49361
5015.7	He_{blue}	1.50033	1.49776	1.49523	1.49970	1.49711	1.49462	1.51333	1.51080	1.50833	1.50526	1.50266	1.50011	1.50364	1.50104	1.49855
4861.3	H_F	1.50235	1.49977	1.49723	1.50171	1.49911	1.49661	1.51546	1.51292	1.51044	1.50738	1.50476	1.50221	1.50576	1.50314	1.50064
4358.3	Hg_g	1.51083	1.50820	1.50562	1.51018	1.50753	1.50499	1.52442	1.52183	1.51933	1.51623	1.51356	1.51098	1.51463	1.51197	1.50943
		1,2,3-Trimethylbenzene C_9H_{12}			1,2,4-Trimethylbenzene C_9H_{12}			1,3,5-Trimethylbenzene C_9H_{12}			*n*-Bucylbenzene $C_{10}H_{14}$			Isobutylbenzene $C_{10}H_{14}$		
6678.1	He_{red}	1.50891	1.50650	1.50412	1.49986	1.49742	1.49498	1.49446	1.49195	1.48951	1.48537	1.48303	1.48064	1.48206	1.47962	1.47721
6562.8	H_α	1.50952	1.50711	1.50473	1.50047	1.49803	1.49559	1.49507	1.49255	1.49011	1.48591	1.48357	1.48118	1.48260	1.48016	1.47774
5892.6	Na_D	1.51393	1.51150	1.50911	1.50484	1.50237	1.49990	1.49937	1.49684	1.49437	1.48979	1.48742	1.48502	1.48646	1.48400	1.48157
5460.7	Hg_e	1.51778	1.51533	1.51293	1.50867	1.50618	1.50369	1.50314	1.50059	1.49810	1.49315	1.49076	1.48836	1.48983	1.48735	1.48490
5015.7	He_{blue}	1.52303	1.52055	1.51814	1.51386	1.51134	1.50892	1.50826	1.50569	1.50318	1.49770	1.49529	1.49288	1.49438	1.49187	1.48941
4861.3	H_F	1.52524	1.52276	1.52034	1.51607	1.51354	1.51101	1.51043	1.50786	1.50534	1.49963	1.49721	1.49480	1.49631	1.49379	1.49132
4358.3	Hg_g	1.53459	1.53206	1.52962	1.52536	1.52278	1.52020	1.51957	1.51697	1.51440	1.50770	1.50523	1.50281	1.50437	1.50181	1.49931
		sec-Butylbenzene $C_{10}H_{14}$			*tert*-Butylbenzene $C_{10}H_{14}$			1,2-Diethylbenzene $C_{10}H_{14}$			1,3-Diethylbenzene $C_{10}H_{14}$			1,4-Diethylbenzene $C_{10}H_{14}$		
6678.1	He_{red}	1.48580	1.48342	1.48102	1.48822	1.48583	1.48338	1.49877	1.49640	1.49400	1.49089	1.48850	1.48609	1.49017	1.48783	1.48542
6562.8	H_α	1.48633	1.48395	1.48154	1.48877	1.48637	1.48392	1.49935	1.49698	1.49458	1.49146	1.48907	1.48666	1.49075	1.48840	1.48599
5892.6	Na_D	1.49020	1.48779	1.48537	1.49266	1.49024	1.48776	1.50346	1.50106	1.49865	1.49552	1.49310	1.49067	1.49483	1.49245	1.49003
5460.7	Hg_e	1.49356	1.49113	1.48870	1.49604	1.49360	1.49110	1.50706	1.50463	1.50221	1.49906	1.49662	1.49417	1.49838	1.49598	1.49355
5015.7	He_{blue}	1.49812	1.49566	1.49322	1.50062	1.49816	1.49564	1.51192	1.50946	1.50703	1.50385	1.50138	1.49891	1.50321	1.50077	1.49832
4861.3	H_F	1.50004	1.49757	1.49512	1.50256	1.50009	1.49755	1.51398	1.51151	1.50908	1.50588	1.50340	1.50092	1.50525	1.50280	1.50035
4358.3	Hg_g	1.50810	1.50559	1.50312	1.51036	1.50815	1.50557	1.52265	1.52012	1.51767	1.51441	1.51188	1.50936	1.51384	1.51133	1.50885

TABLE 7. *Calculated values of the specific dispersion for 60 API–NBS hydrocarbons*

Temperature	$10^4(n_F-n_C)/d$	$10^4(n_E-n_D)/d$	$10^4(n_F-n_C)/d$	$10^4(n_E-n_D)/d$	$10^4(n_F-n_C)/d$	$10^4(n_E-n_D)/d$	$10^4(n_F-n_C)/d$	$10^4(n_E-n_D)/d$	$10^4(n_F-n_C)/d$	$10^4(n_E-n_D)/d$
°C	*n*-Heptane		2-Methylhexane		3-Methylhexane		3-Ethylpentane		2,2-Dimethylpentane	
20	97.8	124.8	98.4	125.7	97.7	124.4	95.5	121.7	100.3	127.0
25	97.7	124.5	98.5	125.7	97.5	124.2	95.5	121.8	100.2	127.0
30	97.6	124.2	98.5	125.8	97.4	123.9	95.6	121.8	100.1	126.9
	2,3-Dimethylpentane		2,4-Dimethylpentane		3,3-Dimethylpentane		2,2,3-Trimethylbutane		*n*-Nonane	
20	96.2	123.4	98.7	126.0	97.4	123.5	98.8	125.0	97.4	124.7
25	96.1	123.2	98.6	125.8	97.1	123.2	98.4	124.5	97.2	124.4
30	96.0	122.9	98.5	125.6	96.8	123.0	98.0	124.0	97.0	124.1
	2,2,5-Trimethylhexane		2,4,4-Trimethylhexane		3,3-Diethylpentane		2,2,3,3-Tetramethylpentane		2,2,3,4-Tetramethylpentane	
20	98.8	126.4	98.2	125.0	94.6	120.2	96.1	123.0	96.8	123.7
25	99.0	126.6	98.2	125.0	94.3	120.0	95.9	122.8	96.8	123.8
30	99.1	126.7	98.2	125.0	93.9	119.8	95.7	122.6	96.9	123.9
	2,2,4,4-Tetramethylpentane		2,3,3,4-Tetramethylpentane		Ethylcyclopentane		1,1-Dimethylcyclopentane		1,*cis*-2-Dimethylcyclopentane	
20	100.8	129.1	95.5	122.2	95.5	121.2	97.3	123.8	97.6	122.2
25	101.0	129.4	95.4	122.1	95.4	121.1	97.2	123.6	97.0	121.3
30	101.3	129.7	95.4	122.0	95.3	121.0	97.1	123.4	96.4	120.4
	1,*trans*-2-Dimethylcyclopentane		1,*cis*-3-Dimethylcyclopentane		1,*trans*-3-Dimethylcyclopentane		*n*-Propylcyclopentane		Isopropylcyclopentane	
20	96.5	122.2	96.3	122.2	97.3	123.2	95.8	122.5	95.7	122.5
25	96.4	122.1	96.0	122.0	97.3	123.2	95.6	122.1	95.5	122.2
30	96.3	122.0	95.8	121.8	97.2	123.1	95.3	121.7	95.4	121.9
	1-Methyl-1-ethylcyclopentane		1-Methyl-*cis*-2-ethylcyclopentane		1,1,2-Trimethylcyclopentane		1,1,3-Trimethylcyclopentane		1,*cis*-2,*trans*-4-Trimethylcyclopentane	
20	96.0	122.0	94.5	120.2	97.0	123.4	98.9	124.8	95.9	122.1
25	95.8	121.7	94.9	120.6	96.9	123.3	98.4	124.2	95.6	121.8
30	95.5	121.3	95.2	121.0	96.7	123.2	97.9	123.6	95.4	121.6
	1,*trans*-2,*cis*-4-Trimethylcyclopentane		1,1-Dimethylcyclohexane		*n*-Propylcyclohexane		Isopropylcyclohexane		1,1,3-Trimethylcyclohexane	
20	96.8	123.1	98.6	124.5	97.4	123.6	96.6	122.5	98.9	126.5
25	96.8	123.1	98.4	124.2	97.4	123.6	96.5	122.5	99.0	126.6
30	96.8	123.2	98.1	124.0	97.4	123.6	96.3	122.5	99.1	126.7
	n-Butylcyclohexane		Isobutylcyclohexane		*sec*-Butylcyclohexane		*tert*-Butylcyclohexane		Benzene	
20	97.0	123.4	97.4	124.2	95.1	121.9	96.6	122.9	190.0	249.1
25	97.0	123.4	97.5	124.3	95.1	121.9	96.8	123.2	189.4	248.6
30	97.1	123.5	97.6	124.4	95.2	122.0	97.0	123.6	189.6	248.9
	Methylbenzene		Ethylbenzene		1,2-Dimethylbenzene		1,3-Dimethylbenzene		1,4-Dimethylbenzene	
20	185.0	243.0	174.9	229.2	180.4	236.9	181.0	237.8	182.4	239.5
25	184.7	242.7	174.7	228.9	180.0	236.4	180.4	237.1	182.0	239.0
30	184.6	242.5	174.9	229.3	179.8	236.3	180.7	237.6	182.2	239.3

TABLE 7. *Calculated values of the specific dispersion for 60 API–NBS hydrocarbons*—Continued

Temperature	$10^4(n_F-n_C)/d$	$10^4(n_g-n_D)/d$	$10^4(n_F-n_C)/d$	$10^4(n_g-n_D)/d$	$10^4(n_F-n_C)/d$	$10^4(n_g-n_D)/d$	$10^4(n_F-n_C)/d$	$10^4(n_g-n_D)/d$	$10^4(n_F-n_C)/d$	$10^4(n_g-n_D)/d$
°C	*n*-Propylbenzene		Isopropylbenzene		1-Methyl-2-ethylbenzene		1-Methyl-3-ethylbenzene		1-Methyl-4-ethylbenzene	
20	166.6	218.2	165.6	217.3	172.4	225.5	173.5	227.1	173.8	227.9
25	166.4	217.9	165.5	217.2	172.1	225.3	173.0	226.6	173.6	227.9
30	166.3	217.9	165.3	217.1	172.5	225.8	173.3	227.0	173.6	227.9
	1,2,3-Trimethylbenzene		1,2,4-Trimethylbenzene		1,3,5-Trimethylbenzene		*n*-Butylbenzene		Isobutylbenzene	
20	175.8	231.0	178.1	234.3	177.5	233.5	159.5	208.2	160.7	209.9
25	175.8	230.9	177.9	234.1	177.8	233.8	159.3	208.0	160.5	210.0
30	176.1	231.4	177.7	233.9	177.7	233.7	159.8	208.8	160.7	209.9
	sec-Butylbenzene		tert-Butylbenzene		1,2-Diethylbenzene		1,3-Diethylbenzene		1,4-Diethylbenzene	
20	159.0	207.6	159.1	207.7	166.2	218.1	166.9	218.6	168.2	220.5
25	158.7	207.5	159.1	207.7	165.9	217.6	166.6	218.4	167.8	220.1
30	159.0	207.8	158.8	207.5	166.3	218.1	166.6	218.4	168.1	220.4

V. Discussion

Figure 3 gives, for the several normal alkylbenzenes measured, plots of the values of the constants n_∞ and C in relation to the number of carbon atoms in the normal alkyl radical. It appears that these relations are such that, when one sufficiently higher member of the series, such as *n*-decylbenzene, is evaluated, it will be possible to set up the complete equation for the intermediate members of the series as well as for some members higher than *n*-decylbenzene, with a knowledge only of the refractive index at one wavelength, as n_D.

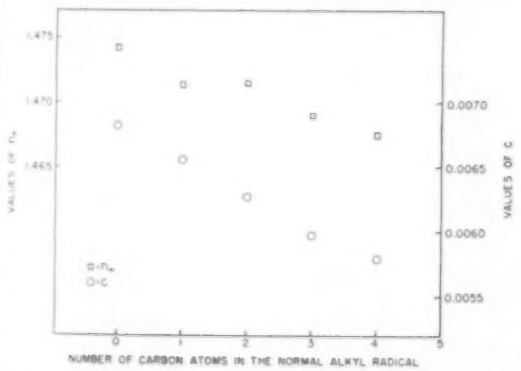

FIGURE 3. *Values of the constants ,n_∞ and C, of the Hartman equation, as a function of the number of carbon atoms in the normal alkyl radical of five alkylbenzenes.*

It is planned to do this for the series of normal alkylbenzenes, normal monoolefins (l-alkenes), normal paraffins, normal alkylcyclopentanes, and normal alkylcyclohexanes.

Grateful acknowledgement is made to Frederick D. Rossini for his many suggestions in the course of the investigation and in the preparation of this report.

VI. References

[1] G. B. Arnold and L. Donn, Anal. Chem. **19,** 666 (1947).
[2] A. F. Forziati and F. D. Rossini, J. Research NBS **43,** 473 (1949) RP 2038.
[3] A. R. Glasgow, Jr., E. T. Murphy, C. B. Willingham, and F. D. Rossini, J. Research NBS **37,** 141 (1946) RP1734.
[4] A. J. Streiff, E. T. Murphy, V. A. Sedlak, C. B. Willingham, and F. D. Rossini, J. Research NBS **37,** 331 (1946) RP1752.
[5] A. J. Streiff, E. T. Murphy, J. C. Cahill, H. F. Flanagan, V. A. Sedlak, C. B. Willingham, and F. D. Rossini, J. Research NBS **38,** 53 (1947) RP1760.
[6] A. J. Streiff, E. T. Murphy, J. C. Zimmerman, L. F. Soule, V. A. Sedlak, C. B. Willingham, and F. D. Rossini, J. Research NBS **39,** 321 (1947) RP1833.
[7] A. J. Streiff, J. C. Zimmerman, L. F. Soule, M. T. Butt, V. A. Sedlak, C. B. Willingham, and F. D. Rossini, J. Research NBS **41,** 323 (1948) RP1929.
[8] L. W. Tilton and H. L. Gurewitz, NBS, private communication.

WASHINGTON, November 4, 1949.

827106—50——4

U. S. Department of Commerce
National Bureau of Standards

Research Paper RP2086
Volume 44, April 1950

Part of the Journal of Research of the National Bureau of Standards

Heats of Combustion and Formation of Cellulose and Nitrocellulose (Cellulose Nitrate)

By Ralph S. Jessup and Edward J. Prosen

This paper gives the results of bomb calorimetric measurements of heats of combustion at 30° C of one sample of cellulose and four samples of nitrocellulose from cotton linters, and of one sample of cellulose and four samples of nitrocellulose from wood pulp. The results have been combined with values for the heats of formation of carbon dioxide and water to obtain values of heats of formation of the celluloses and nitrocelluloses. Empirical equations are given expressing heat of combustion and heat of formation of the nitrocelluloses as functions of nitrogen content.

I. Introduction

The work described in this paper was done at the request of the National Defense Research Committee, and the results were originally reported in their Armor and Ordnance Report No. A-285 (OSRD No. 3932).

The data presented in this paper differ from those given in the above report in the following respects: (1) the results are now expressed in terms of the absolute joule instead of the international joule as the fundamental energy unit; (2) the results have been reduced to the basis that all gases involved in the reactions discussed are in the thermodynamic state of unit fugacity instead of the state of the real gases at atmospheric pressure.

II. Materials

The materials whose heats of combustion have been determined were made available to the National Bureau of Standards through arrangements made by the National Defense Research Committee with the Office of the Chief of Ordnance, War Department.

The lots of cellulose from cotton linters and wood pulp were obtained from the Hercules Powder Co., Radford Ordnance Works, Radford, Va. For the nitrocellulose, the manufacturer, material nitrated, and the nitrogen contents were as follows:

Lot No.	Source of cellulose	Nitrogen	Manufacturer
		Percent	
A 480181	Cotton linters	13.42	Hercules Powder Co., Radford Ordnance Works, Radford Va.
A 480387	do	12.62	
BPA 1963 HRS1	Wood pulp	13.36	
BPA 1964 HRS7	do	12.53	
403-74-2	Cotton linters	12.14	Hercules Powder Co., Parlin, N. J.
416-50	do	11.49	
403-74-1	Wood pulp	12.12	
416-49	do	11.74	

The analyses for nitrogen were made by the Hercules Powder Co. The samples of cellulose and nitrocellulose were regular plant samples. Because of the urgent need for the data, and as the heats of combustion of the actual plant samples were desired, no attempt was made to purify the samples further.

III. Preparation and Weighing of Samples

The following procedure of preparation and weighing of the samples was followed. A batch of cellulose or nitrocellulose sufficiently large to serve for all the experiments on that sample was placed in a desiccator, which was evacuated until the material seemed dry and fluffy. Then portions about 10 percent larger than the amount needed for an experiment, about 2 g, were roughly weighed out and placed in separate beakers. These portions were then wetted with distilled water and were compressed into tight pellets in a pellet press. The pellets then contained approximately 20 to 30 percent of water. These pellets were placed in separate weighing bottles having ground-glass necks and evacuated in a desiccator for about 3 to 8 hr. The bottles were then placed in an oven, kept at 100° C for 1 hr, cooled in a desiccator, stoppered with their ground-glass stoppers, and weighed against a tare (an empty weighing bottle of the same size). They were again placed in the oven at 100° C for intervals of ½ hr until constant weight (within about 0.1 mg) was obtained. This was usually reached within about 2 hr in the oven at 100° C. About 10 percent of water, an amount that was found to produce the best conditions for burning the samples in the bomb, was added to the pellets, and the pellets were transferred from the weighing bottles to the platinum crucible in which they were to be burned. The weighing bottles, together with any particles of sample left in them, were put in the oven at 100° C for 1 hr and reweighed against the tare. From these weighings the weight of dry sample was obtained.

All weights were corrected to the vacuum basis using the factor 1.00080, obtained by assuming a value of 1.25 g/ml for the density of dry cellulose and nitrocellulose.

IV. Apparatus and Method for Measurements of Heats of Combustion

Measurements of heats of combustion were made by burning weighed samples of the material in oxygen in a constant-volume bomb that was part of a calorimetric system described elsewhere [1, 2, 3].[1] The bomb was made of a corrosion-resistant alloy (illium) and had a capacity of 0.380 liter. Two types of experiments were made. In one of these a measured quantity of energy was supplied to the calorimetric system, and the resulting rise in temperature was observed. In the other type of experiment a weighed sample of cellulose, or nitrocellulose, was burned in the bomb, the resulting rise in temperature was observed, and the mass of carbon dioxide formed was determined. The first type of experiment gives the energy equivalent (effective heat capacity) of the calorimetric system, and when the energy equivalent is known, the temperature rise in the second type of experiment is a measure of the heat produced by combustion [4, 5]. For each experiment the mass of the dry sample of material burned, the mass of carbon dioxide formed in combustion in the bomb, and the mass of carbon dioxide formed in subsequent oxidation of gaseous products of incomplete combustion were determined. The mass of carbon dioxide formed by oxidation of the products of combustion was usually 0.01 or 0.02 percent of the mass formed in combustion in the bomb. Correction for incomplete combustion was made on the assumption that the only product of the incomplete combustion was carbon monoxide. The details of the methods used have been described elsewhere [3, 6].

In connection with the correction for the heat of formation of nitric acid in the bomb, the question arose as to whether some nitrous acid might also be formed, especially when the nitrocelluloses were burned in the bomb. To answer this question, tests for nitrous acid were made by W. S. Clabaugh[2] on the washings from the bomb after each of four combustions, two of benzoic acid and two of nitrocellulose. The air initially in the bomb was flushed out with oxygen before burning the two samples of nitrocellulose and before burning one of the samples of benzoic acid but was not flushed out in the case of the second sample of benzoic acid. The amount of nitric acid formed in the second combustion of benzoic acid was, therefore, several times that formed in the first. The amount of nitrous acid found did not exceed 0.5 percent of the total acid formed in any of these experiments. The error introduced into the results of heat of combustion measurements by assuming all the acid to be nitric acid is entirely negligible.

[1] Figures in brackets indicate the literature references at the end of this paper.

[2] Chemistry Division of the National Bureau of Standards.

V. Calibration of Calorimeter

The energy equivalent of the calorimeter for the temperature interval 28.5° to 30° C was determined by burning NBS Standard Sample 39f of benzoic acid in the bomb, using the value 26433.8 absolute joules per gram mass (weight in vacuum), recently obtained in this laboratory [3, 9, 10], for the heat of combustion of this material under the conditions of the standard bomb process at 25° C. Appropriate corrections were made to take account of differences between the actual and standard bomb processes. The results of these calibration experiments are as follows: Series I, five experiments, energy equivalent 13862.6±2.1 (standard deviation of mean) joules per deg C; Series II, six experiments, energy equivalent 13833.9±1.2 (sdm) joules per deg C.

These values of energy equivalent are for the calorimeter containing the same mass of water as in the experiments on the nitrocelluloses, and with the bomb containing 1 g of water and oxygen under a pressure of 30 atm at 30° C. In the measurements on the nitrocelluloses the values used for the energy equivalent differed from the mean values given above by two small corrections, one for the heat capacity of the charge of nitrocellulose and one for the heat capacity of the oxygen in the bomb in excess of that required to fill it to 30 atm at 30° C.

The mean value of the energy equivalent obtained in Series I was used in calculating the results of measurements on the samples of nitrocellulose made from cotton linters and containing 11.49 percent and 12.14 percent of nitrogen. After the measurements on these samples were completed, the insulation of the firing electrode in the bomb failed, and the necessary repairs involved some change in the heat capacity of the bomb. The calorimeter was therefore recalibrated with the repaired bomb. The calibration experiments of the second series were made under the same conditions as those of the first, except that the calorimeter contained a smaller amount of water in the second series. The mean value of energy equivalent obtained in Series II was used in calculating the results of all measurements of heat of combustion, except those on the two samples of nitrocellulose just mentioned.

VI. Calorimetric Experiments on Cellulose and Nitrocellulose

1. Measurements of Heat of Wetting

Since the samples were wet when ignited in the bomb, the observed heat produced by combustion of each sample was lower than that for the dry sample by an amount equal to the heat of wetting of the dry sample with the amount of water added to it. In order to obtain data for correcting the observed heats of combustion for this effect, measurements were made of the heats of wetting of the various materials.

The method used was similar to that described by Katz [7]. Samples of 2 to 5 g of each cellulose and nitrocellulose were placed in weighed glass tubes of about 12-mm inside diameter, one end of which was drawn down to a fine capillary and sealed. The samples were then dried in vacuum (residual pressure less than 10^{-4} mm of mercury) until no water could be detected with the McLeod gage after the vacuum pump had been shut off for several hours. Dry air was then admitted to the vacuum space, and the tubes were removed, corked immediately, and weighed.

To determine the heat of complete wetting, a tube containing dry material was immersed in the water of a calorimeter with the sealed end down and the open end projecting 2 or 3 cm above the top of the calorimeter jacket. The top of the sample of material in the tube was 6 cm or more below the surface of the water in the calorimeter. The temperature of the water in the calorimeter was slightly lower than that of the jacket, so that there was no heat transfer by evaporation of water from the calorimeter and condensation on the jacket. After sufficient time had elapsed for the attainment of a steady state, a series of readings of calorimeter temperature and corresponding time was made. The fine capillary at the bottom of the glass tube was then broken by pressing it against the bottom of the calorimeter vessel, permitting water to rise in the tube and wet the material contained therein. Readings of time and temperature were continued for about 10 min after the rate of temperature change had become constant. Similar measurements were made on samples to which small known amounts of water had been added after drying and weighing.

The results of the measurements of heat of wetting of the completely dry materials are given in table 1, together with values calculated for the nitrocelluloses from the empirical equation:

$$Q = 93.20 - 671f, \quad (0.115 \leqq f \leqq 0.135),$$

where Q is heat of wetting in joules per gram, and f is the mass fraction of nitrogen in the sample.

TABLE 1. *Values for heats of wetting of samples of dry cellulose and nitrocellulose*

Source of cellulose	Nitrogen content	Heat of wetting		Observed minus calculated
		Observed	Calculated	
	Percent	*j/g*	*j/g*	*j/g*
Cotton linters	0.00	47.7		
Do	.00	45.9		
Wood pulp	.00	59.3		
Do	.00	58.6		
Cotton linters	11.49	16.5	16.1	+0.4
Do	11.49	16.6	16.1	+.5
Do	12.14	11.7	11.7	.0
Do	12.62	8.5	8.5	.0
Do	13.42	3.8	3.2	+.6
Wood pulp	11.74	14.9	14.4	+.5
Do	11.74	13.7	14.4	−.7
Do	12.12	11.2	11.9	−.7
Do	12.53	8.7	9.1	−.4
Do	13.36	3.4	3.6	−.2

The results of measurements on samples containing small amounts of water are shown graphically in figure 1, where the abscissa is the mass of water per gram of dry material, and the ordinate is the difference between the heats of wetting of the dry and wet materials expressed as a fraction of the heat of wetting of the dry material. The solid curve in figure 1 represents data calculated from Katz's [7] equation for cellulose. The dashed curve is drawn through the points representing the experimental data obtained in this investigation.

2. Results of Measurements of Heats of Combustion

The results of the measurements of heats of combustion at 30° C are summarized in table 2. The observed values of $-\Delta U_B$, the heat of combustion under the conditions of the bomb process, were corrected for heat of wetting, and reduced, in accordance with the procedure outlined by Washburn [8], to the corresponding values of $-\Delta U_c^\circ$, the decrease in internal energy accompanying the combustion reaction when each of the gaseous reactants and products is in its thermodynamic standard state of unit fugacity at 30° C. The correction for heat of wetting was made on the basis of the observed value for heat of wetting of the dry material, and the data represented by the dashed curve of figure 1.

In column 4 of table 2 are given values of the ratio of carbon dioxide formed in combustion in the bomb and in oxidation of products of incomplete combustion to that calculated from the masses of dry samples, based on the assumption that they were pure cellulose or nitrocellulose represented by the formula $C_6H_{10-x}O_5(NO_2)_x$. If f is the mass fraction of nitrogen in the sample and m the mass of sample burned, then the calculated mass of carbon dioxide was taken as $(1.62859 - 5.23177f)m$. The values of atomic weights used in this and other calculations connected with this report are O = 16.000, C = 12.010, H = 1.0080, and N = 14.008.

3. Further results derivable from experimental data

It will be seen from table 2 that the average values of the ratio (carbon dioxide formed : carbon dioxide calculated) are less than unity by amounts ranging from 0.4 to 0.9 percent, indicating that the samples probably contained at least the corresponding amounts of impurity. If it is assumed

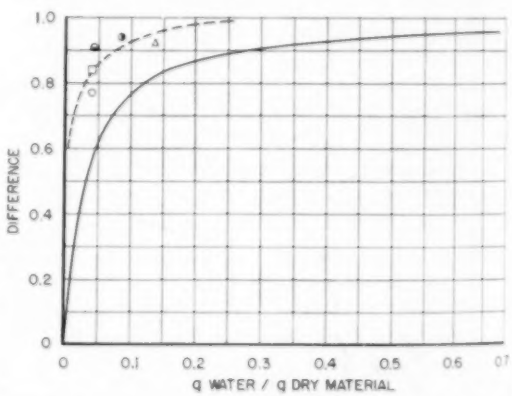

FIGURE 1. *Results of measurements of heat of wetting for samples containing small amounts of water.*

Abscissa, grams of water per gram of dry material. Ordinate, difference between heats of wetting of dry and wet materials expressed as a fraction of the heat of wetting of the dry material. Solid curve, Katz's data on cellulose. Dotted curve drawn to represent data obtained in present work. △, Cellulose from cotton linters; ○, nitrocellulose from wood pulp, 11.74 percent nitrogen; □, nitrocellulose from wood pulp, 12.12 percent nitrogen; ◑, nitrocellulose from cotton linters, 11.49 percent nitrogen; ◒, nitrocellulose from cotton linters, 12.14 percent nitrogen.

TABLE 2. *Experimental data on the heats of combustion* [a]

Source of cellulose	Nitrogen content	Number of experiments	Ratio of carbon dioxide formed to carbon dioxide calculated	Heat of combustion based on the mass of sample burned		Heat of combustion based on the mass of carbon dioxide formed	
				$-\Delta U_B$	$-\Delta U_c^\circ$	$-\Delta U_B$	$-\Delta U_c^\circ$
	Percent			*j/g*	*j/g*	*j/g CO_2*	*j/g CO_2*
Cotton linters	0.00	4	0.99576 ±0.00020 [a]	17320.9	17352.6 ±2.3 [a]	10680.8	10700.4 ±2.9 [a]
Wood pulp	.00	4	[b] .99590 ±0.00076	17343.1	[b] 17385.9 ±18.9	10693.8	10720.3 ±4.4
Cotton linters	11.49	5	[c] .99577 ±0.00013	10667.9	[c] 10667.6 ±3.1	10428.7	10428.8 ±2.4
Do	12.14	3	.99412 ±0.00025	10277.3	10272.7 ±2.6	10406.1	10401.4 ±2.4
Do	12.62	4	[b] .99489 ±0.00014	10013.6	10006.3 ±3.1	10393.0	[b] 10385.5 ±3.3
Do	13.42	4	.99407 ±0.00019	9538.8	9526.6 ±1.9	10357.1	10343.9 ±2.3
Wood pulp	11.74	4	.99338 ±0.00059	10506.3	10504.1 ±7.6	10426.4	10424.2 ±2.2
Do	12.12	4	.99238 ±0.00019	10279.2	10273.9 ±2.8	10415.5	10410.0 ±2.2
Do	12.53	4	.99162 ±0.00015	10029.2	10021.9 ±2.6	10394.0	10386.5 ±1.9
Do	13.36	4	.99079 ±0.00023	9540.1	9527.7 ±2.2	10357.9	10344.6 ±2.1

[a] The values following the ± sign in this table are the standard deviations of the mean.
[b] Mean of three experiments.
[c] Mean of two experiments.

that all the impurity in the samples was inert material that did not enter into the combustion reaction in any way, then the values given in table 2 based on the mass of carbon dioxide formed should be the heats of combustion of pure cellulose and pure nitrocellulose. Under this assumption, however, the values of the nitrogen contents must be adjusted, due to the fact that the nitrogen content of a nitrocellulose containing inert impurity is higher than that reported for the impure sample. If we let R be the ratio (carbon dioxide formed : carbon dioxide calculated) (see table 2), f be the mass fraction of nitrogen as reported (see table 2), and i gram be the amount of impurity per $(1-i)$ gram of $C_6H_{10-x}O_5(NO_2)_x$, then it can be shown that

$$1-i=R+3.212\,5f(1-R).$$

The corrected value, f', of the mass fraction of nitrogen in the nitrocellulose is

$$f'=\frac{f}{1-i}.$$

The derived values for the heats of combustion and formation of cellulose and nitrocellulose, together with the corrected nitrogen contents, are given in table 3. The proper values for the heats of formation of gaseous carbon dioxide and liquid water at 30° C were taken from reference [19].

It was found that the data on the heats of combustion of the nitrocellulose could be represented by linear equations expressing the heat of combustion at 30° C as a function of the corrected nitrogen content. The following equations, which were derived by the method of least squares, represent the heats of combustion per gram of nitrocellulose within about 0.03 percent. For nitrocellulose from cotton linters:

$$\Delta H_c^\circ=-4169.32+14069f' \text{ cal/g } (0.115\leqq f'\leqq 0.135). \quad (1)$$

For nitrocellulose from wood pulp:

$$\Delta H_c^\circ=-4186.36+14200f' \text{ cal/g } (0.115\leqq f'\leqq 0.135), \quad (2)$$

where f' is the corrected fraction of nitrogen in the nitrocellulose.

TABLE 3. *Derived data for cellulose and nitrocellulose*

Source of cellulose	Corrected nitrogen content	$-\Delta U_c^\circ$ at 30° C		$-\Delta H_c^\circ$ at 30° C	$-\Delta H_f^\circ$ at 30° C
	Percent	*j/g CO_2*	*cal/g nitrocellulose*	*cal/g nitrocellulose*	*cal/g nitrocellulose*
Cotton linters	0.00	10700.4 ±2.9 [a]	4165.0	4165.0	1421.9
Wood pulp	.00	10720.3 ±4.4	4172.8	4172.8	1413.2
Cotton linters	11.52	10428.8 ±2.4	2557.0	2548.3	689.5
Do	12.18	10401.4 ±2.4	2464.0	2454.8	647.9
Do	12.66	10385.5 ±3.3	2398.7	2389.1	617.0
Do	13.46	10343.9 ±2.3	2284.7	2274.5	567.0
Wood pulp	11.79	10424.2 ±2.2	2521.0	2512.1	671.2
Do	12.18	10410.0 ±2.2	2466.9	2457.8	646.3
Do	12.59	10386.5 ±1.9	2407.3	2397.8	621.5
Do	13.43	10344.6 ±2.1	2289.2	2279.1	569.4

[a] Standard deviation of the mean.

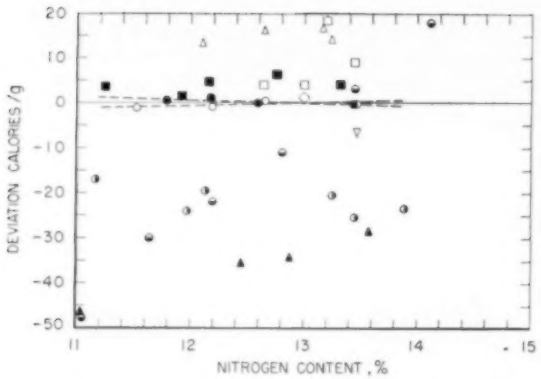

FIGURE 2. *Deviations of values of heat of combustion ($-\Delta H_c^\circ$) derived from results of various observers from eq 3 of the present work.*

○, Present work, nitrocellulose from cotton linters (30° C); ●, present work, nitrocellulose from wood pulp (30° C); ▽, Sarrau and Vieille (15° C) [11]; ◇, Kast [12]; ■, Muraour [13]; ◑, Prettre (20° C) [14]; ▲, Kozo Tomioka [15]; ◒, Schmidt and Becker [16]; □, Milus (25° C) [17]; △, Taylor and Hall (17° C) [18].

If we consider all the nitrocelluloses together, the following equation represents the data within about 0.05 percent:

$$\Delta H_c^\circ = -4176.70 + 14126f' \text{ cal/g } (0.115 \leqq f' \leqq 0.135). \quad (3)$$

Similar equations can be derived expressing $\Delta Hf°$ at 30° C as functions of nitrogen content. Thus the following equation, based on the data on all the nitrocelluloses, represents the values given in table 3 on the nitrocelluloses within about 1.3 cal/g:

$$\Delta H_f^\circ = -5896.88 + 26178f' \text{ cal/g } (0.115 \leqq f' \leqq 0.135). \quad (4)$$

The data on the nitrocelluloses are plotted in figure 2. The abcissa is the nitrogen content of the nitrocellulose, while the ordinate is the deviation from the heat of combustion ΔH_c° given by eq 3. The dotted lines represent eq 1 and 2.

Although there were significant differences between the heats of combustion of cellulose from cotton linters and from wood pulp, 0.18 percent, and between the nitrocelluloses from cotton linters and from wood pulp, maximum 0.1 percent, it is felt that this probably does not indicate a real difference in the heats of combustion of pure cellulose or of nitrocellulose from cotton linters or wood pulp. Rather, the differences are an indication that the impurities in the materials made some contribution to the heat of combustion.

It will be noted that the nitrogen contents of the nitrocelluloses investigated are all intermediate between the nitrogen contents of dinitrocellulose, $f'=0.1111$, and trinitrocellulose, $f'=0.1414$. The values for the heats of combustion and formation of dinitrocellulose and trinitrocellulose,[3] calculated by substitution of $f'=0.1111$ and $f'=0.1414$ into eq 1 and 2, and the corresponding equations for heat of formation, are given in table 4 along with the values for the celluloses.

VII. Results of Previous Measurements

Measurements of heats of combustion or heats of explosion of nitrocelluloses have been reported by Sarrau and Vieille [11], Kast [12], Muraour [13], Prettre [14], Tomioka [15], Schmidt and Becker [16], Milus [17], and Taylor and Hall [18]. In figure 2 the results of various investigators are compared. The values of $-\Delta H_c^\circ$ attributed to previous investigators were derived as follows:

[3] It is of interest to compare the data on cellulose and nitrocellulose with similar data on ethanol and ethyl nitrate. The differences between the heats of formation of cellulose and nitrocellulose range from 24.4 to 25.0 kcal per nitrate group. The corresponding difference between the heats of formation of liquid ethanol and liquid ethyl nitrate (reference [19], tables 25-9 and 23-45 (1948)) is 22.1 kcal. Combination of the latter value with an accurate value for the heat of formation of cellulose would, therefore, have yielded values for the heats of formation of dinitrocellulose and trinitrocellulose in error by about 5 and 7.5 kcal per monomer unit, respectively.

TABLE 4. *Heats of combustion and formation of cellulose, dinitrocellulose, and trinitrocelluiose*

Material	Source of cellulose	$-\Delta U_c^\circ$ at 30° C		$-\Delta H_c^\circ$ at 30° C		$-\Delta Hf°$ at 30° C	
		cal/g	*kcal/monomer unit*	*cal/g*	*kcal/monomer unit*	*cal/g*	*kcal/monomer unit*
Cellulose	Cotton linters	4165.0	675.3	4165.0	675.3	1421.0	230.4
	Wood pulp	4172.8	676.6	4172.8	676.6	1413.2	229.2
Dinitrocellulose	Cotton linters	2614.4	659.2	2606.0	657.1	715.3	180.4
	Wood pulp	2616.9	659.8	2608.6	657.7	712.8	179.7
Trinitrocellulose	Cotton linters	2190.2	650.8	2179.5	647.6	523.9	155.7
	Wood pulp	2188.7	650.4	2178.1	647.2	525.4	156.1

Where sufficient data were given, the reported values of heat of combustion or heat of explosion were corrected to the basis of the energy units used in the present work, and for the Washburn effect [8], and, where necessary, were reduced to a constant pressure basis. The resulting values were then combined with values for heats of formation [19] of the products of the combustion or explosion reaction to obtain the values of $-\Delta H_c^\circ$. The various values were not reduced to a common temperature, because no data on the heat capacities of nitrocelluloses have been found. The differences between the results of different observers are so large that the reduction of the results to a common temperature would not improve the agreement to a significant extent.

VIII. References

[1] H. C. Dickinson, Bul. BS **11**, 189 (1914) S230.
[2] R. S. Jessup and C. B. Green, J. Research NBS **13**, 496 (1934) RP721.
[3] R. S. Jessup, J. Research NBS **29**, 247 (1942) RP1499.
[4] F. D. Rossini, Chem. Rev. **18,** 233 (1936).
[5] F. D. Rossini and W. E. Deming, J. Wash. Acad. Sci. **29**, 416 (1939).
[6] R. S. Jessup, J. Research NBS **21,** 475 (1938) RP1140.
[7] J. R. Katz, Proc. Roy. Soc. Amsterdam **13** II, 958 (1911).
[8] E. W. Washburn, BS J. Research **10,** 525 (1933) RP546.
[9] R. S. Jessup, J. Research NBS **36,** 421 (1946) RP1711.
[10] NBS Circular C475, p. 22 (1949).
[11] Sarrau and Vieille, Compt. rend. **93,** 269 (1881).
[12] H. Kast, Spreng- und Zündstoffe p. 71 (1921). Data taken from reference [15].
[13] Muraour, Data taken from reference [15].
[14] M. Prettre, Mem. Poudres **24,** 223 (1931).
[15] K. Tomioka, J. Cellulose Inst., Tokyo **8,** 88 (1932).
[16] A. Schmidt and F. Becker, Z. ges. Schiess-u. Sprengstoffw. **28,** 280 (1933).
[17] P. R. Milus, Ind. Eng. Chem. **29,** 492 (1937).
[18] J. Taylor and C. R. L. Hall, J. Phys. Chem. **51,** 593 (1937).
[19] Selected values of chemical thermodynamic properties, National Bureau of Standards, Washington, D. C., Series I, Volume **I**, Tables 8–1 (1947) and 23–2 (1948).

Washington, December 14, 1949.

U. S. Department of Commerce
National Bureau of Standards

Research Paper RP 2087
Volume 44, April 1950

Part of the Journal of Research of the National Bureau of Standards

Thermal and Moisture Expansion Studies of Some Domestic Granites

By Arthur Hockman and Daniel W. Kessler

As a part of a study of the physical properties of building stone, thermal expansion determinations were made on 48 samples of domestic granites by the differential interferometer method (with an interferograph recording attachment) over the temperature range $-20°$ to $+60°$ C. Thermal coefficients computed between $-20°$ and $+60°$ C ranged from 4.8 to 8.3×10^{-6} per deg C with an average of 6.2×10^{-6} per deg C. Coefficients obtained on cooling (60° to 0° C) averaged 6.7×10^{-6} per deg C. Expansion curves drawn for all samples indicate slight irregularities in the 0- to 20-deg range in the heating curves of at least 65 percent of the samples. These irregularities are probably caused by moisture changes in the sample during the test.

Moisture expansion determinations were made on the 48 samples by means of the Tuckerman optical strain gage over a 24-hour period at constant temperature. The expansions obtained ranged from 0.0004 to 0.009 percent and averaged 0.0039 percent.

Adverse effects resulting from continued thermal and moisture expansion and contraction of granite are believed to be of some significance in monumental structures that are expected to last for long periods of time.

I. Introduction

Granite is known to be one of the most durable of structural materials. For this reason it has been an ideal choice for monuments, public buildings, shrines, and structures that are expected to last for centuries. There are granite structures in this country that have existed for periods up to 200 yr without showing serious signs of disintegration, yet there is evidence to show that some granite structures have begun to deteriorate in less than 50 yr.

The durability of granite may be adversely affected by one or more of many physical and chemical agencies. The effect of natural temperature changes in contributing to the deterioration of the stone has been recognized by geologists and engineers.[1] It is well known that the rapid heating of granite, as in the case of a fire, will usually cause serious spalling. Not so apparent is the fact that gradients in a granite structure resulting from the usual diurnal temperature changes cause internal stresses which, after numerous repetitions, may have a weakening effect on the stone. It also seems likely that the granite may be affected by the unequal expansion of the different mineral constituents, and the fact that the principal constituents, namely feldspar and quartz, expand unequally along different crystallographic axes.

Expansion effects due to absorption of water by granite have not been generally understood or appreciated. The experimental data acquired in this study definitely prove that granite undergoes a change in length on becoming wet. As in the case of thermal expansion, the repeated expansion and contraction resulting from wetting and drying may have a weakening effect on the stone. Moisture gradients resulting from partial wetting of the stone cause internal stresses, which in the course of time may adversely affect its durability.

The purpose of this study was to accumulate data on the thermal expansion characteristics of granite over the temperature range produced by

[1] The supposition that rocks in general are seriously affected by natural changes in temperature is strongly challenged by some geologists. For example see E. Blackwelder, The insolation hypothesis of rock weathering Am. J. Sci. **26**, 970 (1933).

the usual weather exposures and also on the expansion due to the absorption of water. Most of the published data on thermal expansion of granite were computed from measurements taken at larger temperature intervals than those to which masonry is normally subjected, and these values can be misleading when applied to the seasonal range. In this study coefficients of linear thermal expansion were determined over the range of −20° to +60° C (−4° to 140° F). Since there are very few data published on the moisture expansion of granite, this property was determined on the entire series of samples tested for thermal expansion. This report cites a few examples of granite structures that show some deterioration resulting from temperature and moisture effects.

II. Previous Investigations

A review of the literature on thermal expansion measurements of granite reveals that in 1832, Bartlett [1][2] seeking the cause of fissures in coping joints in a granite structure, measured the thermal expansion of a sample of Massachusetts granite, and samples of marble and limestone. His specimens were 94 in. long, and the temperature range was −14° to +39° C. (See table 1 for results of previous investigations). Also about this time, Adie [2] measured the expansion of two granites (Aberdeen gray and Peterhead red from Scotland), also samples of marble, sandstone, and greenstone. His temperature range was +10° to 98° C. Adie recognized that a sample of greenstone expanded permanently after several successive heatings. Reade [3] in 1886, included four samples of granite in his thermal expansion studies of several types of rocks but did not state the temperature range. In 1895 at the Watertown Arsenal [4] thermal expansion tests were made on eleven samples of granite acquired from eight states. Measured bars, 24 in. by 6 in. by 4 in. were placed in cold water (32° F), then in hot water (212° F), and back in the cold bath. These expansion results evidently represented the combined effects of temperature and moisture.

In 1909 Baldwin-Wiseman and Griffith [5] determined permanent length changes, due to heating, for several samples of sandstones, limestones, marbles, and one sample of granite (Peterhead, Scotland). The temperature range was +20° to 300° C. In 1910, Wheeler [6] studied the effects of six repeated heatings from +19° to 1,000° C of samples of Rhode Island granite, Canadian diabase, and of Italian marble from +19° to 500° C.

The more recent investigations of thermal expansion include those made in 1936 by Griffith [7]. Among the 106 samples of American rocks tested by him, about 20 represent granites generally used for building and monumental purposes. His range was room temperature to 260° C.

In 1939, Willis and DeReus [8] included the measurements of five samples of granite in their study of concrete aggregate. The temperature range was +3° to 60° C. In 1944, Johnson and Parsons [9], applying a test procedure similar to that used in the present investigation, included the measurements of four granite samples in their study of thermal expansion of concrete aggregates.

Comparatively few investigators have studied the moisture expansion of building stone. It seems that in 1886 Schumann [10] (original reference unobtainable) was the first to make a systematic study of moisture expansion of natural stone. Hirschwald [11] repeated these experiments. Using a micrometer microscope, the latter determined length changes of several stone specimens after 2 weeks immersion in water. The average expansion obtained for one sample of granite and four samples of basalt was 0.029 percent.

TABLE 1. *Summary of thermal expansion data on granite obtained by previous investigators*

No. of specimens tested	Temperature range [a]	Mean coefficient of linear thermal expansion per degree C×10⁶	Investigator	Date of publication
	°C			
1	−14 to +39	8.25	Bartlett	1832
2	+10 to 98	8.22	Adie	1836
4		8.85	Reade	1886
11	0 to 100	[b] 7.0	Watertown Arsenal	1895
1	0 to 100	10.2	Baldwin-Wiseman & Griffith.	1909
1	+19 to 172	8.6	Wheeler	1910
20	0 to 100	8.1	Griffith	1936
5	3 to 60	6.7	Willis & DeReus	1939
4	−20 to 60	6.0	Johnson & Parsons	1944

[a] The range for which the coefficients were calculated.
[b] Specimens tested in wet condition.

[2] Figures in brackets indicate the literature references at the end of this paper.

More recent studies of moisture expansion of building stone include those made by Matsumoto [12], Stradling [13], Royan [14], and Kessler [15]. However, the reports of these investigators did not include any data on granite.

An examination of all the published data on thermal and moisture expansion of granites described in the preceding paragraphs reveals; (1) there is a scarcity of data on the thermal expansion characteristics of domestic granites over the seasonal range of temperature; (2) investigators took readings at wide temperature intervals and few made observations on cooling; (3) there are practically no data available on dimensional changes in domestic granites due to absorption of moisture.

III. Description of Samples

The 48 samples used in this study were collected for a previous investigation at this Bureau of other physical properties of the domestic granites [16]. The samples represent the deposits of the principal producing districts of 17 states. Most of these granites have been used for architectural, monumental, or structural purposes.

Geologically, granite is designated as a crystalline rock of igneous origin, and is composed of feldspar, quartz, and one or more accessory minerals such as mica, hornblende, pyroxene, etc. Generally, there are two kinds of feldspar present in the rock, the more abundant usually being a potash feldspar (orthoclase or microcline or both). The other is soda-lime feldspar (plagioclase), and may include one or more of the following species: albite, oligoclase, and andesine. In most granites, quartz ranks second in abundance to the feldspars, a ferro-magnesian mineral (biotite, hornblende, or pyroxene) ranking third. The term "commercial granite" may include such closely related rocks as gneiss, syenite, monzonite, etc. "Black granites", also a commercial designation, include rock species such as diabase, norite, and gabbro, which are somewhat distantly related to the true granites. This study includes several of these "related" granites. Of the 48 granites tested, potash feldspar was the most abundant mineral in 35 samples, soda-lime feldspar in 10, and quartz in 3. Mica was the most abundant of the accessory minerals in 39 samples, hornblende in 4, and pyroxene in 2.

The descriptive portion of table 2 gives the sample numbers, source, classification, texture, and major mineral constituents of all samples tested. The "classification" of a granite is derived from the most abundant accessory mineral, such as "biotite granite," or "hornblende granite", etc. Textures refers to the average size of the feldspar grains and follows the scale given at the end of the table.

TABLE 2. *Description, source, classification, texture, composition, thermal expansion coefficients, and moisture expansion percentages of all samples tested*

(1)	(2)	(3)	(4)	(5)	(6) Thermal expansion—average coefficient of linear thermal expansion per degree C×10⁶			(7)
					Heating		Cooling	
Sample No.[a]	Source	Classification	Texture [b]	Major Mineral Constituents (in descending order of abundance)	−20° to 60°	0° to 60°	60° to 0°	Moisture expansion—length change due to immersion in water for 24 hr at constant temperature (21.5° ± .5° C)
								Percent
1	Vinalhaven, Me	Biotite granite	Fine to medium	Orthoclase, quartz, oligoclase and biotite.	5.8	6.1	6.4	0.0018
2	do	Olivine norite	Fine	Soda-lime feldspars (labradorite to bytownite), hypersthene, olivine and magnetite.	5.9	6.1	6.1	.0008
5	do	Biotite hornblende granite.	do	Orthoclase and microcline, smoky quartz, oligoclase, biotite, hornblende.	6.5	6.7	7.0	.0036
8	Mt. Desert, Me	Biotite granite	do	Orthoclase, smoky quartz, oligoclase and biotite.	4.8	4.9	5.2	.0028
9	Jonesboro, Me	do	Medium to coarse	do	6.8	7.2	7.4	.0020

See footnotes at end of table.

TABLE 2. *Description, source, classification, texture, composition, thermal expansion coefficients, and moisture expansion percentages of all samples tested*—Continued

(1) Sample No.[a]	(2) Source	(3) Classification	(4) Texture[b]	(5) Major Mineral Constituents (in descending order of abundance)	(6) Thermal expansion—average coefficient of linear thermal expansion per degree C×10⁶			(7) Moisture expansion—length change due to immersion in water for 24 hr at constant temperature (21.1° ± .5° C)
					Heating		Cooling	
					−20° to 60°	0° to 60°	60° to 0°	
								Percent
10	Long Cove, Me	Biotite-muscovite granite	Fine to medium	Microcline and orthoclase, quartz, oligoclase, biotite and muscovite.	6.6	6.5	7.1	0.006
11	North Jay, Me	Biotite-muscovite granite	Fine	do	6.2	6.3	6.5	.005
12	Stonington, Me	Biotite granite	Coarse	Orthoclase and microcline, smoky quartz, oligoclase, and biotite.	5.9	6.0	6.4	.005
13	Frankfort, Me	do	Medium	do	6.6	7.1	7.2	.004
16	Highpine, Me	do	Coarse	Microcline and orthoclase, smoky quartz, oligoclase, and biotite.	5.8	5.9	6.3	.008
17	Concord, N. H	Muscovite-biotite granite	Fine to medium	Microcline and orthoclase, quartz, oligoclase-albite, muscovite, and biotite.	7.7	7.7	8.4	.004
18	Redstone, N. H	Biotite-granite	Coarse	Orthoclase, smoky quartz (oligoclase-albite), and biotite.	5.4	5.6	6.1	.007
21	Milford, N. H	Quartz monzonite	Fine	Microcline and orthoclase, oligoclase, smoky quartz and biotite.	5.7	6.0	6.3	.003
24	Fitzwilliams, N. H	Biotite-muscovite granite.	do	Orthoclase and microcline, quartz, oligoclase, biotite and muscovite.	5.4	5.5	6.2	.008
25	Barre, Vt	Biotite granite	do	Orthoclase, smoky quartz, oligoclase-albite, biotite and muscovite.	6.3	6.1	6.8	.005
27	Derby, Vt	Quartz monzonite	Fine to medium	Smoky quartz, oligoclase, microcline and orthoclase, biotite and muscovite.	7.1	7.2	7.7	.002
28	Woodbury, Vt	Biotite granite	Coarse	Microcline and orthoclase, quartz, oligoclase, biotite and muscovite.	6.1	6.2	6.6	.007
30	Windsor, Vt	Hornblende biotite granite.	Fine to medium	Orthoclase, smoky quartz, plagioclase (oligoclase-albite) hornblende and biotite.	5.3	5.6	5.6	.003
33	Quincy, Mass	Riebeckite-aegirite granite.	Coarse	Orthoclase, smoky quartz, riebeckite, aegirite and albite.	5.3	5.3	5.9	.010
37	W. Chelmsford, Mass	Muscovite-biotite granite-gneiss.	Medium	Microcline and orthoclase, oligoclase, quartz, rutile, muscovite and biotite.	5.5	5.6	6.2	.007
39	Chester, Mass	Biotite-muscovite granite-gneiss.	Medium to fine	Microcline, quartz, plagioclase, biotite and muscovite.	6.5	6.6	7.2	.006
40	Milford, Mass	Biotite granite	Coarse	Microcline and orthoclase, quartz, plagioclase (albite-oligoclase), and biotite.	5.9	6.4	6.6	.007
41	Rockport, Mass	Hornblende granite	do	Orthoclase and microcline, smoky quartz, hornblende, and plagioclase (albite-oligoclase).	5.4	5.7	5.9	.003
43	Ansonia, Conn	Muscovite-biotite granite-gneiss.	Fine	Microcline and orthoclase, quartz oligoclase, muscovite and biotite.	7.5	7.5	8.0	.005
45	East Lyme, Conn	Quartz monzonite	do	Quartz, oligoclase, microcline and orthoclase, biotite and muscovite.	7.0	7.1	7.5	.003

See footnotes at end of table.

TABLE 2. *Description, source, classification, texture, composition, thermal expansion coefficients, and moisture expansion percentages of all samples tested*—Continued

(1)	(2)	(3)	(4)	(5)	(6)			(7)
					Thermal expansion—average coefficient of linear thermal expansion per degree C×10⁶			
					Heating		Cooling	
Sample No.[a]	Source	Classification	Texture[b]	Major Mineral Constituents (in descending order of abundance)	−20° to 60°	0° to 60°	60° to 0°	Moisture expansion—length change due to immersion in water for 24 hr at constant temperature (21.5° ± .5° C)
								Percent
46	Waterford, Conn	Quartz monzonite	Fine	Oligoclase, microcline and orthoclase, quartz, biotite and muscovite.	5.3	5.4	6.0	0.0068
47	Branford, Conn	Biotite granite gneiss	Medium to coarse	Microcline and orthoclase, quartz oligoclase, biotite and muscovite.	5.3	5.3	6.2	.0080
53	Mt. Airy, N. C	Biotite granite	Medium	Oligoclase, orthoclase and microcline, quartz and biotite.	6.0	6.2	6.4	.0020
56	Salisbury, N. C	do	do	Orthoclase with a small amount of microcline, plagioclase, quartz and biotite.	7.1	7.3	7.7	.0020
59	Rion, S. C	do	do	Orthoclase and microcline, plagioclase (oligoclase), quartz and biotite.	6.5	6.6	6.9	.0066
62	Newberry, S. C	do	Fine	Orthoclase and microcline, oligoclase, and biotite.	5.5	6.0	6.3	.0040
65	Elberton, Ga	do	Medium to fine	Orthoclase and microcline, oligoclase, quartz and biotite.	6.0	5.7	6.4	.0060
66	do	do	do	do	6.6	6.7	6.8	.0052
67	Stone Mt., Ga	Muscovite granite	Medium	Orthoclase and microcline, plagioclase, quartz, muscovite and biotite.	6.2	6.6	6.7	.0034
73	Amberg, Wis	Biotite granite	do	Orthoclase and microcline, quartz and biotite.	7.9	8.1	8.3	.0032
76	Montello, Wis	Hornblende granite	Fine	Orthoclase and microcline, quartz and hornblende.	6.1	6.2	6.6	.0024
77	Wausau, Wis	Biotite hornblende granite.	Medium	Orthoclase and microcline, plagioclase, quartz, hornblende and biotite.	7.6	7.9	7.9	.0046
79	Isle, Minn	Biotite granite	Medium to coarse	Orthoclase and microcline, quartz and biotite.	8.3	8.3	8.6	.0034
80	Rockville, Minn	do	Coarse	Orthoclase and microcline, quartz, plagioclase and biotite.	6.4	6.4	6.7	.0022
82	Morton, Minn	Biotite granite-gneiss	Medium to coarse	Orthoclase, plagioclase, quartz, microcline and biotite.	5.9	6.0	6.5	.0032
90	Hibbing, Minn	Quartz monzonite	Medium	Orthoclase, plagioclase, quartz, biotite and hornblende.	5.5	5.5	5.9	.0044
91	Peekskill, N. Y	Biotite-muscovite granite.	Medium to fine	Albite, oligoclase, quartz, orthoclase, biotite and muscovite.	5.8	6.1	6.5	.0052
95	St. Peters, Pa	Gabbro	Fine	Plagioclase and pyroxene	6.6	6.6	6.8	.0056
97	Port Deposit, Md	Biotite granite-gneiss	Medium	Oligoclase, orthoclase, microcline, quartz and biotite.	6.6	6.4	7.2	.0062
104	Graniteville, Mo	Biotite granite	do	Plagioclase, microcline, orthoclase, perthite, quartz and biotite.	6.4	6.6	6.6	.0012
106	Marble Falls, Tex	do	Coarse	Quartz, microcline, plagioclase and biotite.	7.0	7.2	7.4	.0038
111	Columbia, National Forest, Wash.	Basalt porphyry	Fine	Plagioclase and high iron glass	6.0	6.2	6.2	.0018
115	Alhambra, Calif	Hypersthene gabbro	do	Plagioclase, pyroxene and hornblende.	5.6	5.7	5.8	.0004

[a] Sample numbers correspond to the serial numbers listed in table 1 of RP1320 Journal of Research NBS **25**, 161 (1940) RP1320.

[b] Texture refers to the average size of the feldspar grains, according to the following designation: fine, less than 0.5 cm; medium, 0.5 to 1 cm; coarse, slightly larger than 1 cm.

IV. Test Method for Thermal Expansion Measurements

1. Apparatus

(a) Differential Interferometer

When the usual interferometer method is applied to measure the expansion of fine grained materials, a relatively small specimen, 2 to 6 mm in height is generally used [17]. However, in order to make the interferometer applicable to the thermal expansion measurement of medium and coarse grained granites it was found necessary to use a test specimen considerably larger than the conventional small one.

For this purpose, a differential interferometer, similar to that applied by Saunders [18], was used to make the expansion measurements. This method is a modification of Fizeau's differential interferometer [19] in which the three adjustable screws used by Fizeau to support the top plate were replaced by a perforated fused quartz tube of a specific height.

In these tests the specimen is 38.42 mm high (avg. size), T-shaped in cross section, and with a maximum width and depth of 12.5 mm. The sides are perforated to reduce its heat capacity to a minimum. Figure 1 is a schematic diagram of the interferometer arrangement used in all tests. The specimen rests on a glass thermometer plate, *e*, and supports an interferometer plate, *b*, on its upper surface. Another interferometer plate, *a*, is supported approximately 0.5 mm above plate *b* by a perforated fused quartz tube 42.65 mm high, the latter also resting on plate *e* and surrounding the specimen, *d*. Plate *a* is polished on both faces. Plates *b* and *e* are polished on the upper faces and fine ground on the lower, with the exception of a small area on plate *e*, which is polished on both faces in order to produce the temperature fringes. The expansion of the specimen on heating causes plate *b* to move toward plate *a*. This results in a movement of the interference fringes in the field. (See section IV–6 for the details of calculations.)

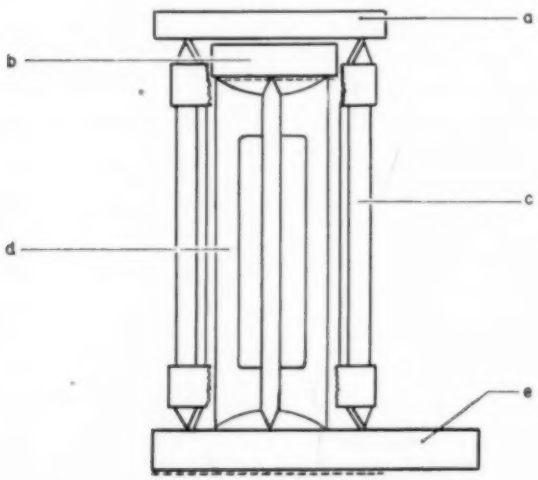

FIGURE 1. *Diagram of differential interferometer.*

a, Top interferometer plate; b, lower inteferometer plate; c, fused quartz tube supporting top plate; d, test specimen; e, thermometer plate.

(b) Thermal Chamber

The thermal chamber (fig. 2) was the same as that used by Johnson and Parsons [9]. A brass cylinder, 9 in. long and 3 in. in diameter was inserted through the top of an ordinary electric refrigerator into a tank of kerosine, which surrounded the freezing coils. The heating element consisted of a hard rubber tube wound with 30 ft of No. 24 Nichrome wire. A removable copper cup, supported from the refrigerator top by steel rods, held all the components of the interferometer. Just beneath the bottom thermometer plate were inserted the three variable junctions of a copper-constantan thermocouple. Three slide wire resistors, an ammeter, and a toggle switch were placed in series with the heating element and the 110-v power source for control of the heating current.

(c) Recording Mechanism

A recording apparatus (fig. 2) previously constructed and used by Johnson and Parsons [9], was a simplified form of the one originally designed by Saunders [20]. This apparatus replaced the eyepiece of the ordinary Pulfrich type interferometer viewing instrument and thus eliminated the tedious job of counting fringes visually. A strip of 35-mm high speed photographic film was drawn from an ordinary camera cartridge over rollers by a sprocket geared to a synchronous motor, at the rate of 1½ in. per hr. A lens focused the interference pattern through a yellow filter upon a screen with a slit ¼ mm wide, which allowed only a very narrow portion of the image to reach the slowly moving film. A side tube with a slotted mirror placed at a 45° angle, permitted

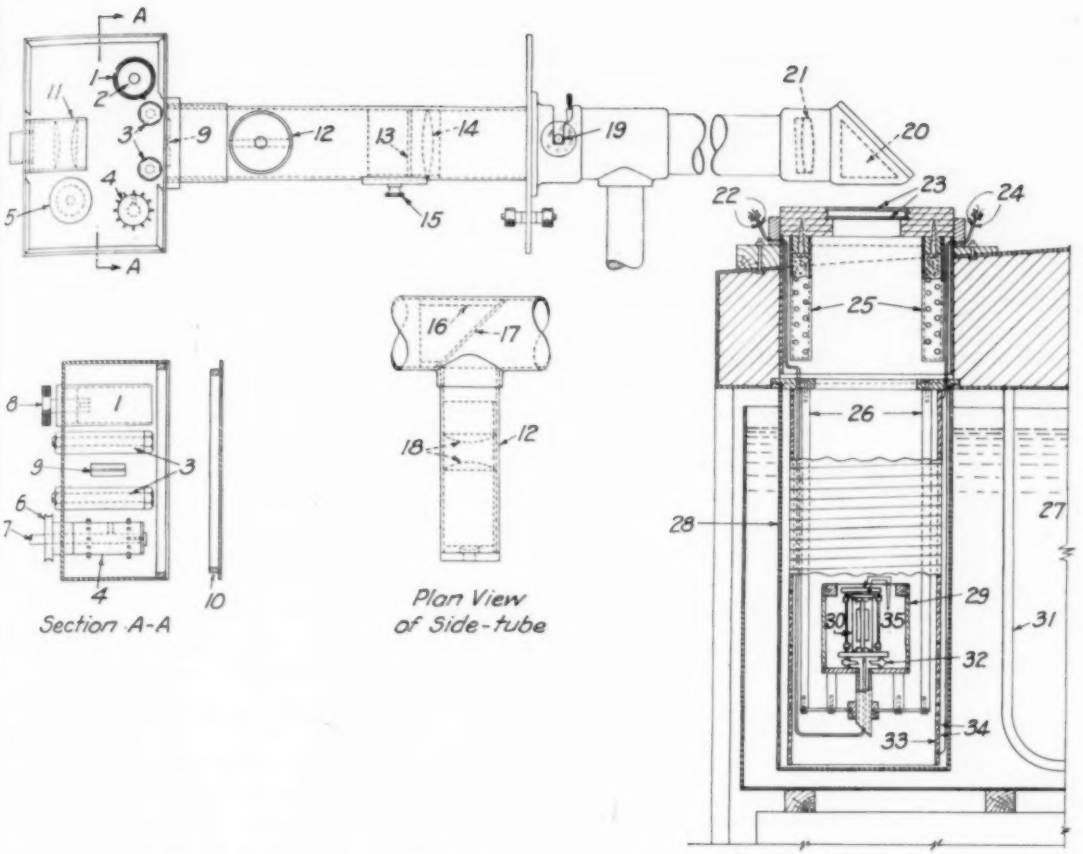

FIGURE 2. *Diagram of viewing instrument, recording camera, and thermal chamber.*

1, Magazine; 2, film cartridge; 3, film rollers; 4, feed sprocket; 5, take-up spool; 6, pulley to take-up spool; 7, drive shaft geared to synchronous motor; 8, rewind knob; 9, slit (aperture); 10, light-tight cover; 11, camera eyepiece and lenses; 12, side-tube eyepiece; 13, yellow filter; 14, objective lens; 15, focus adjustment; 16, mirror support; 17, mirror; 18, side-tube eyepiece lenses; 19, spectrum tube; 20, 90° prism; 21, objective; 22, heating coil terminals; 23, double glass; 24, thermocouple leads; 25, dessicant tubes; 26, steel supports; 27, kerosine; 28, brass cylinder; 29, copper cup; 30, specimen; 31, refrigerator cooling coil; 32, glass ring; 33, hard rubber tube; 34, nichrome wire; 35, interferometer plates.

visual observations for checking purposes during the operation of the recorder (see reference [20] for details of the recording instrument).

2. Temperature Determinations

Temperatures were measured with an optically ground thermometer plate (fig. 1, e) often referred to as an interference or refraction thermometer [21]. This plate gave a satisfactory set of straight interference bands that shifted at a definite rate whenever it was heated or cooled. In order to calibrate this thermometer plate it was placed, together with the other components of the interferometer, into the thermal chamber, and a thermometer fringe count determined for a number of equilibrium temperatures, the latter being measured by a three-junction thermocouple located just beneath the plate. The fringe numbers obtained in this manner were plotted against the temperatures, and a fringe-temperature curve drawn. From this curve it was possible to determine the temperature corresponding to any specifically numbered fringe. During each test the temperature fringes were recorded simultaneously with the expansion fringes.

3. Preparation of the Specimens

Figure 3, a, b, c and d illustrates the stages in the fabrication of a typical test specimen. A rectangular prism, approximately 12.5 mm by

12.5 mm in cross section and approximately 38.5 mm in length was first cut from the granite sample by means of a 6-in. circular diamond saw. Sections were then cut away with the same saw leaving a T-shaped piece having sides approximately 2.5 mm thick (fig. 3, b and c). Next, with the aid of small fine silicon carbide grinding wheels, the specimen illustrated in figure 3, d was completed. The ends of the finished specimen were ground so that there were three polished points at the bottom to contact the glass thermometer plate, and three points at the top to support the lower interferometer plate. Similarly, the quartz tube used to support the upper interferometer plate (fig. 1) had three polished points on its top and bottom surface.

With a fine emery stone and a micrometer gage the heights of the "legs" of the specimen were equalized to within 0.005 mm. The legs of the quartz supporting tube were adjusted to a height of 42.65 mm. By setting up all the various parts of the interferometer and examining through a viewing instrument, the heights of the legs of the specimens were adjusted further to give the desired interference pattern. The finished specimens, which averaged 3.2 g in weight, were dried at 80° C for 4 days and placed in a desiccator until ready for test.

4. Test Procedure

After the desired fringe pattern was obtained, the copper cup containing all the components of

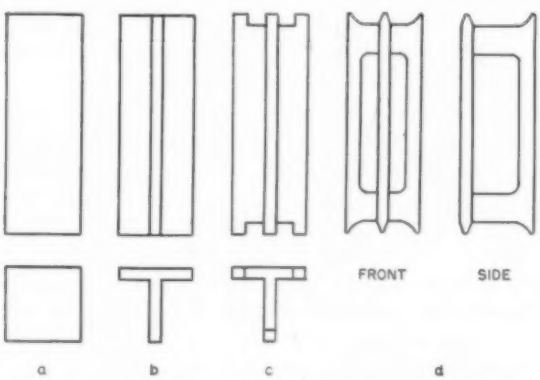

FIGURE 3. *Diagrams showing successive steps in the preparation of a test specimen.*

a, Rectangular prism cut from larger sample; b, sections cut away to form a T-shaped specimen; c, view of b after grinding it to form "legs"; d, views of finished specimen showing points on legs and sections ground away to reduce its mass.

the interferometer was placed, very carefully, into the thermal chamber. The chamber was closed and after a preliminary fast heating to 68° C to stabilize the air films between the points of contact of the specimen and of the quartz tube with the interferometer plates [22], the cooling system was started and allowed to operate overnight. Next morning after the final adjustments were made on the viewing instrument and recording apparatus, the film was inserted, and the initial temperature determined by the thermocouple. The recorder was then started, cooling system turned off, the heating current turned on and increased at 15-min intervals to produce a uniform rise in temperature of approximately 0.4° C per minute. When the final temperature was reached (approximately 65° C), the cooling system was again turned on, and the heating current reduced at regular intervals until the temperature fell just below 0° C. The recorder was then stopped, the chamber reheated to room temperature to prevent condensation inside, and the specimen removed. Finally the film was rewound into the cartridge and removed for development.

5. Description of the Interferogram

The interference pattern when seen through the viewing instrument appears as shown in figure 4, A. When the eyepiece of the instrument is replaced with the recording apparatus, only a narrow portion of the pattern is focused on the moving film (fig. 4, B). Figure 4, C and D are schematic drawings of portions of a typical interferogram resulting from the fringe pattern shown in figure 4, A and B.[3] The fringes become a series of bands that are parallel to the direction of the movement of the film only so long as thermal equilibrium is maintained, such as during the first few minutes of a test. The upper portion of figure 4, C illustrates this condition. When the temperature begins to rise and the specimen expands, there is a corresponding movement of temperature and expansion fringes. To prepare the interferogram for the counting of fringes, penciled lines are drawn parallel to a slit line,[4] through each intersection of an even numbered thermometer fringe with the thermometer reference line. Where each of these penciled lines crosses

[3] Expansion data were read from a 3× enlargement of the interferogram.

[4] A slit line is produced on a film by turning off the source of monochromatic light for about 30 sec during a test, resulting in a narrow underexposed strip.

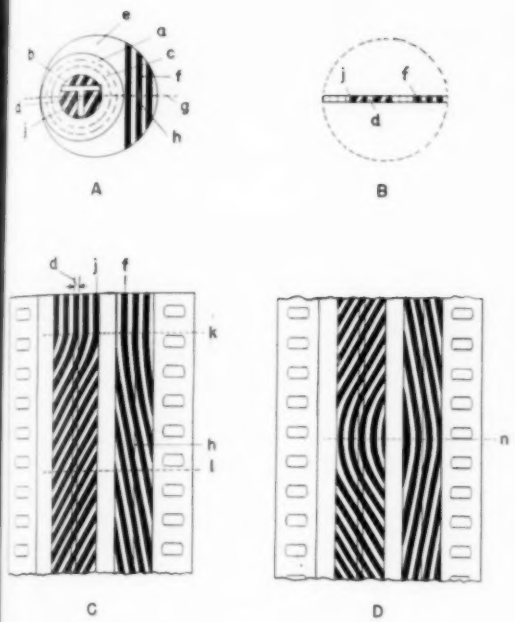

FIGURE 4. *Interferometer and interferogram.*

A, Interferometer as seen through the viewing instrument; B, exposure slit magnified to show fringes; C, section of interferogram at start of test; D, middle section of interferogram: a, top interferometer plate; b, lower interferometer plate; c, fused quartz tube; d, test specimen; e, thermometer plate; f, temperature fringe; g, position of exposing slit in camera; h, thermometer reference mark; j, expansion fringe; k, point where fringes begin to move; l, line (parallel to slit line) drawn through intersection of thermometer fringe No. 1 and expansion fringe No. 6.5; n, maximum temperature and reversal of fringes.

the middle of the specimen trace, the simultaneous expansion fringe number is noted. For example, line *k* passes through temperature fringe No. 0 and expansion fringe No. 0, line *l* passes through temperature fringe No. 2 and expansion fringe No. 6.5.

Fringe data for a typical test were as follows:

Temperature fringe No.	Temperature	Expansion fringe No.
	°C	
0	−22.2	0
2	−10.6	6.9
4	+0.6	11.5
6	11.6	15.5
8	22.1	21.0
10	32.4	27.0
12	42.2	33.8
14	51.8	41.0
16	61.0	49.3

When the maximum temperature was reached and cooling began, the direction of the fringe movement for both expansion and temperature was reversed (figure 4, D, *n*). As the fringes recrossed their respective reference marks they were assigned their previous numbers.

6. Calculation of Results

Since the total number of expansion fringes passing during a test was affected by the expansion of the quartz tube and the interferometer plate, *b*, as well as that of the granite specimen (fig. 1), it was necessary to develop a formula that would include all these factors. The following formula was used for this purpose:

$$\Delta L=\frac{N\frac{\lambda}{2}-C\cdot S\times 10^{-4}+[(A_q\cdot L_q)-A_r\cdot L_r)](T_2-T_1)}{L}$$

where L = length of specimen at initial temperature T_1 in millimeters;

ΔL = linear expansion of specimen in mm/mm from T_1 to any higher temperature, T_2;

N = number of observed fringes;

λ = wavelength of monochromatic light in millimeters;

C = air correction in microns per centimeter.[5]

S = air space between interferometer plates *a* and *b* in millimeters;

A_q = expansion coefficient of fused quartz tube per deg C from T_1 to T_2;[6]

L_q = length of fused quartz tube at T_1 in millimeters;

A_r = expansion coefficient of interferometer plate *b* per deg C from T_1 to T_2;[6]

L_r = height of interferometer plate *b* at T_1 in millimeters.

7. Reliability of Results

In order to check the performance of the apparatus, samples of three different materials, namely, porcelain, glass, and a metal alloy were tested for thermal expansion. These values were compared with those obtained on identical ma-

[5] Data taken from the table of air corrections listed in reference [17].

[6] Expansion coefficient of the fused quartz was determined by the usual interferometer method on a small sample cut from the original piece of quartz tubing. The expansion coefficient of the interferometer plate *b* (Vycor brand glass) was taken from reference [18].

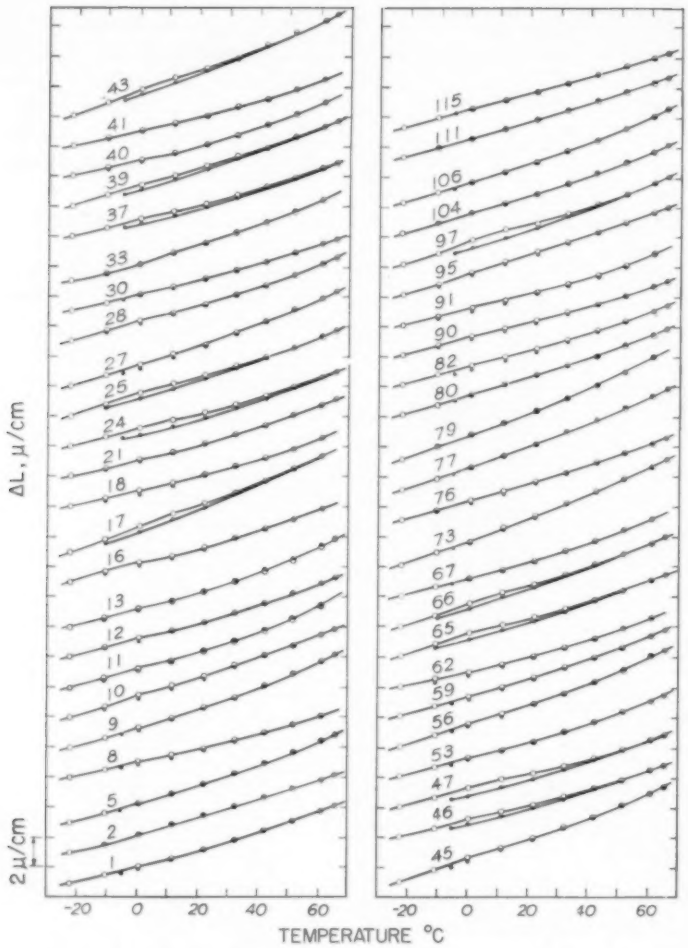

FIGURE 5. *Thermal expansion curves of 48 samples of granite.*

○, Heating points; ●, cooling points; figures refer to sample numbers in table 2.

terials by the Thermal Expansion Section of this Bureau. The results were as follows:

Sample	Coefficient of linear thermal expansion per deg C from −20° to +60° C	
	Hidnert [7]	Authors
BC (Porcelain)	4.5×10^{-6}	4.4×10^{-6}
BG (Glass)	8.7×10^{-6}	8.6×10^{-6}
BF (Alloy)	2.5×10^{-6}	2.5×10^{-6}

[7] Chief, Thermal Expansion Section, National Bureau of Standards.

The results agree within the limits of experimental error.

V. Thermal Expansion Results and Discussion

1. General

Table 2, column 6 gives the mean coefficients of linear thermal expansion for three different temperature ranges of all samples tested, and figure 5 shows their characteristic heating and cooling curves. The coefficients obtained for the 48 samples ranged from 4.8 to 8.3×10^{-6} per deg C between −20° and +60° C with an average of 6.2×10^{-6}. The coefficients of 84 percent of the samples in this same temperature range were between 5 and 7×10^{-6} per deg C. For the

temperature range 0° to 60° C, the average of the coefficients was 6.3×10^{-6} and on cooling (60° to 0° C), it was 6.7×10^{-6} per deg C.

2. Irregularity of Expansion

A general view of all the expansion curves as illustrated in figure 5 reveals more or less smooth regular curves on both heating and cooling. However, on closer scrutiny it can be readily seen that at least 65 percent of the samples expand at a certain rate until the region of 0 to 10 deg is reached, then change to a slower rate for about 10 deg and finally resume a new rate of expansion that continues regularly until the maximum temperature is reached. On the other hand, the cooling curves of all the samples show little evidence of irregularities. Samples 17, 24, 46, 47, 65, and 97 show some of the more pronounced instances of irregular heating curves. These irregularities were reproducible on retesting of the samples.

The irregular expansion appears to be due to moisture changes in the sample during the test. If water is prevented from entering the sample during a test the irregularities disappear. Three samples showing irregular expansions were retested after having been dried at 80° C for 4 days and coated with a synthetic resin water-proofing. The resulting curves (fig. 6) showed virtually no irregularities after the treatment. It might also be noted here that the testing of nonabsorptive materials, such as glass and metal, produced smooth coinciding curves on both heating and cooling.

Since the uncoated samples were dry at the start of each test, absorption of moisture by them is likely during the tests. As the temperature of the surrounding atmosphere is reduced, the relative humidity rises and although the outer wall of the chamber is colder than the sample during the initial cooling part of the cycle, the latter's very dry initial condition might make it receptive to atmospheric moisture. During the early heating part of the cycle the sample is colder than its surroundings, hence condensation of moisture on it might be expected. A portion of this moisture would most certainly be absorbed. Further heating would raise the vapor pressure of the water in the sample above that of the surrounding atmosphere and produce a drying action.

As shown in section VII, granites expand when moisture is absorbed. Absorption of water during the early heating part of the cycle might account for the increased slope of the expansion curve in that range, while loss of moisture at higher temperatures is consistent with the reduced rate of expansion occurring at about 10° C.

The abrupt change in slope observed in some of the curves at 0° C or slightly above might indicate that some of the absorbed moisture was in a frozen state below that temperature. If the sample absorbs water while being cooled to −20° C, there is ample opportunity for the water to become frozen since the sample is maintained at this low temperature for at least 9 hrs. The relative high thermal coefficient of ice might contribute to the over-all expansion at the lower temperatures, while a gradual melting with attendant loss in volume would reduce the observed slope on further heating.

Further evidence to show that irregularities are

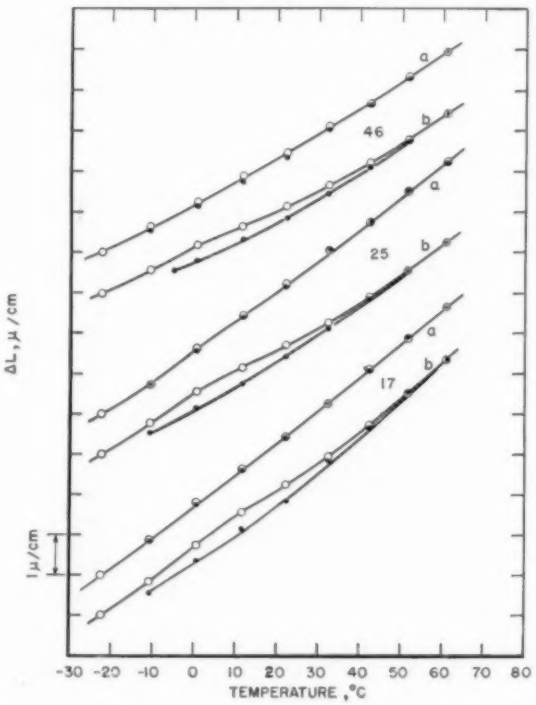

FIGURE 6. *Thermal expansion curves for three samples of granite showing the effect of waterproofing the test specimens.*

○, Heating points; ●, cooling points; figures refer to sample numbers in table 2. a, waterproofed; b, original test.

probably due to moisture in some form is indicated by the fact that six samples showing no irregularities had an average absorption value of 0.08 percent [8] and a moisture expansion value of 0.0026 percent. On the other hand, the six samples showing the most pronounced irregularities had an average absorption value of 0.25 percent and a moisture expansion value of 0.0072 percent. The average absorption and moisture expansion values for all samples were 0.20 percent and 0.0039 percent, respectively.

3. Effect of Mineral Composition

The thermal expansivity of granite is a function of the expansivities of its mineral constituents. There are some data available on the thermal expansion coefficients of the chief minerals in granite. The values in table 3 indicate that the expansion coefficients of quartz differ from those of the feldspars, and that the coefficients of potash feldspar are different from those of the soda-lime feldspars. Furthermore, each mineral expands at different rates along different crystallographic axes. Since a typical granite of this investigation contains four major mineral constituents plus several minor ones, all occurring in random orientation, it would seem impossible to form a precise correlation between mineral constituents and expansivity. Granites of similar mineral composition but from different quarries gave different results.

TABLE 3. *Mean coefficients of linear thermal expansion for some oriented minerals contained in granite*

Mineral	Orientation	Mean coefficient of linear thermal expansion per degree C×10⁶		Source
		−20° to +60°	+60° to 0°	
Quartz	Perpendicular to *c*-axis	13.5	13.5	Johnson & Parsons [9].
Do	Parallel to *c*-axis	7.4	7.7	Do.
Microcline	Parallel to *b*-axis	1.1	1.3	Do.
Do	Perpendicular to *b*-axis	3.5	3.2	Do.
Do	Parallel to *a*-axis	17.1	17.3	Do.
Oligoclase	do	3.1	3.7	Do.
		20° to 100°		
Orthoclase	do	15.0		Kozu and Saiki [23].
Do	Parallel to *b*-axis	0.0		Do.
Plagioclase	Parallel to *a*-axis	11.2		Kozu and Ueda [24].
Do	Perpendicular to 010	3.8		Do.
Hornblende	Perpendicular to 100	6.2		Do.
Do	Parallel to *b*	7.5		Do.
Do	Parallel to *c*	7.2		Do.
Olivine	Parallel to *a*	5.0		Kozu, Ueda & Tsumori [25].
Do	Parallel to *b*	10.0		Do.
Do	Parallel to *c*	8.8		Do.

[8] Absorption values were determined by measuring the percentage gain in weight of cylindrical specimens, 2 in. in diameter and 2½ in. long, after 48-hr immersion in water at room temperature. Moisture expansion tests are described in section VII.

Potash feldspar was the most abundant mineral constituent in 35 of the 48 samples tested. The average of the thermal coefficients obtained for these 35 samples was 6.2×10^{-6} per deg C between −20° and +60° C. For the 10 samples containing soda-lime feldspar as the most abundant mineral constituent, the average of the coefficients was 6.3×10^{-6} per deg C in this same range.

Quartz was the most abundant mineral constituent in 3 of the 48 samples tested. The average of the coefficients for these samples was 7.0×10^{-6} per deg C between −20° and +60° C. Since the average of the coefficients of quartz measured in all directions is higher than those of the feldspars, it seems logical that samples with an abundance of quartz would have higher than average coefficients.

4. Thermal Expansion Data for Other Building Stones

Table 4 shows the range in linear thermal expansion coefficients determined for some other types of stone used for structural purposes.

VI. Test Method for Moisture Expansion

1. Specimens

For convenience in preparation, cylindrical specimens, 2 in. in diameter and 2½ in. long, were cored from the original granite samples. Two plane surfaces opposite each other were ground on each specimen, one to provide a base and the other for attachment of the gage.

2. Apparatus

A brass tank large enough to accommodate two specimens was enclosed within a well insulated box with a cover having three holes. Two of the holes were so spaced as to provide openings for reading the gages, and the other was fitted with a 2-hole rubber stopper for a thermometer

TABLE 4.—*Mean coefficients of linear thermal expansion for some building stones other than granite*

Material	Source	Orientation	Mean coefficient of linear thermal expansion per degree C×10⁶	
			−20° to +60°	+60° to 0°
Limestone	Rockwood, Ala	Parallel to bedding plane.	0.7	−0.1
Do	do	Perpendicular to bedding plane.	1.7	2.9
Do	Bedford, Ind	Parallel to bedding plane.	2.8	3.4
Do	do	Perpendicular to bedding plane.	4.2	4.2
Marble	South Dover, N. Y	"*A*" direction (random).	8.7	9.2
Do	do	Perpendicular to "*A*" direction.	5.2	5.9
Sandstone	McDermott, Ohio	Parallel to bedding plane.	9.2	10.2
Do	do	Perpendicular to bedding plane.	9.5	10.5

and funnel. Two calibrated Tuckerman optical strain gages [26], of 2-in. gage length, reading to 2×10^{-6} in. were used for the expansion measurements (fig. 7). The knife edges of the gages were mounted on thin brass strips attached to the specimen with water-proof cement.

3. Procedure

The specimens were dried at 105° C for 24 hr and cooled in a desiccator. The brass strips were then attached to one plane face of each specimen and, when the cement had hardened

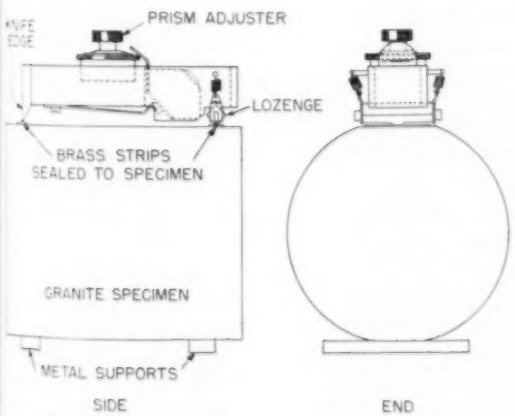

FIGURE 7. *Diagram of Tuckerman optical strain gage mounted on granite specimen.*

sufficiently, the specimens were taken into a controlled temperature room. The gages were then mounted and the knife edges held in firm contact with the metal strips by small rubber bands placed around the specimens and gages. The specimens with the gages were then placed in the brass tank and left overnight to reach an equilibrium temperature (about 21° C). A flask of distilled water was also left standing near the specimens. About 16 hrs later the gages were read and water poured into the tank until the level reached the tops of the specimens. Gage readings were taken at approximately 1-hr intervals for 8 hrs and a final reading after 24 hrs.

During any test, the temperature of the water did not vary more than ±0.5 deg C. The maximum difference in temperature of the water between the time of the first and last reading was 0.2 deg C. Errors due to thermal expansion of the gage or specimen were thereby virtually eliminated.

To verify the fact that the length changes observed in the stone specimens were caused only by the absorption of water, two metal cylindrical specimens were tested in the manner described. The greatest change observed in four tests was 2×10^{-6} in. Since the gages are sensitive only to this amount, it can be assumed that no significant dimensional change took place during these tests.

VII. Moisture Expansion Results

Table 2, column 7, gives the linear moisture expansion results for the 48 samples of granite. The values range from a minimum of 0.0004 percent to a maximum of 0.0090 percent, with an average of 0.0039 percent. Although the immersion period for each test was 24 hrs, five specimens exhibited maximum expansion in 1 hr, and 28 specimens between 2 and 8 hrs.

Figure 8 gives moisture expansion curves for nine samples, together with the corresponding absorption curves. These show results typical for all samples tested. Both the expansion and absorption curves tend to rise sharply during the first few hours and then quickly level off, but there seems to be little correlation between the amounts of expansion and absorption. The moisture expansion values were also compared with density, porosity, and mineral composition but no correlation was found with these properties.

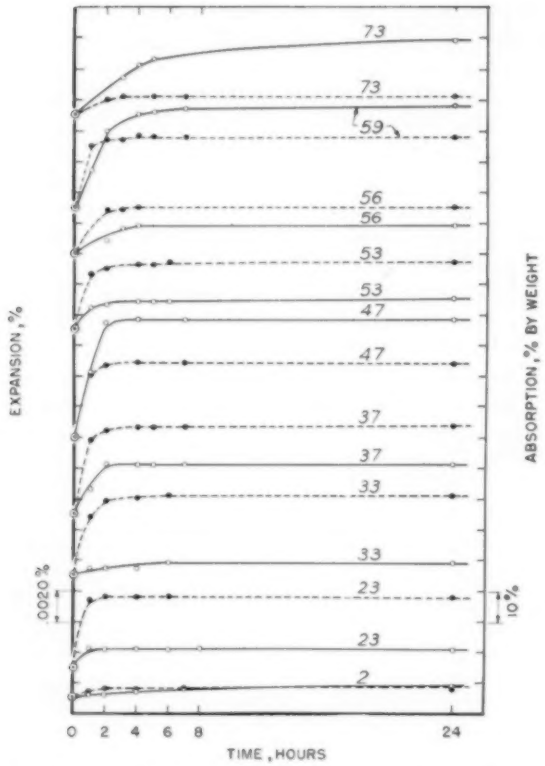

FIGURE 8. *Moisture expansion and corresponding absorption curves of nine granite samples.*

○, Moisture expansion points; ●, absorption points; figures refer to sample numbers in table 2.

Table 5 shows the moisture expansion values obtained for several samples of other types of building stone, tested in the manner described.

VIII. Thermal and Moisture Expansion in Relation to Durability of Granite

Merrill [27] cites several cases of rock weathering, including granite, which he attributed to heating and cooling effects. Temperature changes can produce internal stresses in two ways: (1) a thermal gradient due to heating or cooling of one surface causes unequal expansion of layers at different depths; (2) the various mineral constituents of granite have different expansion rates among themselves and also in different crystallographic directions. Stresses caused by both conditions come into action simultaneously and augment each other. Although such stresses are

TABLE 5. *Moisture expansion values of some building stones other than granite*

Type of stone	Source	Expansion
		Percent
Limestone	Rockwood, Ala	0.0032
Do	Bedford, Ind	.0028
Do	Cedar Park, Tex	.0015
Marble	Gantt's Quarry, Ala	.0010
Do	Whitestone, Ga	.0025
Do	Swanton, Vt	.0010
Sandstone	Amherst, Ohio	.013
Do	Glenmont, Ohio	.010
Do	McDermott, Ohio	.044

usually much lower than those required to produce rupture, frequent repetition and reversal of directions may ultimately cause fractures. These stresses in a compact material like granite are probably greater than in more porous materials.

Two cases can be cited in which rather large spalls occurred at corners of granite masonry where the superimposed loads were not sufficient to account for the fractures. It seems possible that a complication of stresses due to temperature effects might occur in such parts of structures.

One case of cracking has been examined where the facade of a building is made of a granite with unusually large quartz crystals. The polished columns show considerable cracking on the parts most exposed to the sun, while the shaded parts appear to be entirely sound. Several cubic inches of granite have crumbled away from the corner of a column base that is freely exposed to the afternoon sun. This case provides evidence that unequal expansion of the minerals might be causing the deterioration.

The moisture expansion values obtained in this study of granites are not large in comparison with values obtained on certain other types of building materials. In general the total expansion of granites due to moisture (using average values) is equivalent to the thermal expansion produced by a temperature change of about 6 deg C. It was not possible to determine by the methods used in this study if a wet specimen expands at the same rate, due to a thermal change, as a dry specimen. It can be assumed that the two types of expansion occur simultaneously, and the total expansion of a wet granite can be computed as the sum of the moisture and thermal changes. Using the average values for the thermal and moisture expan-

sions, it is found that a 100-ft course of granite may expand 0.05 in. on becoming wet and 0.08 in. due to a 10 deg C increase in temperature, giving a total of 0.13 in. If the course is constrained, there will be an elastic deformation of 0.13 in., and one may estimate the stress produced where the modulus of elasticity (E value) is known. Assuming an E value of 7,000,000 lb/in.^{2}, the resulting compressive stresses would be 760 lb/in.^{2}, which is high in comparison with the superimposed weight stresses in most structures, but rather low in comparison with strength of granite.

A more serious effect might result on coping courses where the masonry has more freedom of movement. The combined effect of thermal and moisture expansion may cause each block to move toward the ends of the structure; but when contraction occurs, there is insufficient tensile strength in the mortar joints to pull the blocks back to their original position, hence cracks at the joints are produced. These cracks become partly filled with dirt and sand from the mortar and the next expansion results in moving the blocks still further. Open joints allow water to enter, and freezing may cause rupture of the mortar in joints at lower levels.

Schaffer [28] points out that a stress gradient is produced by moisture from rains because the stone is soaked to only a slight depth. He believes that frequent repetition of such stresses might produce injurious effects. Observation on granite buildings shows that the surface of granite often scales off, but the scaling is usually confined to small areas of the lower courses. This can be explained by the assumption that salts are carried up into the granite by ground water, and crystals are formed in the pores. The expansive action of the salt crystals in forming causes tensile stresses perpendicular to the exposed face in sufficient amounts to cause the flaking. It seems likely that a compressive stress parallel to the face resulting from a moisture gradient would aggravate the flaking action.

Based on such studies as have been made on structures, it is the authors' belief that most granites are not affected as seriously by thermal and moisture expansion as by other physical and chemical agencies. Deterioration due to expansion probably does not manifest itself appreciably during the normal life of a building, but it may become apparent on certain monumental structures after a long period of time.

IX. Summary

1. Thermal and moisture expansion determinations were made on 48 samples of domestic granites representative of those used in important structures. Complete descriptions are given of the apparatus and test procedures used in making the measurements. The major mineral constituents of the samples were determined by petrographic methods.

2. The linear thermal expansion coefficients for all samples ranged from 4.8 to 8.3×10^{-6} and averaged 6.2×10^{-6} per deg C for the range $-20°$ to $+60°$ C ($-4°$ to 140° F). This average value is smaller than the average (7.7×10^{-6}) obtained by previous investigators, which may be accounted for in part by the lower temperature range explored in the present study. The coefficients of 84 percent of the samples were between 5 and 7×10^{-6} per deg C.

3. Some irregularities in the heating curves were evident in about 65 percent of the samples tested. These irregularities, which occurred somewhere between 0° and $+20°$ C, were probably due to moisture changes in the sample during the test.

4. Although a definite correlation between thermal expansion and mineral composition could not be established from the values obtained because of the heterogeneous composition of granite, the results indicated that granites with exceptionally high percentages of quartz had higher than average coefficients.

5. The moisture expansion values for a 24-hr soaking period at constant temperature, ranged from 0.0004 to 0.009 percent with an average of 0.0039 percent for all samples. The expansion increased rapidly during the first few hours only; thereafter it increased very slowly or remained constant. Little correlation was found between moisture expansion and mineral composition, absorption, specific gravity, or porosity.

6. It is probable that the repeated thermal expansion and contraction of granite resulting from natural weather conditions, is one of the many factors contributing to the eventual disintegration of the stone. These adverse effects of temperature are due mainly to stresses produced by the unequal expansion of layers at different depths and by the unequal expansion of the mineral con-

877106—50——5

stituents. The deterioration resulting from thermal expansion progresses very slowly and probably does not manifest itself appreciably during the normal life of a building, but it may become apparent on certain monumental structures after a long period of time.

There is some evidence that moisture expansion may contribute to the weathering of granite but to a lesser degree than thermal expansion. However, when moisture and thermal expansions occur simultaneously they may cause masonry units to be moved slightly out of position and injure the mortar joints.

The authors thank Peter Hidnert and James B. Saunders of this Bureau for their very helpful suggestions regarding the thermal expansion method used in this investigation.

X. References

[1] W. H. C. Bartlett, Experiments on the expansion and contraction of building stone, Am. J. Sci. & Arts **22,** 136 (1832).

[2] A. J. Adie, On the expansion of different kinds of stone from an increase of temperature with a description of the pyrometer used in making the experiments, Trans. Roy. Soc. Edinburgh **13,** 366 (1836).

[3] T. M. Reade, Origin of mountain ranges (Taylor and Francis, Ltd. London, 1886).

[4] Report on tests of metals, etc. Watertown Arsenal, U. S. War Dept., 322 to 418 (1895).

[5] W. R. Baldwin-Wiseman and O. W. Griffith, Physical properties of building materials, Proc. Inst. Civil Eng. **3,** 179, 290 (1909).

[6] N. E. Wheeler, On the thermal expansion of rock at high temperatures, Trans. Roy. Soc. Can. **3,** 4, 19 (1910).

[7] J. H. Griffith, Thermal expansion of typical American rocks, Iowa Eng. Expt. Sta. Bulletin 128 (1936).

[8] T. F. Willis and M. E. DeReus, Thermal volume change and elasticity of aggregates and their effect on concrete, Am. Soc. Testing Materials **39,** 919 (1939).

[9] W. H. Johnson and W. H. Parsons, Thermal expansion of concrete aggregate materials, J. Research NBS **32,** 101 (1944) RP1578.

[10] Schumann, Protocoll de Verhandlungen der IV General-Versammlung des Vereins Deutscher Cement Fabrikanten (1881).

[11] J. Hirschwald, Handbuch der bautechnischen Gesteingsprufung (Gebrüder Borntraeger, Berlin, 1912).

[12] T. Matsumoto, A study of the effect of moisture content upon the expansion and contraction of plain and reinforced concrete, Univ. of Ill. Eng. Exp. Sta., Bul. No. 126 (Urbana, 1921).

[13] R. E. Stradling, Effects of moisture changes on building materials, Dept. Ind. Sci. Research, Bld. Research Bul. 3 (London, 1928).

[14] N. Royen, Naturstenens tekniska egenskaper och dess anvandning till hysbyggnader och dkydd-rumsanlaggningar, Trans. Chalmers Univ. of Technology, Gothenburg, Sweden No. 8 (1942).

[15] D. W. Kessler, A. Hockman, and R. E. Anderson, Physical properties of terrazzo aggregates, NBS Building Materials and Structures Report BMS98 (1943).

[16] D. W. Kessler, H. Insley, and W. H. Sligh, Physical-mineralogical and durability studies on the building and monumental granites of the United States, J. Research NBS **25,** 161 (1940) RP1320.

[17] G. E. Merritt, The interference method of measuring thermal expansion, J. Research NBS **10,** 59 (1933) RP515.

[18] J. B. Saunders, Expansivity of a Vycor brand glass, J. Research NBS **28,** 51 (1942) RP1445.

[19] H. Fizeau, Uber die Ausdehnung starrer Korper durch die Warme, Ann. Physik **128,** 564 (1866).

[20] J. B. Saunders, An apparatus for photographing interference phenomena, J. Research NBS **35,** 157 (1945) RP1668.

[21] A. Q. Tool, D. B. Lloyd, and G. D. Merritt, Dimensional changes caused in glass by heating cycles, J. Am. Ceramic Soc. **13,** 641 (1930).

[22] J. B. Saunders, Interferometer measurements on the expansion of iron, J. Research NBS **33,** 75 (1944) RP1597.

[23] Kozu and Saiki, Sci. Rep. Toh. Univ. **3,** 2, 205 (1925) as quoted in the Handbook of Physical Constants, Geol. Soc. Am. Special Papers, No. 36, 33 (1942).

[24] Kozu and Ueda, Proc. Imp. Acad. Japan **9,** 262 (1933); **10,** 25 (1933) as quoted in the Handbook of Physical Constants, Geol. Soc. Am. Special Papers, No. 26, 33 (1942).

[25] Kozu, Ueda, and Tsumori, Sci. Rep. Toh. Univ. **3,** 10, 222, (1934), as quoted in the Handbook of Physical Constants, Geol. Soc. Am. Special Papers, No. 36, 33 (1942).

[26] L. B. Tuckerman, Optical strain gages and extensometers, Proc. Am. Soc. Testing Materials **23,** pt. 2, 602 (1923).

[27] G. P. Merrill, Rocks, rock-weathering and soils, p. 158 to 162 (Macmillan Co., New York, N. Y. 1906).

[28] R. J. Schaffer, The weathering of natural building stones, Dept. Ind. Sci. Research, Bldg. Research Spec. Report No. 18, London (1932).

WASHINGTON, October 27, 1949.

U. S. Department of Commerce
National Bureau of Standards

Research Paper RP2088
Volume 44, April 1950

Part of the Journal of Research of the National Bureau of Standards

Separation of 2,3-Dimethylpentane, 1,*cis*-3-Dimethylcyclopentane, and 3-Ethylpentane from Petroleum[1]

By Augustus R. Glasgow, Jr., Charles B. Willingham, and Frederick D. Rossini

This report describes the separation of 3-ethylpentane and the fractionation of 2,3-dimethylpentane and 1,*cis*-3-dimethylcyclopentane from the aromatic-free fraction of petroleum normally boiling in the range 89° to 94° C. These three compounds, together with the four hydrocarbon compounds previously separated, constitute substantially all of the material of this fraction of petroleum. For these seven compounds, the normal boiling points (of high-purity samples not from the present investigation) and the estimated amounts by volume in the original Ponca, Oklahoma, crude petroleum are as follows: 2,3-dimethylpentane, 89.78° C, 0.1 percent; 2-methylhexane, 90.05° C, 0.7 percent; 1,*trans*-3-dimethylcyclopentane, 90.77° C, 0.9 percent; 1,*cis*-3-dimethylcyclopentane, 91.72° C, 0.2 percent; 3-methylhexane, 91.85° C, 0.5 percent; 1,*trans*-2-dimethylcyclopentane, 91.87° C, 0.5 percent; and 3-ethylpentane, 93.47° C, 0.05 percent.

I. Introduction

As part of the work of the API Research Project 6 at the National Bureau of Standards on the fractionation and analysis of hydrocarbons in petroleum [1, 2],[2] the program has been completed on that part of petroleum normally boiling between 89° and 94° C. In earlier work [3, 4], 2-methylhexane, 1,*trans*-3-dimethylcyclopentane, 1,*trans*-2-dimethylcyclopentane, and 3-methylhexane were separated from this fraction, and in the present investigation 2,3-dimethylpentane, 1,*cis*-3-dimethylcyclopentane, and 3-ethylpentane have been determined.[3] This report describes the fractionation of the latter three hydrocarbons and gives the estimated amounts of all seven hydrocarbon components that comprise the aromatic-free fraction of petroleum normally boiling in the range 89° to 94° C.

II. Material Analyzed

The API Research Project 6 at the National Bureau of Standards has had under investigation since 1928 a large quantity of a representative petroleum taken from a well at Ponca, Okla. [1, 2, 6]. All of the material from the original petroleum normally boiling between 89° and 94° C remaining after the previous treatment [3, 4, 7] was blended together for analysis, with the exception of small lots of approximately 50 ml each of the best samples of 2-methylhexane, 1,*trans*-3-dimethylcyclopentane, 1,*trans*-2-dimethylcyclopentane, and 3-methylhexane separated in the previous processing [3, 4]. Before the beginning of the present investigation, the material was again filtered through silica gel [8] to remove traces of toluene and produce a mixture containing only paraffins and cycloparaffins.

III. Method of Analysis and Results

This blend of material normally boiling between 89° and 94° C was distilled analytically at high efficiency. Following the initial distillation shown in figure 1, parts *A*, *B*, *C*, and *D* of the distillate were further processed to fractionate 2,3-dimethylpentane, 1,*cis* 3-dimethylcyclopentane, and 3-ethylpentane, as listed in table 1. Reference [9] gives a description of the distilling columns used.

[1] This investigation was performed as part of the work of the American Petroleum Institute Research Project 6 at the National Bureau of Standards on the "Analysis, Purification, and Properties of Hydrocarbons."

[2] Figures in brackets indicate the literature references at the end of this paper.

[3] See reference [5] for the naming of geometric isomers of the polyalkyl cycloparaffins.

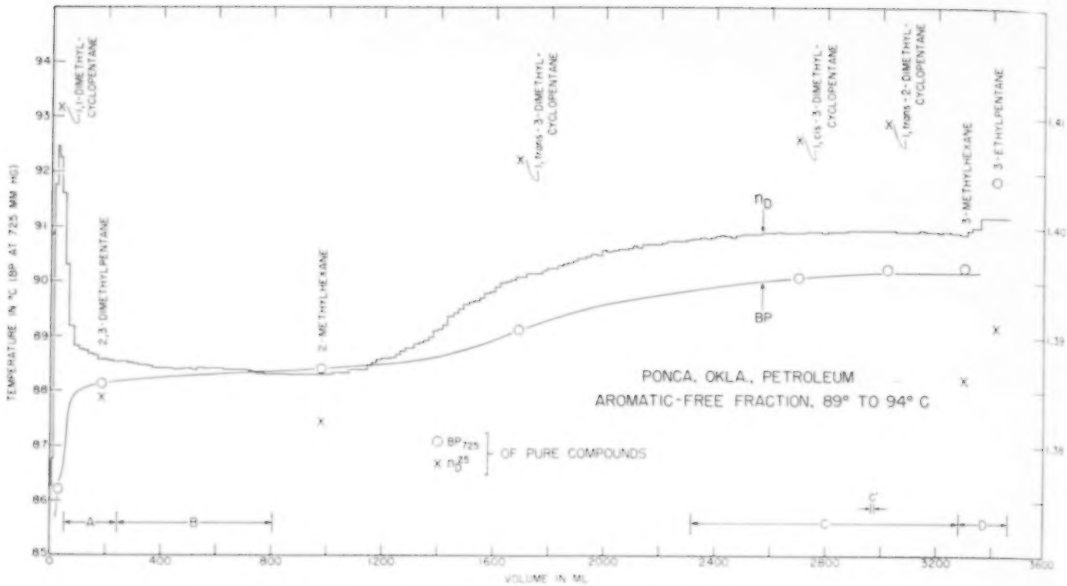

FIGURE 1. *Distillation of the 89° to 94° C (aromatic-free) fraction of petroleum.*

The ordinate scale on the right gives the refractive indices of the fractions of distillate, and the ordinate scale on the left gives the boiling point of the distillate at 725 mm Hg. The scale of abscissas gives the volume of distillate in milliliters. The portions *A* to *D*, enclosed with arrows, were redistilled. The distillate fraction, *C'*, was analyzed by spectrographic infrared absorption measurements, the results of which are given in table 2.

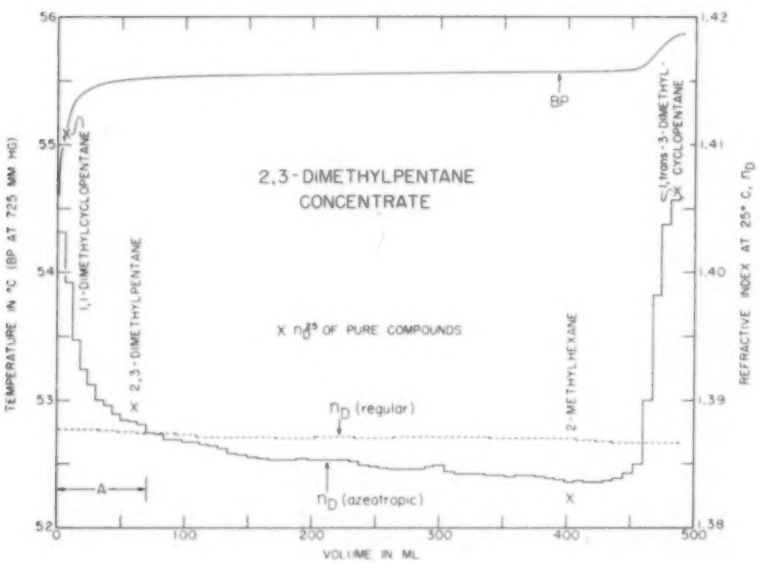

FIGURE 2. *Distillation of the 2,3-dimethylpentane concentrate (part B, fig. 1).*

The ordinate scale on the right gives the refractive indices of the hydrocarbon portion of the fractions of azeotropic distillate, and the ordinate scale on the left gives the boiling point of the azeotropic distillate at 725 mm Hg. The scale of abscissas gives the volume of the hydrocarbon portion of the distillate in milliliters. The portion *A*, enclosed with arrows, was redistilled. The broken curve refers to the previous distribution of the refractive index of this material in the regular distillation (shown by part *B* of fig. 1).

TABLE 1. *Information on the distillation for the analysis and separation of 2,3-dimethylpentane, 1,cis-3-dimethylcyclopentane, and 3-ethylpentane from the aromatic-free fraction of petroleum normally boiling in the range 89° to 94° C.*

Material	Distillation									
	Distilling [a] column number	Number of equivalent theoretical plates at total reflux (approximately)	Reflux ratio (approximately)	Rate of collection of distillate	Pressure of distillation (controlled)	Kind of distillation	Azeotrope-forming substance, if used, and its volume	Volume of hydrocarbon charged	Volume of each fraction of distillate	Results plotted in figure
				ml/hr	*mm Hg*			*ml*	*ml*	
89° to 94° C (aromatic-free) fraction of petroleum.	[b] 3A	200	190/1	4.2	725	Regular		3,530	17	1
2,3-Dimethylpentane concentrate (part B, fig. 1).	1A	150	270/1	1.1	725	Azeotropic	Methanol, 700 ml	550	12	2
2,3-Dimethylpentane concentrate (part A, figs. 1 and 2).	1A	150	270/1	1.1	725	Regular		235	12	3
cis-3-Dimethylcyclopentane concentrate (part C, fig. 1).	1A	150	200/1	1.5	725	Azeotropic	Methanol, 750 ml	878	11	4
cis-3-Dimethylcyclopentane concentrate (part A, fig. 4).	1A	150	150/1	0.5	54	Regular		202	13	5
3-Ethylpentane concentrate (part D, fig. 1).	1A	150	300/1	1.0	725	do		198	7	6
3-Ethylpentane concentrate (part A, fig. 6).	1A	150	300/1	1.0	725	Azeotropic	Methanol, 150 ml	40	6	7

[a] For further details, see reference [9].
[b] Same as column 4 in reference [9].

2,3-Dimethylpentane was fractionated by azeotropic distillation with methanol followed by regular distillation, the results of which are shown in figures 2 and 3. In the azeotropic distillation, the methanol, which comprised about 40 percent by volume of the distillate, was extracted from the hydrocarbon portion by three cold water extractions in a separatory funnel. The best lot from the distillate shown in figure 3 was selected on the basis of boiling point and refractive index as having the highest concentration of 2,3-dimethylpentane. This fraction was examined by spectrographic infrared absorption measurements by the Humble Oil and Refining Company, Houston, Texas, and found to contain 57 percent by volume of 2,3-dimethylpentane. The results are given in table 2.

TABLE 2. *Results of the spectrographic infrared absorption measurements [a, b] of selected samples from the aromatic-free fraction of Ponca, Oklahoma, petroleum normally boiling in the range 89° to 94° C*

Identification of sample	3, 3-Dimethylpentane	1, 1-Dimethylcyclopentane	2, 3-Dimethylpentane	2-Methylhexane	1, *trans*-3-Dimethylcyclopentane	1, *cis*-3-Dimethylcyclopentane	3-Methylhexane	1, *trans*-2-Dimethylcyclopentane	3-Ethylpentane	*n*-Heptane	Methylcyclohexane
	Percentage by volume in the sample										
Part C; figure 1 [b]				2	7	15	37	39			
2,3-Dimethylpentane; figure 3 [a]		1	57	37	3	2	0	0			
Part A; figure 4 [a]				0	3	21	54	22			
Part B; figure 4 [a]				0	3	23	42	32			
Part C; figure 4 [a]				0	2	21	19	58			
Part D; figure 4 [a]				0	2	6	0	92			
Part A; figure 5 [a]				4	19	43	9	25			
Part B; figure 5 [a]				2	8	51	10	29			
Part C; figure 5 [a]				0	7	31	30	32			
3-Ethylpentane; figure 7 [a]						0	0.4	0.8	98.7	0	0

[a] Made by the Humble Oil & Refining Co., Baytown, Tex. A description of the apparatus is given in reference [10].
[b] Made by the Socony-Vacuum Laboratories, Paulsboro, N. J. A description of the apparatus is given in reference [11].

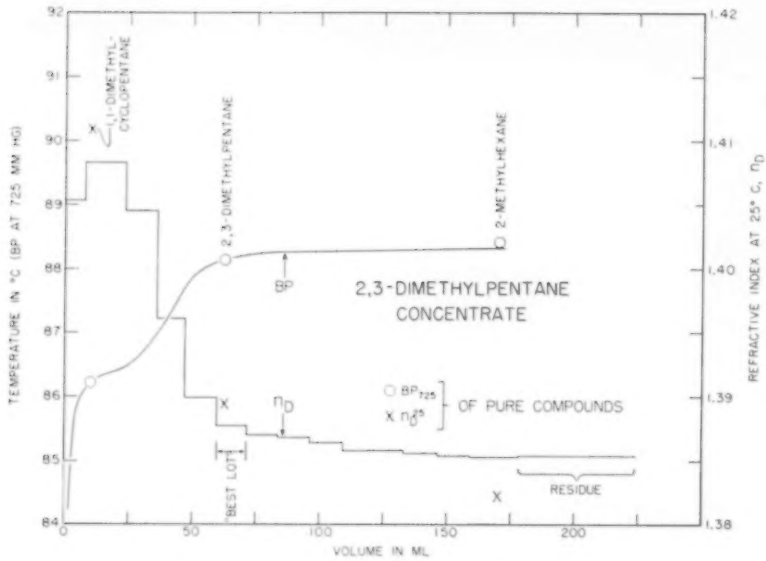

FIGURE 3. *Distillation of the 2,3-dimethylpentane concentrate (part A, figs. 1 and 2).*

The ordinate scale on the right gives the refractive indices of the fractions of distillate, and the ordinate scale on the left gives the boiling point of the distillate at 725 mm Hg. The scale of abscissas gives the volume of distillate in milliliters. The portion labeled "best lot" was analyzed by spectrographic infrared absorption measurements, the results of which are given in table 2.

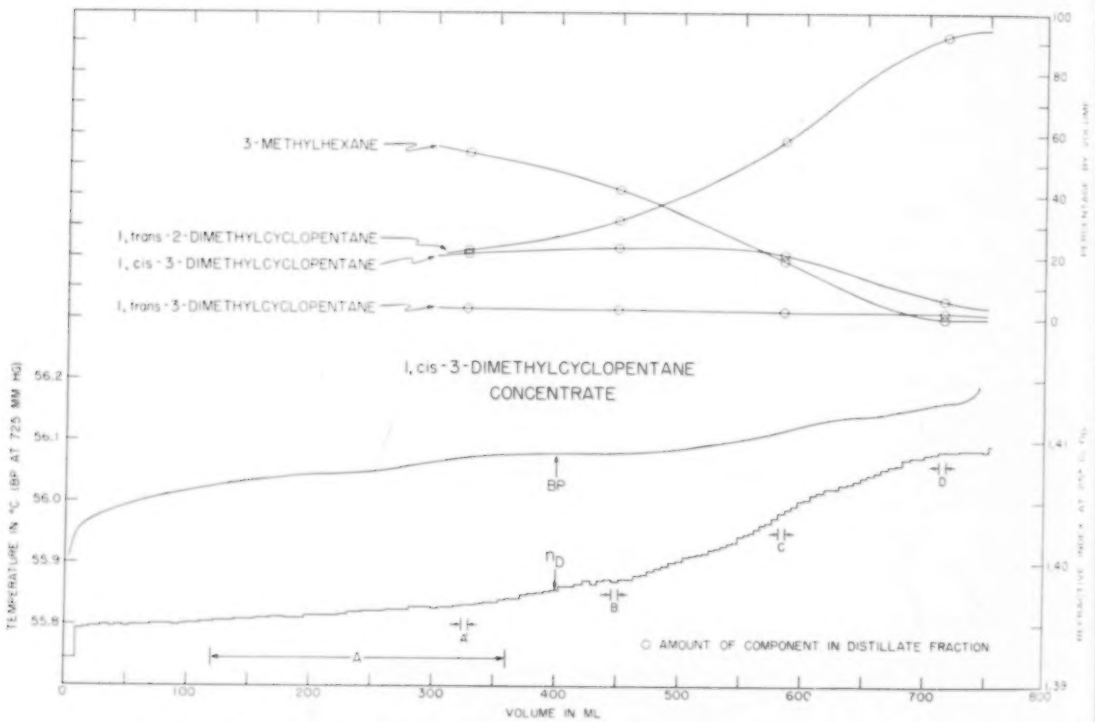

FIGURE 4. *Distillation of the 1,cis-3-dimethylcyclopentane concentrate (part C, fig. 1).*

The ordinates on the right give, on the lower scale, the refractive indices of the hydrocarbon portion of the fractions of azeotropic distillate and, on the upper scale, the percentage by volume of the components in the hydrocarbon portion of the distillate, as determined by spectrographic infrared absorption measurements on fractions labeled *A'*, *B*, *C*, and *D* in the figure. These results are given numerically in table 2 and graphically in the upper portion of the figure. The ordinate scale on the left gives the boiling point of the azeotropic distillate at 725 mm Hg. The scale of abscissas gives the volume of the hydrocarbon portion of the distillate in milliliters. The portion *A*, enclosed with arrows, was redistilled.

The following conclusions may be drawn from the results of the processing of the 2,3-dimethylpentane concentrates: (a) The regular distillation shown in figure 1 substantially separated the components normally boiling near 92° C from 2,3-dimethylpentane and 2-methylhexane normally boiling near 90° C; (b) azeotropic distillation with methanol was effective in further separating 1,1-dimethylcyclopentane and 1,*trans*-3-dimethylcyclopentane from 2,3-dimethylpentane and 2-methylhexane, as shown in figure 2; (c) the regular distillation following the azeotropic distillation further improved the 2,3-dimethylpentane concentrate with additional removal of lower-boiling 1,1-dimethylcyclopentane, as shown in figure 3; (d) regular and azeotropic distillation at 725 mm Hg effects only a partial separation of the two paraffins, 2,3-dimethylpentane and 2-methylhexane. However, regular distillation at reduced pressure should produce a more effective separation because of the increased difference (approximately 1 deg C) in the boiling points [12] of the two isomers at lower pressures (30 to 50 mm Hg).

Following the regular distillation shown in figure 1, 1,*cis*-3-dimethylcyclopentane was fractionated from the components normally boiling near 92° C by azeotropic distillation with methanol followed by regular distillation at a reduced pressure of 54 mm Hg. The results are shown in figures 4 and 5. Part *B* of the distillate shown in figure 5 contained the highest concentration of 1,*cis*-3-dimethylcyclopentane. This portion was examined by spectrographic infrared absorption measurements by the Humble Oil and Refining Company, Houston, Texas, and found to contain 51 percent by volume of 1,*cis*-3-dimethylcyclopentane. The results are given in table 2.

The following conclusions may be drawn from the processing of the material normally boiling near 92° C with respect to the separation of 1,*cis*-3-dimethylcyclopentane: (a) Azeotropic distillation with methanol, as shown in figure 4 and table 2, produces an appreciable separation in the two dimethylcyclopentanes, one from the other, resulting in a nine-fold change in the composition of the two isomers in the distillate, as well as effectively removing 3-methylhexane from 1,*trans*-2-dimethylcyclopentane; (b) the regular distillation at a pressure of 54 mm Hg, as shown in figure 5, effectively removes the 3-methylhexane from the cycloparaffins because of the greater difference in the boiling points [4, 12] at the reduced pressure between the paraffin, 3-methylhexane, and the cycloparaffins, 1,*cis*-3-dimethylcyclopentane and 1,*trans*-2-dimethylcyclopentane.

3-Ethylpentane was separated from the undistilled portion, *D*, in figure 1, by regular distillation followed by azeotropic distillation with methanol. The results are shown in figures 6 and 7, respectively. The best lot from the distillate shown in figure 7 was selected on the basis of boiling point and refractive index as having the highest concentration of 3-ethylpentane. This lot was examined by spectographic infrared absorption measurements by the Humble Oil and Refining Co., Baytown, Tex., and found to contain 98.7 percent by volume of 3-ethylpentane. The results are given in table 2.

The following conclusion may be drawn from the processing of the 3-ethylpentane concentrates: (a) This compound, which occurs in small amount in petroleum, is easily separated by regular and azeotropic distillation.

IV. Amounts in the Crude Petroleum

The calculation of the amounts by volume of the seven compounds in the aromatic-free fraction of Ponca, Okla., petroleum, normally boiling between 89° and 94° C, was made using the data from the analysis of seven representative crude petroleums [13, 14, 15] supplemented by the results of the present investigation, including the spectrographic infrared absorption measurements on selected fractions as listed in table 2.

The spectrographic data served to establish the relative amounts of 1,*cis*-3-dimethylcyclopentane and 1,*trans*-2-dimethylcyclopentane, and of 2,3-dimethylpentane and 2-methylhexane. The data on boiling point and refractive index as a function of volume of distillate were utilized to the fullest extent of their precision by plotting the data on expanded scales of temperature, refractive index, and volume for use in the calculation of the amounts of the individual components as described in reference [16].

The ratios of 2,3-dimethylpentane to 2-methylhexane and of 1,*cis*-3-dimethylcyclopentane to 1,*trans*-2-dimethylcyclopentane found in the present investigation are considered to be representative of the original petroleum on the assumption

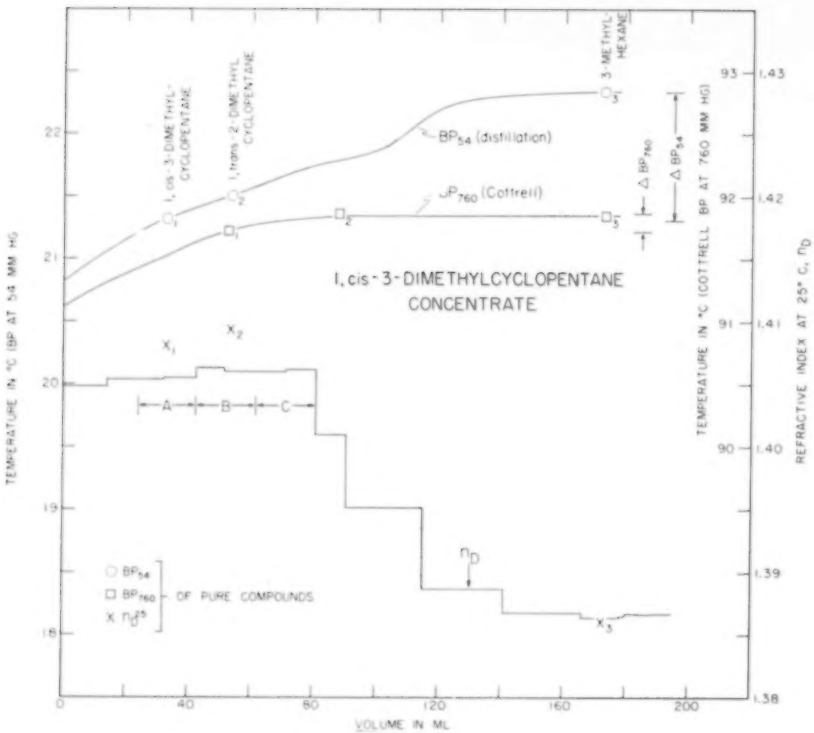
1, cis - 3 - DIMETHYLCYCLOPENTANE
CONCENTRATE
BP54 (distillation)
BP760 (Cottrell)
1, cis - 3 - DIMETHYL - CYCLOPENTANE
1, trans - 2 - DIMETHYL CYCLOPENTANE
3 - METHYL HEXANE
A
B
C
OF PURE COMPOUNDS
TEMPERATURE IN °C (BP AT 54 MM HG)
TEMPERATURE IN °C (COTTRELL BP AT 760 MM HG)
REFRACTIVE INDEX AT 25° C, nD
VOLUME IN ML

FIGURE 5. *Distillation of the 1,cis-3-dimethylcyclopentane concentrate (part A, fig. 4).*

The ordinates on the right give, on the upper scale, the refractive indices and, on the lower scale, the Cottrell boiling points at 760 mm Hg of the fractions of the distillate. The ordinate scale on the left gives the boiling point of the distillate at 54 mm Hg. The scale of abscissas gives the volume of distillate in milliliters. The portions *A*, *B*, and *C*, enclosed with arrows, were analyzed by spectrographic infrared absorption measurements, the results of which are given in table 2. The numbers accompanying the boiling point and refractive index values shown in the figure refer to the following: (1) the 1,*cis*-3-dimethylcyclopentane, (2) to 1,*trans*-2-dimethylcyclopentane, and (3) to 3-methylhexane.

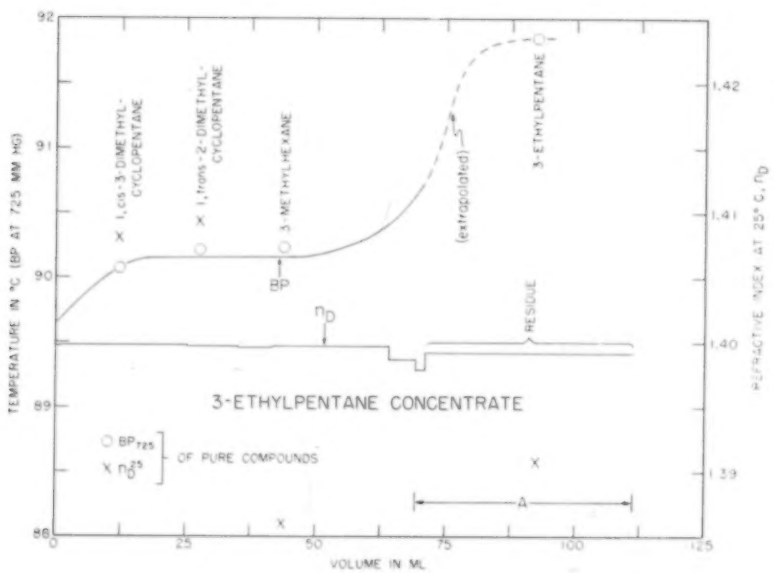

FIGURE 6. *Distillation of the 3-ethylpentane concentrate (part D, fig. 1).*

The ordinate scale on the right gives the refractive indices of the fractions of distillate, while the ordinate scale on the left gives the boiling point of the distillate at 725 mm Hg. The scale of abscissas gives the volume of distillate in milliliters. The portion *A*, enclosed with arrows, was redistilled.

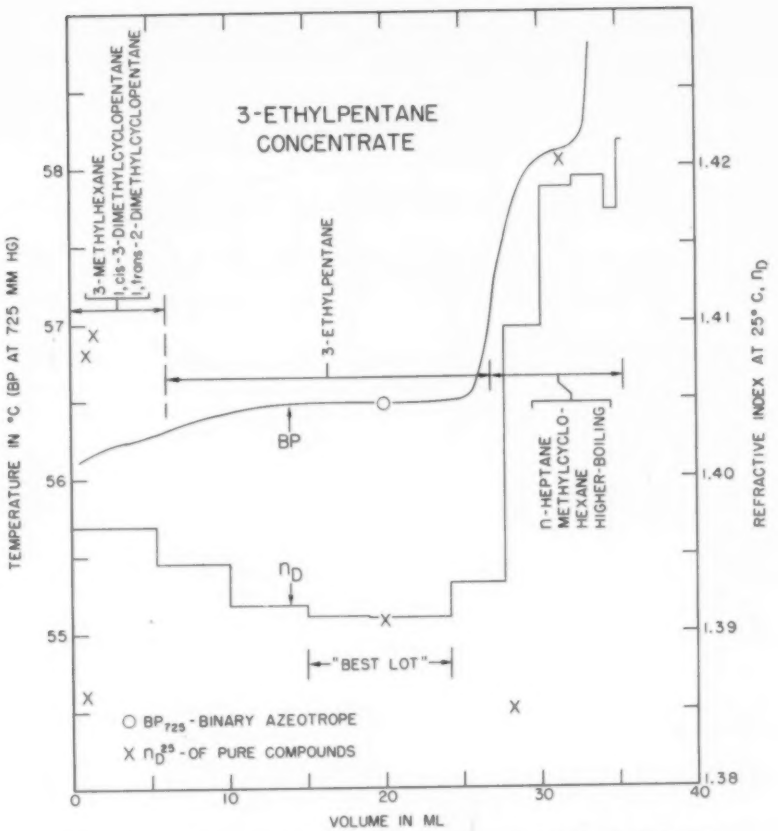

FIGURE 7. *Distillation of the 3-ethylpentane concentrate (part A, fig. 6).*

The ordinate scale on the right gives the refractive indices of the hydrocarbon portion of the fractions of azeotropic distillate, and the ordinate scale on the left gives the boiling point of the azeotropic distillate at 725 mm Hg. The scale of abscissas gives the volume of the hydrocarbon portion of the distillate in milliliters. The portion labeled best lot was analyzed by spectrographic infrared absorption measurements, the results of which are given in table 2.

77106—50——6

that no change in composition of these close-boiling pairs of components, which differ in normal boiling point by 0.27° and 0.15° C [12], occurred during previous processing losses.

The amounts by volume of the seven hydrocarbons in the aromatic-free fraction normally boiling in the range 89° to 94° C and in the original petroleum are give in table 3.

TABLE 3. *Amounts of the seven hydrocarbons constituting the 89° to 94° C aromatic-free fraction of the petroleum*

Component	Boiling point at 1 atm [a]	Relative amount by volume	Amount in the original crude petroleum [b]
	° C		*Percentage by volume*
2,3-Dimethylpentane	89.78	5	0.1
2-Methylhexane	90.05	24	.7
1,*trans*-3-Dimethylcyclopentane	90.77	29	.9
1,*cis*-3-Dimethylcyclopentane	91.72	7	.2
3-Methylhexane	91.85	17	.5
1,*trans*-2-Dimethylcyclopentane	91.87	16	.5
3-Ethylpentane	93.47	2	.05
Total		100	2.95

[a] From reference [17].

[b] For each component, the percentage by volume of the gasoline fraction, 40° to 180° C, is about three times the value in this column.

From the data given in table 3, the following points may be made regarding the composition of the material normally boiling between 89° and 94° C, from the Ponca, Okla., petroleum:

(a) The material is composed entirely of branched paraffins and cycloparaffins in approximately equal amounts.

(b) The relative amounts of the methylhexanes, dimethylpentanes, and ethylpentane are approximately 20, 2, and 1, respectively.

(c) The relative amounts of the three dimethylcyclopentanes are 4, 2, and 1, for the 1,*trans*-3-, 1,*trans*-2-, and 1,*cis*-3- isomers, respectively.

Grateful acknowledgment is made to H. H. Meier and A. A. Draeger, Humble Oil & Refining Co., Baytown, Tex., and to F. P. Hochgesang, Socony-Vacuum Laboratories, Paulsboro, N. J., for the spectrographic infrared absorption measurements reported in table 2 of this paper.

V. References

[1] F. D. Rossini, Petroleum Engr. **14,** 223 (1943).

[2] F. D. Rossini, Anal. Chem. **20,** 110 (1948).

[3] J. H. Bruun and M. M. Hicks-Bruun, BS J. Research **10,** 465 (1933)RP 542.

[4] A. R. Glasgow, Jr., J. Research NBS **24,** 509 (1940) RP1296.

[5] M. B. Epstein and F. D. Rossini, American Petroleum Institute Research Project 44, National Bureau of Standards. Naming of geometric isomers of polyalkyl monocycloalkanes.

[6] F. D. Rossini, Proc. Am. Petroleum Inst. **18,** III 36 (1937); Oil Gas J. **36,** 193 (1937); Refiner Natural Gasoline Mfr. **16,** 545 (1937).

[7] M. M. Hicks-Bruun and J. H. Bruun, BS J. Research **8,** 525 (1932)RP432.

[8] B. J. Mair, A. L. Gaboriault, and F. D. Rossini, Ind. Eng. Chem. **39,** 1072 (1947).

[9] C. B. Willingham and F. D. Rossini, J. Research NBS **37,** 15 (1946)RP1724.

[10] American Petroleum Institute Research Project 44, National Bureau of Standards. Catalog of infrared spectral data. Description of infrared spectrograph, No. 16. Contributed by the Humble Oil and Refining Company.

[11] American Petroleum Institute Research Project 44, National Bureau of Standards. Catalog of infrared spectral data. Description of infrared spectrograph, No. 5. Contributed by the Socony Vacuum Laboratories.

[12] A. F. Forziati, W. R. Norris, and F. D. Rossini, J. Research NBS **43,** 555 (1949)RP2049.

[13] F. D. Rossini, B. J. Mair, A. F. Forziati, A. R. Glasgow, Jr., and C. B. Willingham, Proc. Am. Petroleum Inst. **23,** III 7 (1942); Oil Gas J. **41,** 106 (1942); Petroleum Refiner **21,** 73 (1942).

[14] A. F. Forziati, C. B. Willingham, B. J. Mair, and F. D. Rossini, J. Research NBS **32,** 12 (1944)RP1571; Proc. Am. Petroleum Inst. **24,** III 34 (1943).

[15] A. F. Forziati and F. D. Rossini, American Petroleum Institute Research Project 6, National Bureau of Standards. Unpublished data.

[16] A. R. Glasgow, Jr., A. J. Streiff, C. B. Willingham, and F. D. Rossini, Proc. Am. Petroleum Inst. **26,** III 127 (1946); J. Research NBS **38,** 537 (1947) RP1795.

[17] A. F. Forziati and F. D. Rossini, J. Research NBS **43,** 473 (1949)RP2038.

WASHINGTON, November 22, 1949.

U. S. Department of Commerce
National Bureau of Standards

Research Paper RP2089
Volume 44, April 1950

Part of the Journal of Research of the National Bureau of Standards

Interference Methods for Producing and Calibrating End Standards

By Chauncey G. Peters and Walter B. Emerson

An interferometric apparatus developed at the National Bureau of Standards for ruling meter scales in terms of wavelengths of light requires accurate determination of the length of a decimeter etalon. To compare the results of the interferometric methods of measurement used at this Bureau with those of other national laboratories, etalons of fused quartz having highly polished plane and parallel end surfaces were made and calibrated at this Bureau. They were then sent to the Bureau International des Poids et Mesures, Physikalish-Technische Reichsanstalt, and The National Physical Laboratory for calibration. The lengths of the etalons as determined by the various laboratories are:

Etalon No.	By other Laboratory	By NBS	Difference
	mm	*mm*	*mm*
11	BIPM 99.999 848	99.999 855	−0.000 007
2	PTR 99.999 934	99.999 907	+.000 027
15	PTR 99.999 899	99.999 919	−.000 020
13	NPL 99.999 862 (initial measurements)	99.999 872	−.000 010
14	NPL 99.999 906 (initial measurements)	99.999 888	+.000 018

These results indicate that diverse interferential methods used by the different laboratories give the same lengths to an average deviation of 0.016 μ (1 part in 6,000,000) and to a probable uncertainty much less.

Besides furnishing a direct comparison of the results obtained by different interferential methods, the investigation gives values for the index of refraction of air and also wavelength values for several radiations of krypton and cadmium. These are included in the paper.

Because of inherent advantages of fused quartz etalons as separators for Fabry-Perot interferometers, the methods used in making and calibrating these etalons are given in detail.

I. Introduction

1. Light Waves as Length Standards

Impetus for the use of light waves as standards of length developed from the classical measurements of Michelson and Benoît [1],[1] who in 1893 determined the number of waves of red, green, and blue radiations of cadmium in the standard meter; and those of Benoît, Fabry, and Perot [2], who repeated these measurements in 1905–06 with modified apparatus.

In 1925 the International Astronomical Union provisionally adopted [3] the red radiation of cadmium as the standard for wavelength measurement, assigning as its wavelength for specified conditions of gravity, air temperature and pressure, and operation of the source the value determined by Benoît, Fabry, and Perot; namely $\lambda_R = 6438.4696 \times 10^{-10}$ m. In 1927 the International Conference on Weights and Measures likewise adopted [4] the red radiation of cadmium as the primary wavelength standard with the same value, $\lambda_R = 6438.4696 \times 10^{-10}$ m, but with a specification for the source that differed in some details

[1] Figures in brackets indicate the literature references at the end of this paper.

from that adopted by the IAU. Further changes in the specification of the cadmium source were adopted by the International Committee on Weights and Measures in 1935 [5]. The selection of this particular radiation appears to have been happy in that no definitely superior line has since been discovered in nature. Recently, however, artificial Hg^{198} has been produced, which gives superior radiations. Furthermore, the original value of Benoît, Fabry, and Perot that was adopted for its wavelength is confirmed within the uncertainties of measurements by later determinations, as seen in table 1, compiled by Barrell [6].

TABLE 1. *Determinations of λ_R by various observers*

Date of determination	Observer	Original values	Values corrected and adjusted for normal air	Difference from the mean
		Å	Å	Å
1892-93	Michelson & Benoît (BIPM) [1]	6438.4722	6438.4691	−0.0005
1905-06	Benoît, Fabry, & Perot (BIPM) [2]	6438.4696	6438.4703	+.0007
1927	Watanabe & Imaizumi (Japan) [7]	6438.4685	6438.4682	−.0014
1933	Sears & Barrell (NPL) [8]	6438.4711	6438.4713	+.0017
1933	Kösters & Lampe (PTR) [9, 10]	6438.4672	6438.4689	−.0007
1934-35	Sears & Barrell (NPL) [11]	6438.4709	6438.4709	+.0013
1934-35	Kösters & Lampe (PTR) [11]	6438.4685	6438.4690	−.0006
1937	Kösters & Lampe (PTR) [12]	6438.4700	6438.4700	+.0004
1940	Romanova, Varlich, Kartashev, & Batarchukova (USSR) [13]	6438.4677	6438.4687	−.0009
	Mean		6438.4696	±0.0009

Although individual determinations of λ_R differ by more than one part in 2 million, the mean of all nine corrected determinations is identical with the adopted value. The wavelengths of certain neon and krypton lines have been determined relative to λ_R with high precision, thus making length measurements with these lines equivalent to direct comparisons with the cadmium standard. Repeated intercomparisons of lines from numerous sources over long periods of time show no definite variations in their wavelengths greater than the uncertainty of measurement. It is therefore evident that suitable lines can be confidently adopted as standards of length.

It is a well-known fact that length standards of alloys or other materials have shown considerable change in length with time. The results in table 1 show that the meter bars have, however, during the interval 1892 to 1940, remained constant in length within the limits of error imposed by intercomparison of ruled scales and light waves.

For the past 30 years interferential methods using light waves as length standards have been employed by this Bureau to calibrate standard and commercial end gages. The original methods of making these tests have been adequately described by Peters and Boyd [14]. During the same period other national standardizing laboratories likewise developed methods and apparatus for calibrating gages by means of light waves.

To ascertain the degree of uniformity of interferential calibrations by different laboratories, this Bureau in 1927 submitted four 1-in. Johansson gages, designated: $.B_1$, $:B_1$, $\therefore B_1$, $::B_1$, to the National Physical Laboratory (NPL), the Physikalisch-Technische Reichsanstalt (PTR), and the Bureau International des Poids et Mesures (BIPM) for calibration. A summary of these measurements is given in table 2. The individual measurements differed from the mean by 0.00 to 0.03μ.

TABLE 2. *Calibration of 1.0-in. gages by different laboratories*

Measured by—	Length at 20° C			
	$.B_1$	$:B_1$	$\therefore B_1$	$::B_1$
	mm	mm	mm	mm
NPL	25.400 054	25.400 059		
PTR			25.400 08	25.400 0
BIPM			25.400 10	25.400 1
NBS	25.400 11	25.400 06	25.400 09	25.400 0

In view of the availability, reproducibility, permanency, and adaptability of light waves for precise measurements of end gages, their use is favored for calibrations up to the maximum length to which they may be directly applied with accuracy. One further step in their evaluation as length standards remains; i. e.: to determine the precision with which the prototype meter line scale itself may be reproduced by means of light waves. A meter so reproduced will give a direct check, within the errors of ruling and measuring, of the accuracy of the lengths that have been assigned to the waves employed.

2. Purpose of this Investigation

This Bureau has developed apparatus for ruling meters in terms of light waves, reversing the pro-

cedure of Michelson and Benoît. The method selected requires the stepping-off of a meter by using a decimeter end gage that has been measured in terms of standard waves. An accurate direct interferometric calibration of this decimeter gage is imperative, because any uncertainty in its length is multiplied by a factor of 10 in the meter ruled with it. Although the 1927 comparisons gave good agreement among observers for 1-in. gages, no international comparisons were then available for gages of 1-decimeter length for which the path difference approaches the limits of satisfactory interference set by the inherent characteristics of the radiations.

The purpose of the present investigation was to to determine the accuracy of this Bureau's interferential measurements of decimeter lengths. To do this, decimeter end gages of fused quartz were calibrated at the NBS, then two of these were sent to the NPL, two to the PTR, and two to the BIPM. Although decimenter gages had been prepared from the same material (a special steel) as that to be used in ruling meters, it seemed advisable in this investigation to use gages that were capable of more precise measurement than were steel gages. From considerations of permanency, low thermal expansivity, and the perfection with which optical surfaces may be polished plane and parallel, fused quartz glass was selected as the most suitable material. Although this is too fragile for commercial gages, its fragility proved no real handicap in the present investigation. The results obtained by the use of these fused quartz gages give a critical test of the uniformity of measurements by interferential methods at the various standardizing laboratories.

3. Data

In order to meet the more exacting requirements of present-day gage calibrations, interferential methods employed at the NBS have been modified somewhat since the paper of Peters and Boyd was published. Detailed information is therefore given of these present methods, together with the results obtained at this Bureau for 12 fused quartz decimeter end gages, including 5 that were also measured by standardizing laboratories that use other interferential methods.

As an auxiliary investigation, gages of fused quartz, combined with fused quartz plates to form a Fabry-Perot interferometer, proved adaptable to the determination of the refractive index of air and to the determination of other useful wavelengths by comparison with the standard cadmium wavelength. The results of preliminary measurements of the refractive index of air and also the wavelength values that were obtained for several radiations of cadmium and krypton are included. Because of the proved value of these fused quartz gages and consequently their possible value to other investigators, the procedure in making them is included in this paper.

II. Procedure in Making the Gages

1. Preparation of Blanks

Fused quartz was obtained commercially in the form of cylindrical slugs (diameter 8 cm, length 11 cm). These slugs were clear except for scattered minute bubbles, which did not affect their use for end gages. Each slug was sawed into blanks 2 cm square and slightly over 10 cm long, which were afterward heated in an electric furnace to 1,145° C, held at this temperature 35 min and cooled in the furnace to 900° C at the rate of 1° C per minute. The heating current was then cut off, increasing the cooling rate somewhat. This heat-treatment left the quartz in about the same strain-free condition when examined in polarized light as that of well-annealed optical glass. After cooling, the blanks were machine-ground on all faces and finished with 303 emery to within 15 fringes (4.5μ) of the correct length.

2. Finishing of the Gages

First an attempt was made to work the gages in multiple. Four over-length blanks were cemented together and fused quartz blocks 1 by 2 by 5 cm were cemented at the ends of the blanks, as shown in figure 1, to prevent rounding of the edges during polishing. The surfaces were then ground and polished to correct form and length. Multiple working of the gages proved unsatisfactory however, for after the pressure on the blanks (which resulted from the cementing operation) was released the gage surfaces were found to be distorted and their parallelism destroyed. Final procedure was to work each blocked-up end surface of each gage separately. Blocks of fused quartz 1 by 2 by 3 cm were cemented to one end of a blank,

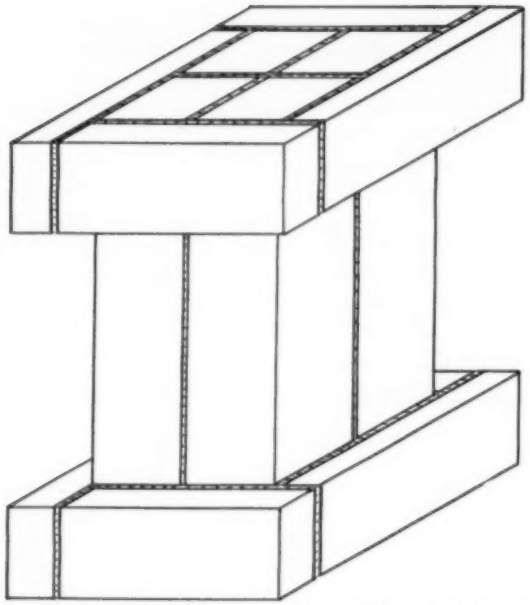

FIGURE 1. *Gage blanks mounted for multiple working of their end surfaces.*

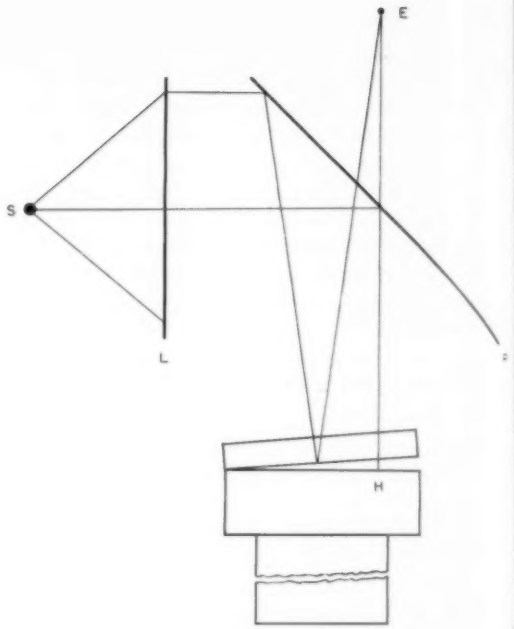

FIGURE 2. *Apparatus for inspecting the gage surfaces.*

after which that end surface was fine-ground with 304 emery on a cast iron lap and pitch-polished plane, using opticians lump rouge. During the early polishing operation, surfaces were inspected with the simple interferometric testing device of Peters and Boyd shown in figure 2 consisting of source, S, of monochromatic light, diffusing glass plate, L, and a thin glass plate, P, set at 45 deg to perpendicular EH from the eye to the surface. As a surface approached its final form, more precise measurements were made with apparatus described below.

After one end of a gage had been finished, the blocks were removed and applied to the unfinished end, which was then worked to make it plane, parallel to and 100 mm distant from the first surface. Length measurements were first made with a Zeiss optimeter until the gage was within 6 or 7 fringes (2μ) of the required length, and errors in parallelism were down to 1 fringe. At this stage more sensitive methods of measuring both parallelism and length were substituted. It was found necessary to continue to completion work once started on a surface because of slippage of the cemented blocks with time and, for this reason, rapidity was an added requirement of the test methods.

3. Method of Checking Parallelism and Planeness of the Ends

The apparatus for testing parallelism and planeness of the ends is illustrated in figure 3. Three quartz end gages (1, 2, 3), each 2 by 2 by 10.03 cm, made accurately to the same length, were wrung to quartz flat B. To the other end of each of these, quartz flat A was also wrung. The adjacent surfaces of A and B were thus plane and parallel (to 0.01λ), and 10.03 cm apart. S is a thin wooden strip that was attached to the rear of supports 1 and 2 by means of wax. Gage G is in position for test. The assembled apparatus is shown in figure 4.

The procedure for testing parallelism of surfaces was to insert a gage between the plane surfaces of A and B and to incline it slightly to the vertical by so resting it against the strip S as to give a spacing of about 2 mm to the straight fringes that were formed by interference of helium light reflected from the lower surface of A and from the top of the gage. These fringes were viewed normally by means of a Pulfrich instrument [15], which is a self-contained device for illuminating and viewing the surfaces and for measuring deviations and displacements of the fringes. The

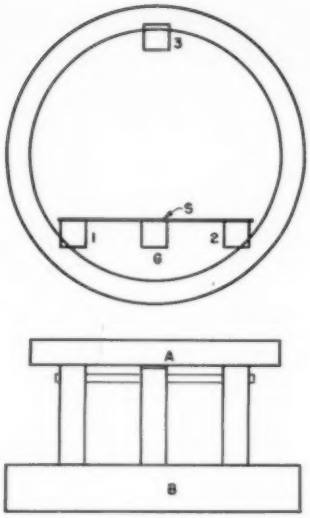

FIGURE 3. *Apparatus for testing parallelism and planeness of the gage surfaces.*

cross wires of this instrument were made parallel to the fringes in direction *ab*, figure 5. Next, the instrument was refocused upon a lower set of fringes formed by interference at the upper surface of *B* and the bottom of the gage. The condition of parallelism required that the latter set of fringes should also be parallel to the cross wires, i. e., the upper and lower sets of fringes should be mutually parallel. The deviation from this condition was a measure of lack of parallelism. For example: if distance e from the fringe to the cross wire differs from f by one-third the distance between two fringes, then the gage lengths at edges *a* and *b* differ by ⅓ fringe (0.1μ). This difference in length at opposite edges, or lack of parallelism, will be termed the "slope" of the gage. In order to compensate for possible slope in the apparatus, the gage was measured in one position, rotated 180 deg. and remeasured; the recorded slope of a gage is the mean of these measurements. The slope was determined at *a*,

FIGURE 4. *Assembled apparatus for testing the gages.*

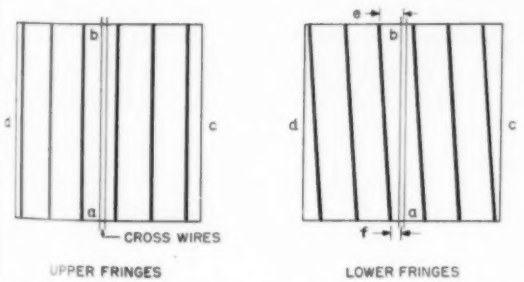

FIGURE 5. *Upper and lower sets of interference fringes.*

b and *c*, *d* for each gage. These tests could be made rapidly and consequently served as a convenient basis for correcting errors in parallelism. The accuracy of the method was verified by length measurements at opposite edges of the gages.

For making accurate measurements of planeness with the same apparatus, the procedure was to place the tested surface beneath plate *A* as shown by *G* in figure 3. Its curvature was determined by placing straight edge *E*, figure 6, above

the fringe pattern and measuring the departure of a fringe from a straight line. If a surface was higher at its center than at its edges by ¼ fringe, then the end of the gage was considered ¼ fringe (0.1μ) convex. In general, departures from planeness assumed the form of regular curvatures.

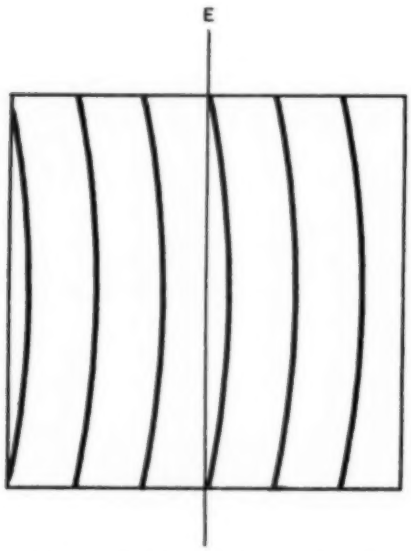

FIGURE 6. *Method of determining surface curvature.*

4. Rapid Method for Checking Lengths

In order to expedite length measurements during the making of the gages, a comparator that is an adaptation of the interferometer described by Priest [16] was used. This is shown in figure 7 and also in figure 4 (slightly to the left of center). For temperature stability, the base and the interferometer support were machined from a heavy steel casting. A, figure 7, is a stainless steel anvil with two parallel strips, each 0.5 mm wide, which supports alternately a standard quartz gage and the gage to be tested. The bottom of anvil A and the top of the base on which it rests were lapped plane, wrung together, and then held by means of screws. B is a glass flat that is cemented in a recess in the top of the block. D is another glass flat that rests upon adjustable screw points S, S and is held in place by spring plungers P above S, S which press down lightly in depressions in the top of plate D, above and in line (L_3) with the supporting screws. Contact C is a small ball that is cemented into a depression in D. Lines

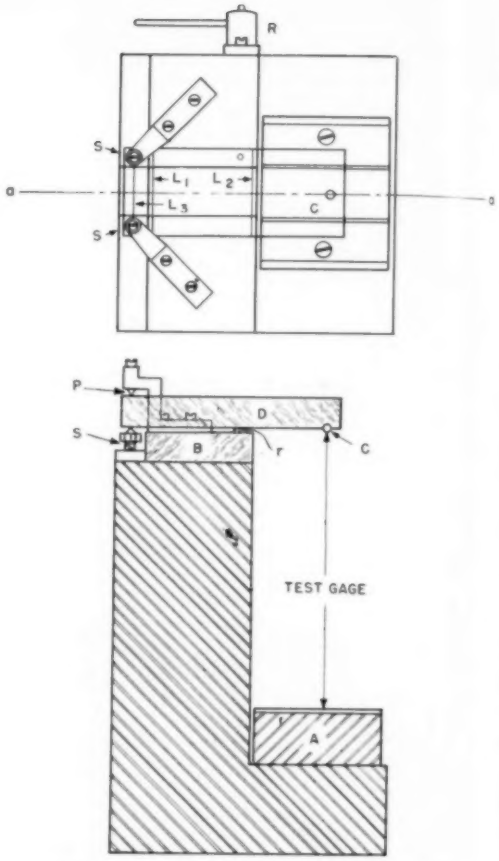

FIGURE 7. *Interferometric length comparator.*

L_1 and L_2 are ruled transversely on plate B; their separation equals one-half the distance between L_3 and C. Screws S, S are adjusted to place the surface of D parallel to and slightly above B. A device R, operates a small rod r, which permits the making or breaking of contact at C. If the inclination of D with respect to B is relatively small, straight fringes are seen when the surfaces are illuminated and viewed normally. The number of fringes between L_1 and L_2 depends upon the inclination of the adjacent surfaces of B and D and the length of the light wave.

In testing, a standard gage is first inserted between C and A and the fringes between L_1 and L_2 counted. The count is repeated after substituting the unknown gage for the standard. The length of the tested gage will be

$$l = l_s + (n - n_s)\lambda, \text{ in which}$$

l = the length of the unknown gage

l_s = the length of the standard gage

n = the number of fringes between L_1 and L_2 with the unknown gage

n_s = the number of fringes between L_1 and L_2 with the standard gage

λ = the wavelength of the source

n and n_s may be positive or negative with respect to each other, and their signs must be considered in the equation. If the fringes are viewed with a Pulfrich instrument, n and n_s may be determined to 0.1 fringe by inspection; thus, the difference in length of the two gages can be quickly measured to 0.1 wavelength (0.06μ).[2]

Measurements were made immediately after each attempted correction (in which great care had to be taken to avoid over-correction) when the gage was at a nonuniform and indeterminate temperature that was higher than that of the standard gage as a result of the polishing operation. Consequently, the end point of each attempt depended upon the judgment of the operator in allowing for contraction of a gage upon cooling.[3]

5. Gages Produced

Following the above procedure, fifteen decimeter gages were made and later, using modified testing apparatus, six 50-mm gages, one 35-mm gage, and two 25-mm gages were produced.

After removal of the end blocks, the edges of the gages were bevelled slightly. The gages were then carefully measured again for planeness and parallelism by the methods as described, and twelve of the decimeter gages were found satisfactory for use as standards. Table 3 gives the planeness and parallelism of these gages, and figure 8 will aid in its interpretation. Let a, b, c, d be the medial points of the edges of one face of a gage and e, f, g, h be the corresponding points of the opposite face. The headings of columns 2 to 6 refer to the directions in which the planeness measurements were made. (It will be noted that one face—always the surface first brought to final correction—is more nearly plane than the other face). The edge containing a was taken as the standard edge in subsequent calibrations. Column 6 gives the combined curvature of the gage surfaces in plane $abfe$. Subscripts A, B, C, D, later associated with a gage number, refer to lengths at a, b, c, and d, respectively.

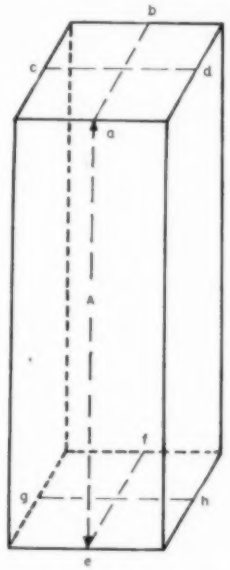

FIGURE 8. *Lettering assigned to a gage to aid in the interpretation of the measurements.*

TABLE 3. *Planeness and parallelism of twelve fused quartz decimeter gages*

Gage	Planeness					Parallelism	
	a, b	c, d	e, f	g, h	a,b+e,f	A>B	C>D
(1)	(2)	(3)	(4)	(5)	(6)	(7)	(8)
	μ	μ	μ	μ	μ	μ	μ
3	[a]0.005c	0.005c	0.011c	0.004c	0.016c	−0.004	+0.057
5	.002c	.000	.004v	.000	.002v	−.006	+.003
6	.006c	.004v	.025c	.025c	.019c	−.011	+.006
7	.005c	.004c	.035c	.007c	.040c	+.002	+.035
8	.010c	.001v	.015c	.010c	.025c	−.007	+.012
9	.005c	.001v	.001c	.001c	.007c	−.002	+.002
10	.018c	.001v	.006c	.003c	.024c	+.007	−.041
11	.000	.002v	.012c	.003c	.012c	+.006	−.016
12	.001c	.004c	.013c	.027c	.014c	+.002	−.033
15	.002v	.002v	.009v	.011v	.011v	−.015	+.021
16	.000	.001c	.032c	.032c	.032c	−.032	−.004
17	.003v	.013c	.005v	.003v	.008v	+.007	−.034

[a] c=concave; v=convex.

[2] In making the fused quartz gages, the total length could not be controlled to this accuracy.

[3] Subsequent measurements using more precise methods show the importance of having the surfaces plane and parallel for accurate calibrations; and, in view of the difficulty experienced in meeting simultaneous requirements of flatness, parallelism, and exact length, the attainment of exact length should have been subordinated to the first two requirements. The making of fused quartz gages to the accuracy of those here produced requires a high degree of skill in optical polishing. The present gages resulted from the exceptional capability of E. L. Robinson of this Bureau who applied to the task the knowledge, skill, and technique acquired over many years in producing optical parts of the highest refinement of workmanship.

III. Calibrating the Gages

1. General Methods

The length of a gage may be determined by: (a) Interferential comparison with a standard gage of known length. (b) Direct interferential measurement of the distance between its faces.

(a) Comparative Method

Method (a) is a relatively simple and very accurate means for calibrating a gage when the length of a like standard is known to the required accuracy. If the gages are of the same material, shape, and finish and are placed side-by-side for comparison, departures from standard temperature conditions tend to affect the gages alike. Only the differential effect on the gages will in this case be included in the measurements and, consequently, the requirements for temperature control and measurement are not specially exacting. Furthermore, the difference in length of the standard and tested gage is usually small and may be measured with great accuracy by means of simple interferometric apparatus. These considerations reduce the necessary equipment to simple temperature apparatus, two interferometer plates, a source of monochromatic radiations, and an instrument for viewing and measuring fringe displacements.

(b) Direct Method

If a standard gage of the required accuracy is not available or if the length of a standard itself is required, accurate calibrations may be made by direct measurement with light waves for gage lengths less than 5 in. The measuring requirements of this method are more exacting than for method (a) and therefore, more elaborate and sensitive apparatus is needed. Accurate knowledge of the temperature and thermal expansivity of a gage is also necessary, because the full difference in length at standard temperature (20° C in US) and at the existing temperature must be taken into account. This is of major importance in calibrating steel gages but less so with fused quartz, which has a thermal expansivity one-thirtieth that of steel. Furthermore, since the order of interference (number of waves) to be determined is large, the lengths of the waves must be accurately known. This requires knowledge of the density and refractive index of the medium surrounding the etalon in order that wavelengths at standard conditions may be converted to wavelengths at existing conditions.

Measurements are sometimes made in vacuum and, when so made, require exact values of refractive indices and dispersions in order to correct air wavelengths to vacuum wavelengths; and require also a correction for the expansion of the gage with reduced pressure (compressibility correction). These corrections must be applied for the total existing atmospheric pressure.

2. Adaptations of the General Methods to the Calibration of Decimeter Gages

Adaptations of these general methods were used in calibrating the fused quartz gages. Because of the simplicity and accuracy of the comparative method, the following procedure given in greater detail was used:

Two of the 12 gages were selected as reference standards. These were carefully compared with each other, and relative lengths of the remaining gages were determined by comparison with each standard. For computational convenience, one standard was assumed to have a mid-side length of 100.000 000 mm.

Actual lengths of the two reference standards were next determined by direct measurement with wavelengths of the standard radiation of cadmium and of two homogeneous radiations of krypton. Later, the actual lengths of the other gages were likewise determined.

From these measurements a corrected value was obtained for the length of each reference standard, by means of which the previously determined relative lengths were converted to actual lengths.

Thus, two values resulted for each of the rest of the 12 gages—one, by comparison with the two reference standards; and the other, by direct measurement with light waves. Although lengths so determined were not independent values, they gave a basis for appraising the measurements and eliminating any unduly large difference in the two values.

IV. Relative Lengths

1. Description of the Comparative Method

Comparative lengths of the fused quartz gages were determined by the method illustrated in figure 9 and in figure 4 at extreme right.

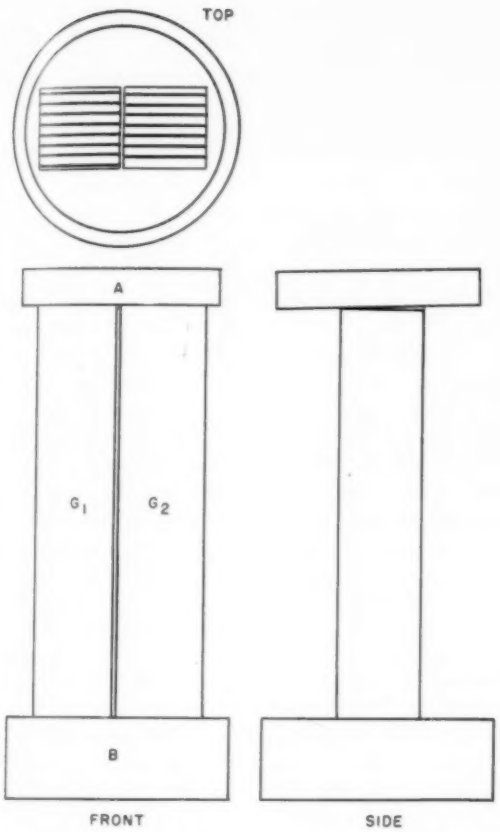

FIGURE 9. *Method for comparing two gages.*

Gages G_1 and G_2 were wrung [4] side-by-side on the fused quartz base B (diameter, 57 mm, thickness, 20 mm) having the top surface plane to 0.01λ. Upper quartz plate A (diameter 50 mm, thickness, 9 mm) having its lower surface plane to 0.01λ was placed on top of the gages forming a wedge that produced about 10 fringes across the surfaces.

The combination was placed in a chamber regulated at 20°±0.01° C by means of apparatus described by Souder and Peters [18,19]. Although this accurate temperature control was unnecessary for comparing fused quartz gages, it was essential when for a special test a quartz and a steel gage were compared.

The source of illumination was a helium tube incorporated in a Pulfrich viewing instrument, which disperses the light. The relative displacement of the two sets of fringes formed by reflection from the lower surface of A and the upper surfaces of the two gages was measured at adjacent edges of the gages for the red, yellow, and green lines of helium. Difference in length of the gages was calculated from the measured displacements of the fringes and the wavelengths of the light.

2. Comparative Measurements: Relative Lengths of the Gages

Gages 5_A and 9_A were selected as reference standards.[5] Gage 9_A was 0.085μ longer than 5_A as found by the above method of comparison. Assuming 5_A to be 100.000 000 mm and 9_A to be 100.000 085 mm, the relative lengths of the remaining gages were determined by comparison with each of these as standard. Table 4 shows that the lengths of a gage obtained by comparison with 5_A and 9_A agree within from 0.001 to 0.022μ, thus assuring the reliability of the comparative measurements. The "average difference" of −0.001μ confirms the relative values that were determined for 5_A and 9_A. Relative midside lengths given in table 4 were later used (section VI) to obtain lengths at the center of the gages.

Additional measurements included intercomparisons of six 50-mm fused quartz gages and comparisons of the 100-mm reference standards with combinations of these 50-mm gages and, also, with 100-mm and 4-in. steel gages.

[4] The method of wringing is as follows:
The surfaces are first cleaned with alcohol and absorbent cotton and then covered with a thin film of grease by thoroughly rubbing with an otherwise clean cloth freshly impregnated with petroleum jelly. This film is reduced in thickness by vigorous polishing with clean surgical cotton until no trace of film is visible in reflected light. Although the surfaces are apparently free from lint and dust, tiny particles sometimes remain, or are attracted to the surfaces by the electric charge produced by polishing. A camel's-hair brush is helpful in removing these particles. Next, the gage, slightly tilted, is held with a bottom edge resting lightly on the plate surface near an edge. The gage is then slid across the plate—sweeping ahead any particles that may be present as it goes—to the desired place and moved simultaneously to vertical position in actual contact. The surfaces are next brought intimately together by pressing lightly on the gage. Contact is indicated by a black appearance at the contacted edge of the gage, which gradually spreads over the entire surface provided particles have been successfully removed. The presence of particles is indicated by a colored or grayish appearance around them in the field of black contact. When particles are in evidence, the surfaces must be separated and the process of wringing repeated. Separation is effected by several hours immersion in water. Our experience in comparing standard end gages indicates that the separation of the surfaces when properly wrung into contact is less than 0.005 μ. Separations of this magnitude have been found by others [17].

[5] Subscript A refers to the length of a gage at the center of edge a as noted in section II.

TABLE 4. *Relative mid-side length of the gages by comparison with 5_A and 9_A*

Gage	Length at mid-side by comparison—		Difference in length by comparison with 5_A and 9_A
	With 5_A (assumed length = 100.000 000 mm)	With 9_A (length by comparison with 5_A = 100.000 085 mm)	
	mm	*mm*	*μ*
3_A	99.999 926	99.999 909	+0.017
5_A	100.000 000	(100.000 000)	.....
6_A	99.999 781	99.999 796	−.015
7_A	100.000 017	100.000 032	−.015
8_A	100.000 025	100.000 010	+.015
9_A	100.000 085	100.000 085	.....
10_A	100.000 104	100.000 039	−.002
11_A	99.999 994	99.999 972	+.022
12_A	100.000 025	100.000 093	−.014
15_A	100.000 018	100.000 031	−.013
16_A	100.000 021	100.000 030	−.009
17_A	99.999 958	99.999 957	+.001
Average difference by comparison with 5_A and 9_A			−0.001

V. Lengths by Direct Interferential Measurement

1. Description of the Direct Method

(a) General Plan

The Fabry-Perot method was selected for direct measurements of length because of the accuracy and convenience with which temperatures may be controlled and because of the sharply defined fringes it furnishes. In its application to gage measurements, the gage itself, G, serves as a separator for two Fabry-Perot interferometer plates.

The arrangement of the apparatus is shown in figures 10 and 11. Interferometer P_1P_2 is placed within constant temperature chamber, A. The transmitted waves, after multiple reflections, produce a system of interference rings that is focused by lens L_2 upon slit F of the spectrometer. The images of the slit corresponding to different wavelengths from the source, S, are separated by the spectrometer. Each image will be crossed by arcs of the ring system formed by that particular radiation, and the diameters of these circular fringes are measured either directly by means of a micrometer eyepiece at E, or the fringes are photographed and then measured. The optical distance between the interferometer plates may be determined from the measured diameters of the rings and the wavelengths of the source.

(b) Interferometer

The interferometer was formed by wringing interferometer plates to the ends of the gage. Plates of optical glass (thermal expansivity 9×10^{-6}) proved unsatisfactory for combining with fused quartz separators (expansivity 4×10^{-7}). Because of the differential expansion, distortion of the plates resulted after wringing unless gage and plates were at the same temperature when brought together, and distortion likewise resulted whenever the temperature of the combination was

FIGURE 10. *Apparatus for direct interferential measurement of length.*

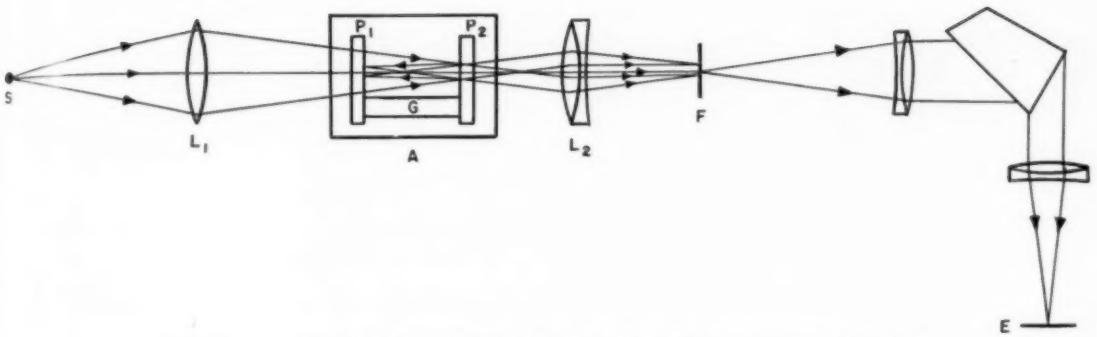

FIGURE 11. *Assembled apparatus for direct interferential measurement of length.*

different from the wringing temperature. Distortion was avoided by using plates of fused quartz selected for its optical homogeneity. These were plane to 0.01μ, and one surface of each was coated with a thin silver film by sputtering from a silver electrode in vacuum. The silver coating was removed from sufficient area to permit the gage to be wrung to the quartz glass surface. Two pairs of plates (diameter 56 mm, thickness 9.5 mm) and (diameter 68 mm, thickness 8.5 mm) respectively, resilvered as required, were used during the measurements. Interferometers thus constructed were sufficiently plane and parallel to give measurable fringes with several different radiations for a 250-mm path.

To avoid errors caused by bending of the gage, consideration was given to the method of supporting the interferometer in its horizontal position. Measured lengths differing by 0.15μ were obtained when the combination was supported at its ends and middle, respectively. Any error attributable to bending was finally reduced to the required limit by supporting the interferometer at points 10 mm from the ends of the gage.

(c) Constant Temperature Apparatus

During the measurements the interferometer *I*, figure 12, was maintained at 20° ±0.01°C in a water-jacketed tubular brass container. The ends of this tube were closed with optically flat glass plates, one of which was permanently sealed in a recess at one end of the tube, whereas the other was removable to permit access to the interferometer chamber. Slidable metal baffles B_1, B_2 provided with windows isolated the central part of the chamber where the temperature was most uniform. Light from the source was diaphragmed by means of cardboard disks placed in B_1 and B_2. A copper tube led from the inteferometer chamber to the outside and, through this, air could be either admitted through a drying train or the container evacuated. Calcium chloride was used as a drying agent within the chamber.

For proper regulation of the temperature, water was circulated (by means of a motor-driven propeller) between the tube containing the interferometer and a surrounding brass tube, and given directional flow around the inner tube by means of vanes and baffles (not shown) soldered to the tubes. The bath liquid was water-cooled by coil *C* and electrically heated by coil *H*. A relay operated by thermostat *J* regulated the amount of heat supplied. Temperature of the bath was measured by means of an exceptionally rapid mercury thermometer calibrated at frequent intervals by the Bureau's Thermometry Section. This constant temperature apparatus was encased in a wooden box and insulated with mineral wool.

With the glass plates attached to the tube ends and with baffles and diaphragms in place for calibration of decimeter gages, the interferometer chamber was explored with differential thermocouples, one junction of each couple being in contact with the thermometer bulb. Exploration showed that after the apparatus had been operating 3 or more hr the chamber attained the temperature of the bath to 0.01° C, provided room temperature was within 1.0° C of the bath temperature. Under these conditions no measurable gradient existed in the inner chamber.

(d) Spectrometer

The present method differs from that of Peters and Boyd by using a constant deviation spectrom-

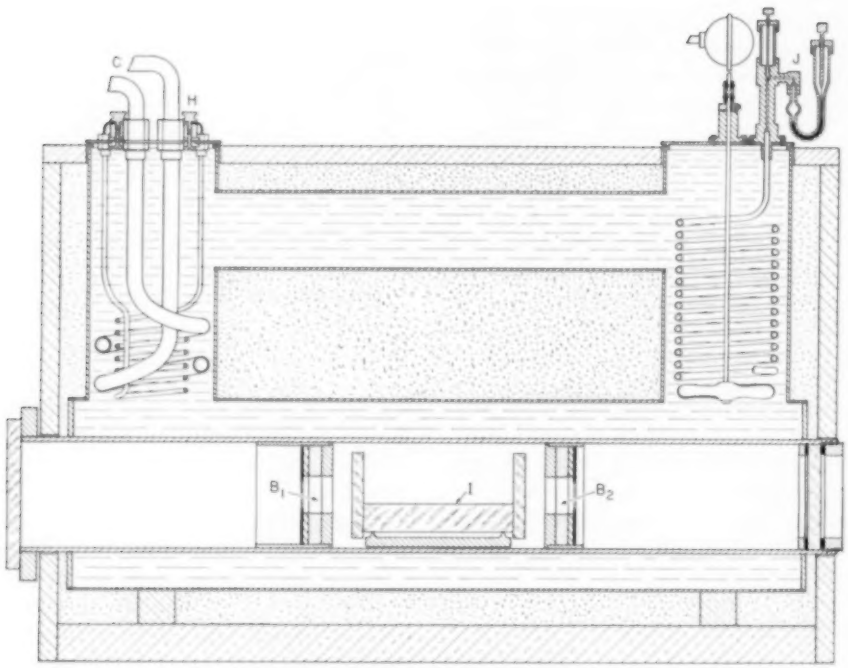

FIGURE 12. *Constant-temperature apparatus.*

eter (Hilger 78: index 1.74 for the *D* line) rather than a diffraction grating for dispersing light.

In the preliminary work ring diameters were usually measured by means of a micrometer eyepiece, but in the final calibrations a camera replaced the eyepiece and the fringes were photographed for permanent record using Eastman Type III—*F* plates. Three or four exposures were made on each plate for a given source, with periods ranging from 30 sec to 12 min—to suit the individual lines. Gage lengths computed from the photographed rings agreed with those obtained by direct visual measurement with the micrometer eyepiece.

(e) Barometer

Atmospheric pressures were measured by means of a standard mercury barometer that had been calibrated by the Aeronautical Instrument Section of this Bureau. Observations were recorded to the nearest 0.05 mm, although the limiting accuracy of the measurements probably did not exceed 0.1 mm.

(f) Sources of Light

Neon, krypton, and cadmium discharge tubes were used during the investigation. The final calibrations were however based solely upon measurements with the red radiation (λ_R= 6438.4696 A) of cadmium as a primary standard and upon two green radiations (λ_{G_1}=5562.2255 A, λ_{G_2}=5570.2892 A) of krypton as secondary standards.

The cadmium tubes were obtained from Meggers and were similar to those used by Meggers and Humphreys [20] for wavelength comparisons. These were operated in a furnace maintained at 320° C.

The krypton tubes were used either "side-on" or "end-on" without affecting the results. Final measurements were made with the tubes end-on because of the greater intensity of the lines. The values given above for the krypton wavelengths were obtained by Meggers and Humphreys by comparison with the standard wavelength λ_R.

(g) Reduction of Observations

(1) *Method of calculation.* The optical separation, L, of the interferometer surfaces at the center of the ring system is given by the equation

$$L=\left(\frac{N}{2}\right)\lambda, \tag{1}$$

in which N is the order of interference (the number of waves of length λ in the distance $2L$ over which the light travels).

Equation 1 may also be stated as

$$2L=N\lambda=(n+a)\lambda, \qquad (2)$$

in which n is the order of interference at the first ring, and a is the fraction of a wave that N differs from n. Thus N consists of an integral number n plus fraction a.

The fractional difference a for a given radiation may be computed from the measured diameters of two or more rings by the method of Childs [21] and Burns and Kiess [22] in the form given by Humphreys [23]. In the present work, results in general were based on the value of a determined from five measured rings.

In order to determine n, fractional values a_1, a_2 . . . for several radiations of known wavelength λ_1, λ_2 . . . are required, together with an approximate value, l, for L which may usually be obtained micrometrically to within 1 or 2μ. The subsequent computing procedure is given by Meggers [24] and modified by Peters [25].

(2) *Conversion of wavelengths at standard conditions to wavelengths at conditions of measurement.* Since light waves vary in length with air density, their known lengths at standard conditions (15° C; 760 mm) must be converted to lengths at the existing temperatures and pressures. Conversion factor (f) is sufficiently accurate for this purpose:

$$f=\frac{\mu_{15}}{\mu_t} \text{ where } \mu_t=1+\frac{(\mu_{15}-1)P288}{760T},$$

in which μ_{15} and μ_t are refractive indices at 15°C and at the observed temperature, T is the observed absolute temperature, and P is the observed pressure.

(3) *Correction for phase change at reflection and film thickness.* Calculated length L is the distance between reflecting surfaces of the silver films, whereas the required length is that between the clear glass surfaces onto which a gage is wrung. Therefore, a small correction that is equal to the thickness of the silver films plus or minus the phase change that occurs on reflection at their surfaces must be applied to L.

To determine the magnitude of this correction, a quartz glass test flat is placed over each interferometer plate so as to cover both clear and silvered parts. Each plate gives two systems of fringes arising from the interference between the front and back surfaces of the separating air films. The system at the silvered area, owing to the combined effect of difference in thickness of the air film and difference in phase change by reflection, is displaced (less than 1 order) relative to the system at the clear portion. The combined displacement for the two plates multiplied by $\lambda/2$ gives the required correction to L.

(4) *Correction for curvature and slope.* The length thus determined is the separation of the glass surfaces of the interferometer plates at the center of the ring system, which lies outside the gage. This will also be the required axial length of the gage (unless account is taken of the very thin wringing films) provided its surfaces are plane and parallel. For gages that are not plane and parallel, the difference in length at the center of the ring system and at the center of the gage may be calculated from the measured planeness and parallelism of the gage surfaces and the approximate distance between the center of the ring system and the gage. In order to make this calculation, it must necessarily be assumed that, upon wringing, the surfaces of the plate conform to the surfaces of the gages. The validity of this assumption depends greatly upon the contour and regularity of curvature of the surfaces and emphasizes the necessity of having plane and parallel gages for precise calibrations.

(5) *Illustration of computations.* Table 5 illustrates the method for making the computations for a 100-mm gage. Column 1 gives the wavelengths used; 2, the number of rings from the center of the ring system; 3, the measured diameter of the rings; 4, the square of these diameters; 5, the difference in squares of the diameters of successive rings; 6, the fractional part a of the order at the center of each ring system; 7, the order of interference N or the number of waves in double the distance between reflecting surfaces of the plates at the center of the ring system; and 8, the distance in millimeters between these reflecting surfaces.

TABLE 5. *Computations for a 100-mm gage*

1	2	3	4	5	6	7	8
λ (Angstrom units)	Ring	D_6; D_5; etc.	D_6^2; D_5^2; etc.	$D_6^2-D_5^2$; $D_5^2-D_4^2$; etc.	α	N	$L\left[\frac{N}{2}\lambda\right]$
							mm
Kr 5562.2255	6th	1026	10527				
				1803	0.839		
	5th	934	8724				
				1852	.711		
	4th	829	6872				
				1845	.725		
	3'd	709	5027				
				1891	.658		
	2'd	560	3136				
				1804	.738		
	1st	365	1332				
					.734	359 563.734	99.998 729
Kr 5570.2892	6th	979	9584				
				1893	.063		
	5th	877	7691				
				1839	.182		
	4th	765	5852				
				1820	.216		
	3'd	635	4032				
				1842	.189		
	2'd	468	2190				
				1770	.237		
	1st	205	420				
					.177	359 043.177	99.998 717
Cd 6438.4696	6th	1123	12611				
				2166	.822		
	5th	1022	10445				
				2109	.953		
	4th	913	8336				
				2142	.892		
	3'd	787	6194				
				2098	.952		
	2'd	640	4096				
				2230	.837		
	1st	432	1866				
					.891	310 628.891	99.998 734

Optical separation of interferometer surfaces, uncorrected for air density	99.998 727
Optical separation corrected to density of air at 760 mm; 15° C, $L\times(f=1.0000096)$	99.999 687
Correction for phase change at reflection and film thickness	+0.000 010
Combined slope and curvature correction to convert the distance between plates at the center of fringe system to the separation at the axis of the gage	−.000 021
Axial length of the gage	99.999 676

2. Measurements

(a) Preliminary Measurements

Before making final direct measurements of the 100-mm gages, steps were taken to assure the accuracy of the integral order of interference.

Direct measurements by the Fabry-Perot method were first made of two 50-mm fused quartz gages with krypton and neon sources. These furnish a large number of spectral lines that are sufficiently homogeneous in structure to stand interference over this shorter path. The following lengths were obtained from visual measurements of the fringe diameters:

Gage	Length at center of fringe system (measured)	Length at A (edge) (converted)
	mm	*mm*
2	50.000 580	50.000 556
4	49.999 897	49.999 890
	Sum 100.000 477 (1)	

Next, gages 2 and 4 were wrung together, and their combined length was determined in the same manner from measurements of photographed interference patterns for three lines of krypton. Lengths thus obtained were:

λ	Measured length of combination at center of fringe system
A	*mm*
5562	100.000 503
5570	100.000 507
5870	100.000 497
	Mean 100.000 502 (2)

The small difference (0.025 μ) between (1) in which gages 2 and 4 were measured individually and (2) in which the gages were measured in combination established the integral order of interference for the decimeter etalon.

Later, 50 mm gages 4 and 5 were measured directly, using the standard radiation of cadmium and the two secondary standard radiations of krypton. Values for gage 4 were computed from diametric measurements of photographed fringes; values for gage 5 (first wringing) were computed from visual measurements of the diameters by two observers. Later, the interferometer plates were removed from gage 5 and rewrung (second wringing) to the gage. The length of this etalon was measured both visually and photographically. The results of the determinations, table 6, show no systematic or appreciable difference for (a)

TABLE 6. *Lengths of two 50-mm fused quartz etalons at the center of the ring system by direct measurement with light waves*

Gage	Date	Observer	Length at center of ring system						Mean of three radiations
			Using cadmium (λ6438.4696)		Using krypton (λ5562.2255)		Using krypton (λ5570.2892)		
			Visually	From photo.	Visually	From photo.	Visually	From photo.	
			mm	*mm*	*mm*	*mm*	*mm*	*mm*	*mm*
4	Feb. 4, '35	1		49.999 885		49.999 894		49.999 886	
				49.999 884		49.999 885		49.999 885	
								49.999 886	
								49.999 887	
			$M=49.999\ 885$		$M=49.999\ 890$		$M=49.999\ 886$		49.999 887
	FIRST WRINGING								
	Dec. 10, '34	1			49.999 933		49.999 940		
	Dec. 11, '34	2			49.999 936		49.999 927		
					49.999 933		49.999 940		
	Dec. 12, '34	2			49.999 922		49.999 931		
					49.999 923		49.999 931		
7	SECOND WRINGING								
	Jan. 31, '35	1	49.999 935	49.999 944	49.999 953		49.999 943	49.999 935	
				49.999 935		49.999 933		49.999 933	
								49.999 937	
	Jan. 31, '35	1		49.999 928		49.999 930		49.999 929	
				49.999 930		49.999 927		49.999 927	
								49.999 925	
								49.999 935	
			$M=49.999\ 934$		$M=49.999\ 932$		$M=49.999\ 933$		49.999 933

two observers, (b) visual or photographic measurements, or (c) the three spectral sources. The mean values given in the last column of table 6 are equivalent to the following mid-edge lengths;

$$4_A = 49.999\ 880 \text{ mm}$$

$$5_A = 49.999\ 932 \text{ mm}$$

This value for 4_A is but 0.01 μ different from that found previously with krypton and neon radiations. Using these values for 4_A and 5_A, the comparative lengths (table 7) of other 50-mm quartz gages were obtained. As a check upon the accuracy of the comparisons, gages 2 and 3 and gages 4 and 7 were wrung together and compared. From table 7, combination $2_A+3_A=$ 99.999 486 mm and combination $4_A+7_A=$ 99.999 144 mm; or a difference in length of -0.342 μ, whereas the difference found by direct comparison of the combinations was $+0.358$ μ.

TABLE 7. *Lengths of the 50-mm gages by comparison with 4_A and 5_A*

Gage	Length by comparison			Length-preliminary direct measurements
	Compared with 4_A (4_A=49.999 880 mm)	Compared with 5_A (5_A=49.999 932 mm)	Mean	
	mm	*mm*	*mm*	*mm*
2_A	50.000 563	50.000 552	50.000 558	50.000 556[a]
3_A	49.999 922	49.999 933	49.998 928	
4_A	49.999 880	49.999 900	49.999 890	49.999 880[a]
5_A	49.999 912[a]	49.999 932[a]	49.999 922	
6_A	49.999 723	49.999 743	49.999 733	
7_A	49.999 257	49.999 251	49.999 254	

[a] Direct measurements.

Approximate lengths were next established for the 100-mm reference standards by the following procedures:

(a) By comparison with combinations of the 50-mm gages that are summarized in table 7.

(b) By comparison with an NBS standard 4-in.

steel gage. This gage had been measured directly with light waves and had also been compared with combinations of 1-in., 2-in., and 50-mm steel gages, which in turn had been calibrated directly with light waves. Its length was confirmed within 0.000002 in. (0.05 μ) by comparing it with gages that had been certified by other national standardizing laboratories. In making these comparisons, gages were placed in the constant temperature chamber at least 4 hrs before measurements were taken.

The following approximate lengths were thus obtained for the reference standards.

Reference standard	Length by comparison—	
	With combinations of 50-mm quartz gages	With 4-in. steel gage
	mm	*mm*
5_A	99. 999 901	99. 999 890
9_A	99. 999 972	99. 999 981

These measurements established the lengths of the reference gages to well within 1 fringe; and the preliminary measurements *in toto* assured the exact integral orders of interference for decimeter etalons when the red radiation of cadmium and the two green radiations of krypton were used.

(b) Final Measurements

Final direct measurements of reference standards 5 and 9 were made at 20° C with cadmium and krypton sources; and it was considered advisable to measure in the same manner the gages to be calibrated by other laboratories.

Calibrations for most of the gages are based upon two wringings of gages and plates. Three exposures were usually made for each source, with times ranging from 30 sec to 12 min for the individual lines. Although several radiations of cadmium and krypton gave fringes that were measured, only the three standard lines were used for computing gage lengths because of uncertainty as to the homogenity of the other lines. The individual values computed from the three standard radiations usually agreed to 0.01μ, as shown in table 8.

No orderly difference was found in measurements made with large and with small interferometer plates. These plates were resilvered from time to time, and the combined corrections for film thickness and phase change for pairs of plates ranged from 0.000 to 0.041μ, for different coatings.

Measurements of a given etalon when undisturbed in its position within the constant temperature chamber gave the same lengths within 0.01-μ on successive days during which barometric pressure varied from 750 to 761 mm Hg. The same values were, however, not always obtained for successive wringings of gages and plates. The maximum difference observed (0.065μ for gage 16; table 8) is greater than would be expected from wringing or from correcting for curvature and slope, and greatly exceeds that obtained with 50-mm gages. Upon reviewing the measurements, the most likely explanation appeared to be that discordance resulted from the method that was used to adjust the etalon to its correct lateral position in the constant temperature chamber. The adjustment was effected by applying a slight pressure to the rear face of an interferometer plate by means of a rod. This operation could conceivably strain the gage and result in a bending that might not be relieved upon removal of the pressure. This explanation was verified in later work by the excellent agreement obtained for successive

TABLE 8. *Lengths at the center of the ring system by direct measurement with krypton and cadmium wave lengths*

[Two or more wringings were made for nine of the gages]

Gage	Wringing No.	Length at center of ring system				
		Krypton		Cadmium	Mean of Kr and Cd values for each wringing	Mean length for all wringings
		$\lambda = 5562.2255$	$\lambda = 5570.2892$	$\lambda = 6438.4696$		
		mm	*mm*	*mm*	*mm*	*mm*
3	1	99.999 831	99.999 828	99.999 840	99.999 833	99.999 82
	1	99.999 878	99.999 881	99.999 891	99.999 883	
	2	99.999 859	99.999 874	.....	99.999 867	
5	3	99.999 870	99.999 874	99.999 877	99.999 874	
	4	99.999 864	99.999 853	99.999 856	99.999 858	99.999 87
6	1	99.999 696	99.999 699	99.999 696	99.999 697	99.999 67
7	1	99.999 953	99.999 938	99.999 941	99.999 944	
	2	99.999 906	99.999 902	99.999 911	99.999 906	99.999 92
8	1	99.999 926	99.999 921	99.999 929	99.999 925	
	2	99.999 909	99.999 906	99.999 899	99.999 905	99.999 93
9	1	100.000 001	100.000 003	100.000 004	100.000 003	
	2	99.999 961	99.999 959	99.999 967	99.999 962	99.999 98
10	1	100.000 046	100.000 040	100.000 041	100.000 042	
	2	100.000 026	100.000 027	100.000 029	100.000 027	100.000 02
11	1	99.999 858	99.999 861	99.999 859	99.999 859	
	2	99.999 880	99.999 878	99.999 865	99.999 874	99.999 87
12	1	99.999 920	99.999 925	99.999 924	99.999 923	
	2	99.999 963	99.999 956	99.999 978	99.999 966	99.999 92
15	1	99.999 959	99.999 962	99.999 964	99.999 962	
	2	99.999 896	99.999 897	99.999 923	99.999 905	99.999 93
16	1	99.999 892	99.999 891	99.999 907	99.999 897	
	2	99.999 957	99.999 959	99.999 967	99.999 962	99.999 93
17	1	99.999 862	99.999 859	99.999 870	99.999 864	99.999 91

wringings when other adjusting procedures were used.

By the use of the corrections in table 9, the lengths that were determined at the center of the ring system (located 5 mm from the edge of a gage) by direct measurement with light waves were converted to mid-edge lengths and to axial lengths of the gages. These are given in table 10.

TABLE 9. *Corrections for planeness and parallelism of the gage surfaces*

Gage	Total curvature [a]	Slope ($A>B$)	Correction to center of gage from center of ring system			Total correction to edge, A, from center of fringe system
			Curvature correction	Slope correction	Total correction applied	
	μ	μ	μ	μ	μ	μ
3	−0.016	−0.004	−0.024	+0.003	−0.021	−0.007
5	+.002	−.006	+.003	+.005	+.008	+.003
6	−.019	−.011	−.029	+.008	−.021	−.008
7	−.040	+.002	−.060	−.002	−.062	−.021
8	−.025	−.007	−.038	+.005	−.033	−.011
9	−.007	−.002	−.011	+.002	−.009	−.003
10	−.024	+.007	−.036	−.005	−.041	−.013
11	−.012	+.006	−.018	−.005	−.023	−.008
12	−.014	+.002	−.021	−.002	−.023	−.008
15	+.011	−.015	+.017	+.011	+.028	+.009
16	−.032	−.032	−.048	+.024	−.024	−.008
17	+.008	+.007	+.012	−.005	+.007	+.003

[a] The algebraic sum of the curvatures of the end surfaces in directions a-b and c-d. A (−) value indicates a resulting concavity, a (+) value indicates convexity.

TABLE 10. *Lengths at the center and mid-edge by direct measurement*

Gage	Lengths by direct measurement		
	At center of ring system	At center of gage (axial length)	At mid-edge, A, of gage
	mm	mm	mm
3	99.999 833	99.999 812	99.999 826
5	99.999 871	99.999 879	99.999 874
6	99.999 697	99.999 676	99.999 689
7	99.999 925	99.999 863	99.999 904
8	99.999 915	99.999 882	99.999 901
9	99.999 983	99.999 974	99.999 980
10	100.000 035	99.999 994	100.000 022
11	99.999 867	99.999 844	99.999 859
12	99.999 945	99.999 922	99.999 937
15	99.999 934	99.999 962	99.999 943
16	99.999 930	99.999 906	99.999 922
17	99.999 864	99.999 871	99.999 867

VI. Summary of Comparative and Direct Measurements of the Gages

Before the comparative calibrations of the decimeter gage can be summarized, the relative mid-side lengths given in table 4 must be converted to actual lengths at the axis. Lengths in table 4 are based upon the assumption that $5_A = 100.000\ 000$ mm and by comparison with this, $9_A = 100.000\ 085$ mm. The actual lengths of the reference standards as found by direct measurement were $5_A = 99.999\ 874$ and $9_A = 99.999\ 980$ mm. Instead, however, of using the measured lengths of the reference standards to convert table 4 values to actual values, lengths $5_A = 99.999\ 898$ mm; $9_A = 99.999\ 982$ mm were used. These corrected values (see table 11) were derived from the directly measured lengths of all gages and the very accurate comparisons of each reference standard with the other gages upon which table 4 is based. These corrected lengths are considered more reliable than those obtained from the relatively few direct measurements of the standards. The corrected lengths of 5_A and 9_A are 0.024 and 0.002μ greater than the directly measured lengths and, since the final comparative length of a third gage was taken as the mean of its comparisons with 5 and 9, its value is increased 0.013μ, using corrected lengths. The difference (0.084μ) in the corrected lengths of 5_A and 9_A concords better with the difference (0.085μ) that was obtained in the original comparisons of 5_A and 9_A than does the difference of 0.106μ resulting from the direct measurements of the two gages. Table 12 shows the close agreement of the pre-

TABLE 11. *Corrected length of 5_A and of 9_A derived from the direct measurement of all gages*

Length of comparison gage by direct measurement	Derived length of reference standard	
	Gage 5_A [a]	Gage 9_A [a]
mm	mm	mm
$3_A = 99.999\ 826$	99.999 900	100.000 002
$5_A = 99.999\ 874$	99.999 874	99.999 959
$6_A = 99.999\ 689$	99.999 908	99.999 978
$7_A = 99.999\ 904$	99.999 887	99.999 957
$8_A = 99.999\ 904$	99.999 879	99.999 979
$9_A = 99.999\ 980$	99.999 895	99.999 980
$10_A = 100.000\ 022$	99.999 918	100.000 001
$11_A = 99.999\ 859$	99.999 865	99.999 972
$12_A = 99.999\ 937$	99.999 912	99.999 983
$15_A = 99.999\ 943$	99.999 925	99.999 997
$16_A = 99.999\ 922$	99.999 901	99.999 977
$17_A = 99.999\ 867$	99.999 909	99.999 995
Corrected, length	99.999 898	99.999 982

[a] The derived lengths of 5_A and 9_A were obtained by correcting the directly measured lengths of the comparison gages of column 1 by the differences that were obtained by comparing these gages with the standard gages.

liminary calibrations of 5_A and 9_A with the measured and corrected lengths.

TABLE 12. *Lengths of reference standards by various methods*

Method of derivation	5_A	9_A
	mm	*mm*
From direct and comparative measurements of 12 gages (corrected value)	99.999 898	99.999 982
By direct measurement with light waves	99.999 874	99.999 980
By comparison with combinations of 50-mm gages that had been measured directly	99.999 901	99.999 972
By comparison with 4.0 steel gage	99.999 890	99.999 981

The length of each gage at its *A* edge was obtained from the comparative values given in table 4 by using the corrected values of 5_A and 9_A for the conversion. Lengths at the center of the gages (axial lengths) were obtained from the mid-edge lengths by applying the slope and curvature corrections in table 9.

The axial lengths determined by comparing the gages with the reference standards and also those determined by direct measurement with light waves are summarized in table 13. It will be noted that the greatest difference in length (Δ) of any gage by the two methods is 0.024 μ.

TABLE 13. *Summary of axial lengths by direct measurement and by comparison*

Gage	Axial length					
	By direct measurement (1)	By comparison—			Δ (1)−(2)	Final value, Mean of (1) and (2)
		With 5_A	With 9_A	Mean (2)		
	mm	*mm*	*mm*	*mm*	μ	*mm*
3	99.999 812	99.999 810	99.999 792	99.999 801	+0.011	99.999 807
5	99.999 879	[a] 99.999 903	99.999 902	99.999 903	−.024	99.999 891
6	99.999 676	99.999 666	99.999 680	99.999 673	+.003	99.999 675
7	99.999 863	99.999 874	99.999 888	99.999 881	−.018	99.999 872
8	99.999 882	99.999 901	99.999 885	99.999 893	−.011	99.999 888
9	99.999 974	99.999 977	[a] 99.999 976	99.999 977	−.003	99.999 976
10	99.999 994	99.999 974	99.999 975	99.999 975	+.019	99.999 985
11	99.999 844	99.999 877	99.999 854	99.999 866	−.022	99.999 855
12	99.999 922	99.999 908	99.999 921	99.999 915	+.007	99.999 919
15	99.999 962	99.999 935	99.999 947	99.999 941	+.021	99.999 952
16	99.999 906	99.999 903	99.999 911	99.999 907	−.001	99.999 907
17	99.999 871	99.999 860	99.999 858	99.999 859	+.012	99.999 865

[a] From corrected values of 5_A and 9_A.

VII. Comparison of the Calibrations by the Various Standardizing Laboratories

Following completion of the measurements the gages were assigned NBS numbers, and two, together with their calibration certificates, were submitted to each of the following laboratories for calibration: Bureau International des Poids et Mesures, Physikalish-Technische Reichsanstalt, and National Physical Laboratory. Either final or preliminary reports have been received for five of the gages.

1. Methods Used at the Other Laboratories

The following methods were used at the other testing laboratories:

(a) Bureau International des Poids et Mesures

The gage was wrung to the plane surface of a fused quartz base plate and placed in an industrial interferometer,[6] which carried a glass interferometer plate at a short distance from the upper surface of the gage. Lengths were determined from measurements of the Fizeau fringes between the part of the glass plate over the gage and the upper face of the gage, and those between another part of the glass plate and the upper surface of the quartz base plate. The radiations used were two yellow lines of mercury and one yellow and two green lines of krypton.

(b) Physikalish-Technische Reichsanstalt

Gages sent to the PTR were likewise calibrated by the use of Fizeau fringes. At this laboratory

[6] Presumably the industrial interferometer described by Pérard [28]. The general principle of this method is similar to the comparative method used with the decimeter gages. Monochromatic light is obtained, however, by passing radiations from a source through a dispersive system of prisms to a slit, from which it is projected vertically onto the interferometer by means of a total reflecting prism and mirror. Fringes are viewed with a telescope

a gage was mounted horizontally with one surface wrung to a fused-quartz base plate. The distance from the middle of the other surface of the gage to the base surface was measured interferometrically, statedly by the PTR method,[7] which is different from that employed at the BIPM. The standard radiation of cadmium and five lines of krypton were used—the wavelengths of the krypton lines having been determined by comparison with the standard wavelength of cadmium.

(c) The National Physical Laboratory

One end of a gage was wrung to a crystalline quartz plate. A second crystalline quartz plate was supported about 15 mm above the upper surface of the gage by means of a fused quartz tube that enclosed the gage and had plane and parallel end faces in wringing contact with the upper and lower plates. Light from the source was projected vertically to the interferometer producing, by reflection from the lower surface of the upper plate and the top surface of the gage and likewise from adjacent surfaces of the plates, two systems of Haidinger fringes. These were focused upon the slit of a spectrograph. The calibrations were based upon four wave-lengths of krypton.

It will be noted that the interferential methods used by the above laboratories and the NBS differ among themselves. For calibrating fused quartz gages, which do not require the exacting temperature control necessary for the direct measurement of steel gages and for which the Fabry-Perot method is particularly adaptable, some of the other methods have certain advantages, namely: (1) bending of a gage is eliminated at the BIPM and NPL by measuring it in a vertical position; and (2) the errors introduced by wringing together imperfect surfaces are less by the BIPM and PTR methods, which require but one wringing.

2. Summary and Comparison of the Calibrations

A summary of the results at present available is given in table 14, in which the NBS bracketed lengths are those originally given in the gage certificates. These differ less than 0.010μ from the final derived lengths, which are based upon additional planeness and parallelism measurements not included in the original computations.

[7] The method in common use at the PTR is basically a modification of Michelson's interferometer. A brief description of it is given by Dr. Kösters in a report by the special committee on wavelengths of light. [27].

TABLE 14. *Axial length of fused quartz gages by different laboratories*

Gage No.		Testing laboratory	Measured length			Notes
Original	NBS		Direct method	Comparative method	Mean	
			mm	*mm*	*mm*	
		BIPM	99.999 840			
			99.999 856			
11	11		99.999 848		99.999 848	
		NBS	99.999 844	99.999 866	99.999 855	Final calculated length.
			[99.999 844]	[99.999 857]	[99.999 851]	[Reported length].
		PTR	99.999 934		99.999 934	
16	2	NBS	99.999 906	99.999 907	99.999 907	Final calculated length.
			[99.999 914]	[99.999 906]	[99.999 910]	[Reported length].
		PTR	99.999 899		99.999 899	
12	15	NBS	99.999 922	99.999 915	99.999 919	Final calculated length.
			[99.999 929]	[99.999 910]	[99.999 920]	[Reported length].
		NPL	99.999 862			Before immersion.
			99.999 926			Measured 7 hr after partial immersion for several hr.
7	13		99.999 927			Measured 5 hr after drying 16 to 17 days in a desiccator.
		NBS	99.999 863	99.999 881	99.999 872	Final calculated length.
			[99.999 861]	[99.999 873]	[99.999 867]	[Reported length].
		NPL	99.999 906			Before immersion.
			99.999 969			Measured 16 hr after partial immersion for several hr.
8	14		99.999 982			Measured 5 hr after drying 16 to 17 days in a desiccator.
		NBS	99.999 882	99.999 893	99.999 888	Final calculated length.
			[99.999 882]	[99.999 886]	[99.999 884]	[Reported length].

The agreement of the NBS calibrations with those of the other laboratories may be stated as follows:

Gage NBS 11: BIPM value—NBS value = -0.007μ

Gage NBS 2: PTR value—NBS value = $+0.027\mu$

Gage NBS 15: PTR value—NBS value = -0.020μ

Gage NBS 13: NPL values—NBS value = -0.010μ [1] to $+0.055\mu$ [2]

Gage NBS 14: NPL values—NBS value = $+0.018\mu$ [1] to $+0.094\mu$ [2]

[1] From NPL initial measurements.

[2] From NPL measurements after wetting and drying treatment noted in table 14.

Comparison of the NBS with the NPL calibrations is less definite than with the BIPM and PTR determinations. Apparent increases in length resulted from various wetting and drying treatments of the gages at the NPL when measured interferentially, although purely mechanical methods of measurement gave no change. Extensive interferometric comparisons at the NBS of two gages, one being alternately immersed in water and dried for several days, agreed with the NPL mechanical measurements, giving no change as great as 0.005μ.[8]

3. Discussion and Conclusion

The NBS calibrations differ from the BIPM calibration by $+0.007\mu$; from the PTR calibrations by $+0.020$ and -0.027μ; and from the initial measurements at the NPL by $+0.010$ and -0.018μ. The lack of agreement with the NPL measurements that were made after wetting and drying the gages has been mentioned.

Gages 2 and 15 were returned to this Bureau after calibration by the PTR. Repeated comparisons of these gages (each having one surface plane and the other 0.03μ concave), made with the plane and concave surfaces wrung in different sequence to the base plate, gave values that dif among themselves as much as the PTR calib tions differ from those of the NBS. Later te give a possible explanation for the differen obtained and show the importance of plane e surfaces for precise calibrations. These te were made with 50-mm fused quartz gages havi one plane and one concave surface, each bei wrung alternately to a fused-quartz base plat A shorter mid-side length was measured when t concave surface was wrung to the plate, th indicating a "flattening" of the concave surface the magnitude depending upon the intimacy contact of the wrung surfaces.

Agreement of the calibrations by the vario observers is thus limited by uncertainties measurement that may be attributed to lack planeness of the gages. The greatest differen (0.027μ) in the independent calibrations ca reasonably be ascribed entirely to lack of planene of the gages. It may certainly be concluded tha the diverse interferential methods used by th BIPM, PTR, NPL, and NBS give the sam lengths to a maximum uncertainty of 0.027 (1 part in 3,700,000) and to a probable uncertain much less.

The results give assurance that decimete lengths can be measured by the Fabry-Pero method to the accuracy required for ruling standard meter scales. In the light of the infor mation obtained from this investigation, the sur faces of the steel decimeter gages to be used i stepping-off the meter scales should be reworked to the highest planeness attainable through present technique. Improvement in the gages, in the temperature control, and in the measuring ap paratus may reasonably be expected to reduce the uncertainty of calibration to 0.02μ for the steel gages. This is equivalent to 0.2μ in a meter or 1 part in 5 million.

VIII. Application of Fused Quartz Gages to Other Investigations

Fabry-Perot interferometers are commonly used for determining refractive indices of gases and for wavelength comparisons. Fused quartz etalons similar to those used in the gage calibrations are particularly suitable for these measurements because of the rigid construction and low thermal expansivity of the etalons, and the planeness and

[8] It is suggested that distortion in the interferometer system may account for the changes obtained interferentially at the NPL. Distortion of interferometer surfaces has been observed at the NBS when glass plates were combined with a fused quartz gage (section V, 1, (b)) and also when a fused quartz plate was combined with a steel gage of high wringing quality. In the latter case a small change in temperature caused appreciable distortion of the plate, although its thickness was 20 mm. Since differences in thermal expansivity between fused quartz and materials such as glass, steel, and crystalline quartz are approximately the same, distortion may reasonably have been experienced in the NPL combination of fused and crystalline quartz. The NPL lack of fused quartz interferometer plates of the required size was noted in its report. These have since been acquired, and repetition of the measurements with these plates may clarify the present uncertainties.

allelism of the interferometer surfaces. In- s and wavelengths are calculated directly from measured orders of interference between tes; consequently, they are not subject to the ertainties of gage calibrations in which meas- d optical lengths must be transferred to me- anical lengths at the center of the gages.

1. Refractive Index of Dry Air

The refractive index of air, n, may be defined as

$$\frac{\text{Number of waves in thickness } (t) \text{ of air}}{\text{Number of waves in thickness } (t) \text{ of vacuum}},$$

d may be determined by obtaining the order of erference of monochromatic radiations in air d in vacuum.

Preliminary measurements to test the suita- ity of fused quartz Fabry-Perot etalons for dex determinations were made in April, 1934. ese consisted of five individual determinations 15° C of the refractive index of dry air con- ining a normal carbon dioxide content, and of o similar determinations at 20° C. In this ork the orders of interference with a 50-mm alon were obtained alternately in air and vacuum r 23 radiations of krypton and neon. Correc- ons were made for the expansion of the etalon in cuum, using $C=9.9\times10^7$ [28] as the coefficient compressibility. Index values so obtained are mpared in a subsequent table with those of ars and Barrell at the NPL; Pérard at the IPM; Kösters and Lampe at the PTR; and eggers and Peters at the NBS, to which reference ill first be made.

In 1918 Meggers and Peters [29] determined the fractive index of air at 0°, 15°, and 30° C for ore than 200 wavelengths of Cu, Fe, Ne, H, and between 2,218 and 9,000 A. Their results were esented in tables giving the observed index at ch wavelength, and also in more convenient bles giving the indices as calculated from dis- rsion equations that were derived from the bserved data.

In 1934 Pérard [30] determined the indices at ve wavelengths in the visible spectrum at tem- eratures between 0° to 100° C and derived from these the following dispersion equation for CO_2-free dry air:

$$(N-1)10^6=\left[288.02+\frac{1.478}{\lambda^2_{air}}+\frac{0.0316}{\lambda^4_{air}}\right]\frac{h(1+\beta h)}{760(1+760\beta)}\,\frac{1}{1+0.003716\theta}$$

in which λ = wavelength in air (microns),
h = pressure (mm),
θ = temperature (° C),
$\beta=2.4\times10^{-6}$ (which can be taken as zero without appreciable error).

In 1934 Kösters and Lampe [9, 10] gave the following equation for the index of CO_2-free dry air at 20° C

$$(n_{t,B}-1)=\left(268.036+\frac{1.476}{\lambda^2_{vac}}+\frac{0.01803}{\lambda^4_{vac}}\right)\frac{1+\alpha\cdot20}{1+\alpha\cdot t}\,\frac{B}{760}10^6,$$

in which λ = wavelength in vacuum (microns),
$\alpha=0.00367$.

In 1937 Sears and Barrell [31, 32] gave the following equations for CO_2-free dry air, which were derived from determinations with eight wavelengths in the visible spectrum:

$$(n_{T,p}-1)=(n_{20,760}-1)\,\frac{p(1+\beta p)}{760(1+760\beta)}\,\frac{1+20\alpha}{1+\alpha T},$$

$$(n_{20,760}-1)10^6=267.8725+\frac{1.5189}{\lambda^2_{vac}}+\frac{0.01246}{\lambda^4_{vac}},$$

in which λ = wavelength in vacuum (microns)
$\beta=0.73\times10^{-6}$
$\alpha=0.003674$

Table 15 gives the indices calculated by Sears and Barrell from the various equations at eight wavelengths and converted by them to like conditions of CO_2-free, dry air at 15° C, 760 mm Hg. The values of Pérard, Sears and Barrell, and Kösters and Lampe are appreciably higher then those of Meggers and Peters, which are admittedly low because, for lack of the necessary data, no correction was applied for the increased length of the etalons in vacuum, although they were the

first to call attention to this required correction. Furthermore their equation does not fit their observations particularly well in the red end of the spectrum and for this reason their observed values are more reliable than the curve values in this region. For example: $(n\text{-}1)$ for the 6,438 Cd line (15° C; 760 mm) is 2758×10^{-7} by their equation, whereas their observed data for this spectral region gives 2761×10^{-7} which, if corrected by 3×10^{-7} for increase in the length of the etalon when changing from atmospheric to vacuum conditions gives $(n-1)=2764\times10^{-7}$ as found by the other observers.

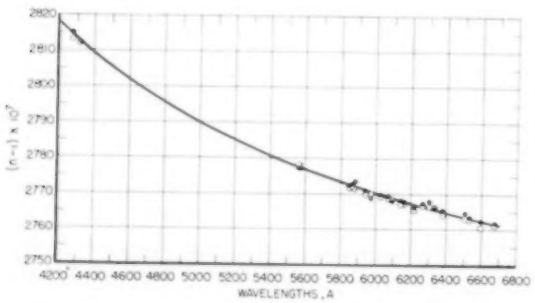

FIGURE 13. $(n-1)\times10^7$ *for dry air; normal* CO_2; *15°C; 760 mm, by various observers.*

———, Pérard, Kösters, and Lampe; Sears & Barrell. ●●● ○○○ Peters and Emerson.

The indices determined in the present preliminary study are seen in figure 13: circles are the mean $(n-1)$ values of five determinations at 15° C, while dots are the means of two determinations at 20° C, which have been converted to 15° indices using Meggers and Peters' optical coefficients. The full line in figure 13 represents the average dispersion curve obtained by converting the equation values of Pérard, Sears and Barrell, and Kösters and Lampe for CO_2-free air to values for air having a normal CO_2 content.

In general the present observations lie close to the average curve of the other observers, although a slight difference in the form of that curve and one drawn through the observed points is indicated. Unfortunately, several of the neon lines used are not suitable for a 100-mm path, causing departures of 1 or 2×10^{-7} from a smooth curve. Also the accuracy of determinations with the 4,274 and 4,320 A Kr lines is questionable, because with optical paths of this magnitude the limiting order of interference was approached for these wavelengths causing the fringes to be indistinct.

TABLE 15. $(n-1)\times10^7$ *for dry, carbon-dioxide-free air at 15° C; 760 mm by various observers*

Source	Wavelength	$(n-1)\times10^7$ by different observers				
		Meggers and Peters (1)	Pérard (2)	Kösters and Lampe (3)	Sears and Barrell (4)	Mean: Observers (2, 3, and 4)
	A					
Cd(R)	6438.4696	2757.5	2763.7	2764.3	2763.4	2763.8
He(Y)	5875.623	2764.4	2771.2	2772.0	2771.2	2771.5
Hg(G)	5460.7430	2771.1	2778.5	2779.4	2778.6	2778.8
Cd(G)	5085.8212	2778.8	2786.8	2787.7	2787.0	2787.2
Cd(B)	4799.9104	2786.0	2794.6	2795.6	2794.8	2795.0
Cd(V)	4678.1493	2789.6	2798.4	2799.4	2798.6	2798.8
He(V)	4471.477	2796.4	2805.7	2806.6	2805.8	2806.0
Hg(V)	4358.325	2800.6	2810.2	2811.1	2810.2	2810.5

2. Wavelengths by Comparison With the Standard Wavelength

In calibrating the decimeter gages by direct measurement with light waves, krypton and cadmium sources were alternated, and the order of interference was determined for all lines that gave measureable fringes. From these data the wavelengths of several Kr and Cd radiations were obtained by comparison with wavelength λ_R of the standard radiation of Cd in the following manner:

The optical path was taken as the product of the order of interference and the wavelength employed. The order of interference, as determined, included the phase change at reflection from the silver surfaces. The combined correction for film thickness and phase change evaluated for red, yellow, green, and blue radiations of helium indicated that any difference in optical path attributable to selective phase change within this spectral range was too small in comparison with the total path to introduce appreciable error in the determined wavelengths. Consequently, the optical path obtained for the standard radiation was considered common to all visible radiations of Cd and Kr. This optical path divided by the order for a given line gave, then, the wavelength of that line for the atmospheric conditions at which the measurements were made. The final step was to convert these values to wavelengths at 15° C and 760 mm Hg.

The gage data were sufficient to give the values shown in table 16 for the wavelengths of the 5,562;

5,570; 5,871 Kr and the 4,800; 5,086 Cd radiations with an optical path of 200 mm.[9] Wavelengths

TABLE 16. *Wavelength determinations with a 200-mm optical path*

Series	Wavelengths (krypton)			Wavelengths (cadmium)	
	A	A	A	A	A
1	5562.2256	5570.2897	5870.9166	4799.9114	5085.8216
2	55	90	57	14	13
3	42	84	43	.....	22
4	63	98	77	23	14
5	48	92	55	13	13
6	64	94	72	.....	26
7	66	90	58	18	14
8	53	92	55	.....	08
9	41	81	50	.....	09
10	50	92	66	.....	17
11	60	97	.....	.....	08
12	39	80	44	.....	07
13	52	86	57	.....	05
14	57	94	82	.....	19
15	56	.2900	61	.....	16
16	55	.2893	70	14	17
17	59	96	72	21	18
18	58	93	59	23	05
19	57	91	55	17	15
20	59	96	60	19	13
21	47	91	58	.....	17
22	56	96	66	11	06
23	50	91	55	11	08
24	52	88	54	11	07
25	55	89	47	22	12
26	62	.2900	65	15	.....
27	54	.2891	53	.....	13
28	47	85	44	13	17
29	48	91	62	18	18
30	43	82	47	17	10
31	62	.2903	68	14	13
32	56	.2895	61	14	11
33	59	96	59	.....	16
34	58	96	60	.....	15
35	61	98	56	.....	.....
36	51	88	56	.....	02
37	47	91	.....	.....	21
38	55	92	60	16	.....
39	56	92	63	19	16
Mean	5562.2254	5570.2892	5870.9159	4799.9116	5085.8213
Avg dev [1]	0.00052	0.00039	0.00066	0.00031	0.00042
Avg dev [2]	.00008	.00006	.00011	.00007	.00007

[1] Average deviation of the observations from the mean.
[2] Average deviation of the mean.

[9] Three exposures were customarily made with each source for a given series. These usually gave three determinations of the order of interference for the 5,438 standard line and two or three determinations for each of the other lines, except the 4,800 Cd for which a single observation was ordinarily obtained. The tabulated wavelengths are based upon the average values of the order of interference of all determinations in a series with the standard radiation and with a given radiation.

Although the 5,650; 5,672; 5,944 Kr and the 4,678 Cd lines also gave measurable fringes with several etalons, the data are too scanty to include in table 16.

determined for these radiations by various investigators are given in table 17.

Jackson's values for Kr wavelengths are greater than those given by the other observers and exceed the average values of those observers by 0.0011, 0.006, and 0.0010 A for the 5,562; 5,570; 5,871 radiations. The uniformity of the values, particularly for the 5,562; 5,570 lines, by observers 1, 3, and 5 indicates an incompatability of Jackson's results with theirs. The preponderance of determinations giving shorter values makes the inclusion of Jackson's wavelengths questionable when arriving at the most reliable values for the wavelengths. The following wavelengths based upon the determinations of Meggers and Humphreys, Meggers and Burns, Pérard and Peters and Emerson are considered by the authors to be the most reliable values now available: Kr_1, 5562.2255; Kr_2, 5570.2893; Kr_3, 5870.9157.

TABLE 17. *Wavelength determinations by different observers*

Observer	Wavelength				
	Krypton			Cadmium	
	(1)	(2)	(3)	(4)	(5)
	A	A	A	A	A
Meggers and Humphreys [20].	[a] 5562.2255	[a] 5570.2892	[a] 5870.9154	.....	.....
	[b] 5562.2254	[b] 5570.2893	[b] 5870.9153	.....	.....
Meggers and Burns [33]. [c]	.....	.....	.....	4799.9139	5085.8230
Sears and Barrell [34] [d]	.....	.....	.....	4799.9104	5085.8212
Pérard [30, 35] [e]	5562.2257	5570.2894	5870.9159	4799.9113	5085.8224
Jackson [36] [f]	5562.2266	5570.2899	5870.9167	.....	.....
Peters and Emerson [g]	5562.2254	5570.2892	5870.9159	4799.9116	5085.8213

[a] By comparison with a cadmium standard, using 25- and 35-mm etalons.
[b] By comparison with neon standards, using 43-mm etalons.
[c] Values are based upon measurements with optical paths up to 80 mm.
[d] Values are based upon measurements with 20- to 240-mm opticel paths.
[e] Values are based upon measurements with optical paths of 10 to 260 mm for the krypton lines and of 10 to 190 mm for the cadmium lines.
[f] Values are the means of determinations with optical paths of 20, 40, and 60 mm.
[g] Values obtained with an optical path of 200 mm.

The greater discordance by the various observers for the 4,800 and 5,086 Cd wavelengths may be attributed to nonhomogeneity of these lines; studies by Michelson and Pérard have confirmed the presence of satellites that affect the wavelength measurements and give different wavelength values when paths of different length are used. The hyperfine structure of these and other cadmium lines has been studied in detail by Schüler and Bruck [37] and by Schüler and Keyston [38].

877106—50——7

IX. References

[1] A. A. Michelson and J. R. Benoît, Travaux et Mémoires du Bureau International des Poids et Mesures **11,** 85 (1895).

[2] J. R. Benoît, C. Fabry and A. Perot, Travaux et Mémoires du Bureau International des Poids et Mesures **15,** 131 (1913).

[3] Trans. Intern. Astronomical Union **2,** 232 (1925).

[4] Comptes rendus, Septième Conférence Générale des Poids et Mesures 52 (1927).

[5] Procès-verbaux des Séances, Comité International des Poids et Mesures, Deuxième Série **XVII,** 91 (1935).

[6] H. Barrell, Rev. Métrologie, 2d Série, **VII, 33,** (Feb. 1947).

[7] N. Watanabe and M. Imaizumi, Proc. Imp. Acad. Tokyo **4,** 351 (1928).

[8] J. E. Sears and H. Barrell, Phil. Trans. Roy. Soc. (London) [A], **233,** 143 (1934).

[9] W. Kösters and Lampe, Phys. Zeit. **35,** 224 (1934).

[10] W. Kösters and Lampe, Compt. rend., Huitième Conférence Générale des Poids et Mesures 79 (1933).

[11] Procès-verbaux des Séances, Comité International des Poids et Mesures, 2d Série, **XVII,** 113 (1935). Results are given by Kösters and Sears for repetitions of the 1933 measurements at the PTR and the NPL.

[12] W. Kösters and Lampe, Werkstatt, und Werksleiter **32,** 527 (1938), Rev. Métrologie, 2d Série, **IV,** 147 (1943).

[13] Romanova, Varlich, Kartasher et Batarchukova: Compt. rend. (Doklady) de l'Académie des Sciences de l'URSS **37,** 46 (1942) (In English).

[14] C. G. Peters and H. S. Boyd, BS Sci. Pap. **17,** 677 (1922) S436.

[15] C. Pulfrich, Z. Instr. **18,** 261 (1898).

[16] I. G. Priest, BS Sci. Pap. **15,** 669 (1919–20) S365.

[17] F. H. Rolt, Gauges and fine measurements **1,** 164 (1929).

[18] W. H. Souder and C. G. Peters, Tech. Pap. BS 157 (1920).

[19] W. H. Souder and C. G. Peters, Dental Cosmos (March 1920).

[20] W. F. Meggers and C. J. Humphreys, J. Research NBS **13,** 293 (1934) RP710.

[21] W. H. J. Childs, J. Sci. Inst. **3,** 99 to 129 (1926).

[22] K. Burns and C. C. Kiess, Pub. Allegheny Obs. **6,** 125 (1927).

[23] C. J. Humphreys, J. Research NBS **5,** 1041 (1930) RP115.

[24] W. F. Meggers, BS Bull. **12,** 203 (1915) S179.

[25] C. G. Peters, BS Sci. Pap. **20,** 635 (1926) S521.

[26] Albert Pérard, Applications Pratiques des Interférences Lumineuses: Travaux et Mémoires du Bureau International des Poids et Mesures **18,** 11 (1930).

[27] W. Kösters, Procès-verbaux des Séances, Comité International des Poids et Mesures, 2d Série, **XVII,** 82 (1935).

[28] W. B. Emerson, J. Research NBS **18,** 683 (1937) RP1003.

[29] W. F. Meggers and C. G. Peters, BS Bull. **14,** 697 (1918) S327.

[30] A. Pérard, Travaux et Mémoires du Bureau International des Poids et Mesures **19,** 78 (1934).

[31] J. E. Sears and H. Barrell, Procès-verbaux des Séances, Comité International des Poids et Mesures, 2d Série, **XVIII,** 94 (1937).

[32] J. E. Sears and H. Barrell, Phil. Trans. Roy. Soc. (London) [A] **238,** 1 to 64 (Feb. 1939).

[33] W. F. Meggers and K. Burns, BS Sci. Pap. **18,** 185 (1922–23) S441.

[34] J. E. Sears and H. Barrell, Proc. Roy. Soc. [A], **139,** 202 (1933).

[35] A. Pérard, Réunions de l'Institut d'Optique 6 Année, 10 (1935).

[36] C. V. Jackson, Proc. Roy. Soc. [A], **138,** 409 (1932).

[37] H. Schüler and H. Bruck, Z. Phys. **56,** 291 (1929).

[38] H. Schüler and J. E. Keyston, Z. Phys. **67,** 433 (1931).

Washington, October 6, 1949.

U. S. Department of Commerce
National Bureau of Standards

Research Paper RP2090
Volume 44, April 1950

Part of the Journal of Research of the National Bureau of Standards

A Note on the Formation and Structure of Iron Dendrites in a Magnesium Alloy

By Harry C. Burnett, Jr. and Herbert C. Vacher

Metallographic examination of commercially pure magnesium that had been heated to 1,000° C in an iron crucible revealed iron dendrites. Further examination by the microradiographic method showed that the dendrites grew at uniform rates in the dodecahedral directions.

During a metallographic examination of commercially pure magnesium, several six-pointed, star-shaped inclusions were observed, see figure 1. This magnesium had been heated to 1,000° C in an Armco iron crucible and stirred with an iron rod. The presence of similar inclusions in magnesium has been reported by Beck [1] and by Fahrenhorst and Bulion,[2] who concluded that they were iron dendrites. Fahrenhorst and Bulion reported that the solubility of iron in liquid magnesium at the melting point (650° C) was 0.025 percent, and at 1,200° C it was 0.84 percent. These values were substantially verified by Mitchell.[3]

Fahrenhorst and Bulion discussed the manner of growth of iron dendrites but did not clearly state whether they grew in the cubic or the octahedral directions or a combination of both. There are six cubic directions, and if the iron dendrites grew only in these directions the maximum number of branches in a plane passing through the nucleus would be four, and they would include angles of 90°. Likewise, there are eight octahedral directions and if the dendrites grew in these directions only, the maximum number of branches in a plane passing through the nucleus would also be four, but they would include angles of 70° and 110°. The dendrite in figure 1, which is a plane section through the nucleus, has six branches. It can be concluded that the growth of the dendrite was not in the cubic or octahedral directions alone.

If iron dendrites grew in magnesium in both the cubic and octahedral directions simultaneously, the maximum number of branches in a plane passing through the nucleus would be six—two in cubic directions and four in octahedral directions. The angle between adjacent branches in the octahedral directions would be 70°, and the angle between adjacent cubic and octahedral directions is 55°. Starting with a cubic direction the angular spacing between adjacent branches is 55°, 70°, 55°, 55°, 70°, and 55°. In order to test this possibility, the angles between the more perfectly developed branches *A*, *B*, *C*, and *D* in figure 1 were measured as accurately as possible and were found to be 60° between *A* and *B*, 62° between *B* and *C*, and 58° between *C* and *D*. These results preclude the possibility that the iron dendrites grow in a combination of cubic and octahedral directions. Since the maximum number of branches in any one plane passing through the center of a dendrite that had grown in the *dodecahedral* directions would be six, and the angular spacing between the branches would be 60°, it may be presumed that the branches of iron dendrites in magnesium grow in the twelve dodecahedral directions.

In order to obtain more complete data on the appearance of iron dendrites, microradiographs were made. A specimen, ⅜ in. by ¾ in. having a thickness of 0.010 in. was prepared from the same material in which was found the dendrite shown in figure 1. Copper radiation was used with a specimen-to-film distance of 28 cm. The photomicroradiograph in figure 2 shows a cluster of dendrites. A study of these and others shows

[1] Adolph Beck, The technology of magnesium and its alloys, p. 43 (1941).
[2] E. Fahrenhorst and W. Bulion, Metallography of magnesium and its alloys, p. 27 (1947).
[3] D. W. Mitchell, Solubility of iron in magnesium, Metals technology, Am. Inst. Min. Met. Engr. **15**, No. 1 (Jan. 1948).

that there are certain characteristic details that indicate that the dendrites grew in twelve directions, that is, in the dodecahedral directions.

In interpreting the photomicroradiographs in figures 2, 3, a, 4, a, 5, a, and 6, a, it should be kept in mind that the images are silhouettes of three-dimensional inclusions made by projecting them perpendicularly onto a flat photographic plate. In these photomicroradiographs it will be noted that certain branches are lighter than others, that the number of branches varies, and that the angles between the branches differ. To consider these variations systematically a model was made of a hypothetical dendrite that grew at the same rate in all twelve dodecahedral directions. It was then photographed using a long focal-length lens so that the photographs would simulate a photomicroradiograph, with the exception that variation in spoke intensity could not be produced. The positions of the model were such that the optical axis of the camera coincided with an octahedral axis, figure 3, b; a dodecahedral axis, figure 4, b; a cubic axis, figure 5, b; and an icositetrahedral axis, figure 6, b. The orientations of the spokes of the model (dodecahedral directions) in the photographs 3, b, 4, b, 5, b, and 6, b, are shown in the stereographic projections 3, c, 4, c, 5, c, and 6, c respectively. The plane of projection in each case corresponds to the photographic film. The photomicroradiographs were then inspected to

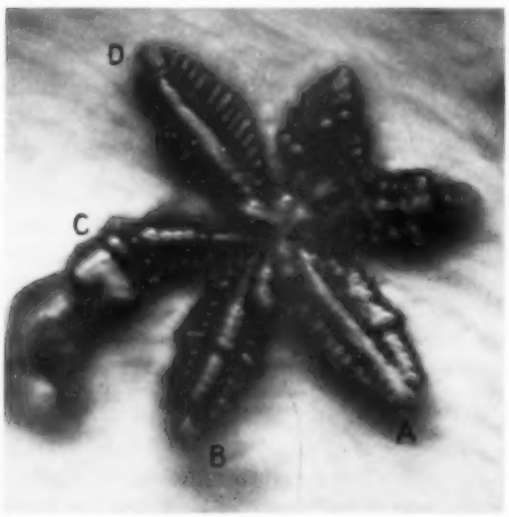

FIGURE 1. *Iron dendrite in magnesium.*
Etched with glycol reagent. ×1,000.

FIGURE 2. *Photomicroradiograph of a cluster of iron dendrites in magnesium.* ×250.

determine if the appearance of certain single dendrites conformed to the appearance of the photographs of the model in the afore-named positions.

The photomicroradiograph of the large dendrite in figure 3, a is in good agreement with the photograph of the model figure 3, b. In this orientation, all twelve spokes of the model are visible. Six long spokes spaced 60° apart that are in the plane of the photographic plate, and six spokes that appear shorter due to being inclined 55°. The angular spacing between the twelve spokes when they are projected onto the plane of the photographic plate is 30°. Only three of the inclined spokes are shown on the stereographic projection figure 3, c. The other three are on the opposite side of the projection. Inspection of the photomicroradiograph, figure 3, a shows that the long branch at the left is not developed completely nor is the short branch at the lower right. However, it is noted that there is a semblance of six long branches and six short branches as shown in figure 3, b, also that the two long branches at the right have minor branches. These minor branches appear to have grown parallel to the long major branches, which should be the case if they grew in dodecahedral directions as shown in figure 3, c. The relative lengths of the short and long branches compare favorably with the photograph of the model, figure 3, b, which indicates that the dendrite was growing at the same rate in all twelve directions.

In figure 4, a there is a large well-developed dendrite having six long branches. The branches to the left and right are darker than the upper and lower branches. This can be explained by postulating that growth was the same amount in the

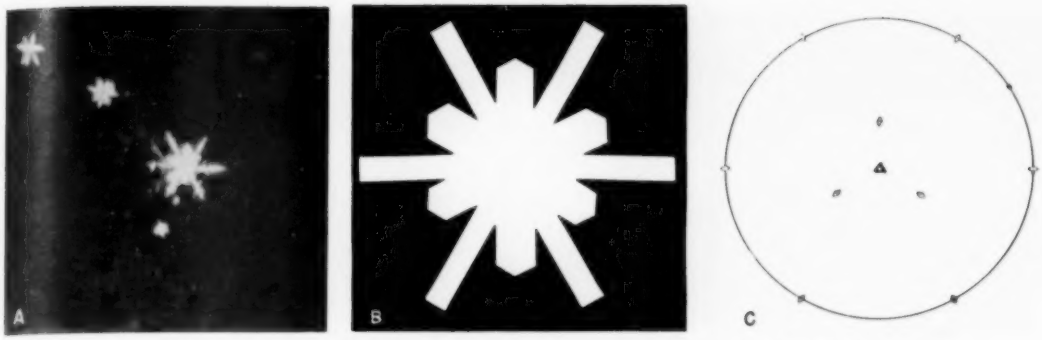

FIGURE 3. *Appearance of an iron dendrite when viewed in octahedral orientation.*

A, Photomicroradiograph of iron dendrites in magnesium. x250; B, photograph of a model dendrite that grew at the same rate in the twelve dodecahedral directions; C, stereographic projections showing the orientations of the branches of the iron dendrites and the spokes of the model dendrite.

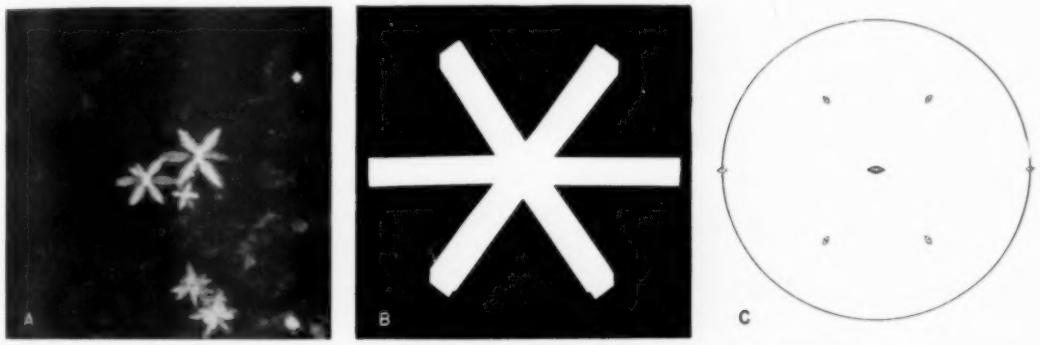

FIGURE 4. *Appearance of an iron dendrite when viewed in dodecahedral orientation.*

A, Photomicroradiograph of iron dendrites in magnesium. x250; B, photograph of a model dendrite that grew at the same rate in the twelve dodecahedral directions; C, stereographic projections showing the orientations of the branches of the iron dendrites and the spokes of the model dendrite.

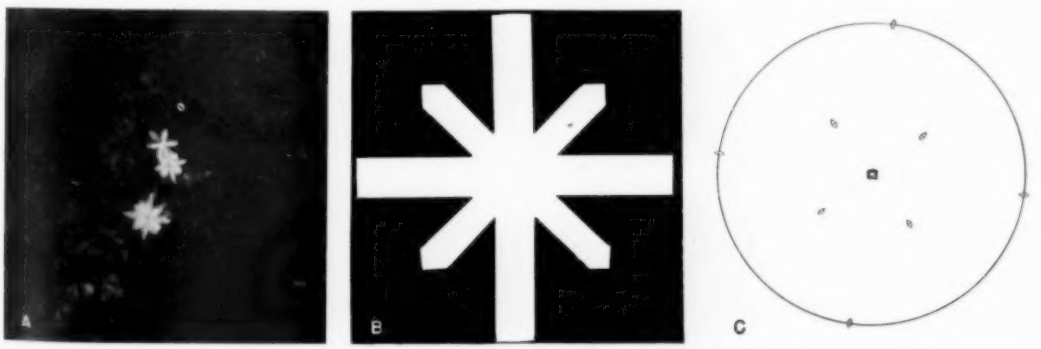

FIGURE 5. *Appearance of an iron dendrite when viewed in cubic orientation.*

A, Photomicroradiograph of iron dendrites in magnesium. x250; B, photograph of a model dendrite that grew at the same rate in the twelve dodecahedral directions; C, stereographic projections showing the orientations of the branches of the iron dendrites and the spokes of the model dendrite.

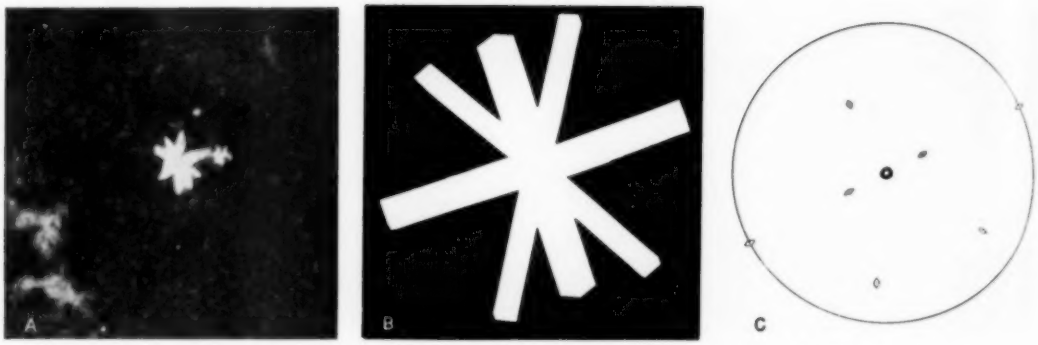

FIGURE 6. *Appearance of an iron dendrite when viewed in icositetrahedral orientation.*

A, Photomicroradiograph of iron dendrites in magnesium. x250; B, photograph of a model dendrite that grew at the same rate in the twelve dodecahedral directions; C, stereographic projections showing the orientations of the branches of the iron dendrites and the spokes of the model dendrite.

twelve dodecahedral directions. If the orientation shown in figure 4, c is assumed, then there are two branches to the right and left, in the plane of the photograph, eight inclined branches are in pairs, each pair lying in a plane perpendicular to the plane of the photograph, thus the image of each inclined branch is the result of the absorption of X-rays through two branches, whereas in the left and right branches the X-rays have been absorbed in only one branch. It is noted that the angles between the spokes in figure 4, b, starting with the one at the left, are 55°, 70°, 55°, 55°, 70°, and 55°. These angles are apparent between the branches in figure 4, a.

The lower dendrite in figure 5, A and the one in the lower left corner of figure 2 have four long and four short branches. The four long branches are darker than the four short ones, and the angles between the short and long branches appear to be 45°. The appearance of these dendrites in the photomicroradiographs also can be explained on the basis that growth was in the twelve dodecahedral directions with orientations as shown in figure 5, c. The four long and darker branches are directions in the plane of the photograph, and the four short but lighter branches are pairs of inclined directions in planes perpendicular to the plane of the photograph.

The photomicroradiograph in figure 6, A is explained on the basis that the dendrite has the orientation indicated in figure 6, b, and 6, c. The angles between the spokes in figure 6, b, starting with the one in the lower left corner, are 58°, 32°, 32°, 58°, 58°, 32°, 32°, and 58°. These appear to agree closely with the angles between the branches in the photomicroradiograph.

As a result of these observations it has been concluded that:

1. Photomicroradiography is a useful tool in determining the number and angular spacing of dendritic arms.

2. Iron dendrites in magnesium grow from a nucleus in the twelve dodecahedral directions.

3. All twelve dendritic arms appear to grow at the same rate.

WASHINGTON, November 18, 1949.